

**UCLA**

**UCLA Electronic Theses and Dissertations**

**Title**

Time-resolved Mechanisms of Organic Reactions: Methodology and Applications

**Permalink**

<https://escholarship.org/uc/item/7f6712w1>

**Author**

Yang, Zhongyue

**Publication Date**

2017

Peer reviewed|Thesis/dissertation

UNIVERSITY OF CALIFORNIA

Los Angeles

Time-resolved Mechanisms of Organic Reactions:

Methodology and Applications

A dissertation submitted in partial satisfaction of the

requirements for the degree Doctor of Philosophy

in Chemistry

by

Zhongyue Yang

2017

© Copyright by

Zhongyue Yang

2017

## ABSTRACT OF THE DISSERTATION

Time-resolved Mechanisms of Organic Reactions:  
Methodology and Applications

by

Zhongyue Yang

Doctor of Philosophy in Chemistry

University of California, Los Angeles, 2017

Professor Kendall N. Houk, Chair

This thesis focuses on the study of time-resolved mechanism of organic reactions with molecular reaction dynamics simulations. Gas-phase trajectory simulations were performed on (1) dimethyldioxirane C-H oxidation, which show how polar acetone solvation favors diradical recombination, leading to the retention of stereospecificity; (2) dehydro-Diels-Alder reactions, which reveal intrinsic dynamic features for concerted and stepwise pathways, where concerted pathway involves a vibrational excitation, while stepwise pathway involves a rotational excitation; (3) cyclopentadiene dimerization, in which two-stage pathway, as originally proposed by Woodward and Katz, is involved in 13% of the reactive trajectories, presenting a typical “dynamically stepwise” feature with time gap between formation of two bonds longer than 60 fs;



and (4) sixteen reactions with potential energy surface bifurcation, where a linear correlation was found between TS bond lengths and the product ratio, serving as an empirical model to assist the discovery of new bifurcating reactions, and estimate product ratio without the expense of MD simulations.

The thesis reports the development of a new computational method, environment-perturbed transition state sampling, (EPTSS) to enable the study of reaction dynamics in solvent and in enzyme. EPTSS integrates the conformational sampling of solvent/enzyme and quasi-classical sampling of reacting molecules, which was inspired by Truhlar and Gao's ensemble-average variational transition state theory. The method has been applied to (1) water-accelerated Diels-Alder reaction, which shows how water molecules dynamically participate the reaction and forms enhanced hydrogen bonds; (2) phosphoric acid-catalyzed allylboration reactions, in which an intrinsic synergy of enhancement between the  $\text{CH}\cdots\text{O}$  and  $\text{OH}\cdots\text{O}$  hydrogen bonds were observed, and the enhancement is diminished in toluene solvent; and (3) SpnF-catalyzed Diels-Alder reaction, which first demonstrates how enzyme dynamically control the product ratio of bifurcating reactions.

The dissertation of Zhongyue Yang is approved.

William M. Gelbart

Peter M. Felker

Shenshen Wang

Kendall N. Houk, Committee Chair

University of California, Los Angeles

2017

The thesis is dedicated to Prof. Houk for his 75<sup>th</sup> birthday and for a FANTASTIC adventure of

research in the realm of physical organic chemistry;

To the memory of Prof. Ronald Breslow, whose classic work initiated our study;

To my parents, who support me with their love and wisdom;

To Wenhao, who makes me realize that being in love is so inspiring and incredible.

TABLE OF CONTENTS

TABLE OF CONTENTS

<b>TABLE OF CONTENTS.....</b>	<b>vi</b>
<b>LIST OF FIGURES .....</b>	<b>xii</b>
<b>LIST OF SCHEMES .....</b>	<b>xx</b>
<b>LIST OF TABLES.....</b>	<b>xxi</b>
<b>ACKNOWLEDGEMENT.....</b>	<b>xxii</b>
<b>VITA.....</b>	<b>xxiv</b>
<b>Chapter 1. The Dynamics of Chemical Reactions: Atomistic Visualizations of Organic Reactions, and Homage to Van't Hoff.....</b>	<b>1</b>
<b>1.1 Abstract.....</b>	<b>1</b>
<b>1.2 Introduction.....</b>	<b>1</b>
<b>1.3 Organic reaction dynamics .....</b>	<b>4</b>
<b>1.4 Dynamics of Pericyclic Reactions in the Gas Phase, Solution and Enzyme .....</b>	<b>10</b>
<b>1.5 Conclusion .....</b>	<b>15</b>
<b>1.6 Reference .....</b>	<b>16</b>
<b>Chapter 2. Molecular Reaction Dynamics in the Gas Phase.....</b>	<b>26</b>

## TABLE OF CONTENTS

<b>2.1 Molecular Dynamics of Dimethyldioxirane C-H Oxidation .....</b>	<b>26</b>
<b>2.1.1 Abstract.....</b>	<b>26</b>
<b>2.1.2 Introduction.....</b>	<b>26</b>
<b>2.1.3 Computational Method .....</b>	<b>30</b>
<b>2.1.4 Results and Discussion.....</b>	<b>31</b>
<b>2.1.5 Conclusion .....</b>	<b>38</b>
<b>2.1.6 Reference .....</b>	<b>38</b>
<b>2.2 Distortion-Controlled Reactivity and Molecular Dynamics of Dehydro-Diels–Alder Reactions.....</b>	<b>43</b>
<b>2.2.1 Abstract.....</b>	<b>43</b>
<b>2.2.2 Introduction.....</b>	<b>43</b>
<b>2.2.3 Computational Methods.....</b>	<b>46</b>
<b>2.2.4 Results and Discussion.....</b>	<b>47</b>
<b>2.2.5 Conclusion .....</b>	<b>56</b>
<b>2.2.6 Reference .....</b>	<b>57</b>
<b>2.3 Molecular Dynamics of the Two-Stage Mechanism of Cyclopentadiene Dimerization: Concerted or Stepwise? .....</b>	<b>62</b>
<b>2.3.1 Abstract.....</b>	<b>62</b>

## TABLE OF CONTENTS

<b>2.3.2 Introduction .....</b>	<b>63</b>
<b>2.3.3 Computational Methods.....</b>	<b>66</b>
<b>2.3.4 Results and Discussion.....</b>	<b>67</b>
<b>2.3.4.1 Transition state structure of cyclopentadiene dimerization.....</b>	<b>67</b>
<b>2.3.4.2 Distribution of trajectories in the cyclopentadiene dimerization .....</b>	<b>69</b>
<b>2.3.4.3 Bond formation via dynamically concerted and dynamically stepwise fashion.....</b>	<b>70</b>
<b>2.3.5 Conclusion .....</b>	<b>74</b>
<b>2.3.6 Reference .....</b>	<b>74</b>
<b>2.4 Relationships Between Product Ratios in Ambimodal Pericyclic Reactions, and Bond Lengths in the Transition Structure .....</b>	<b>77</b>
<b>2.4.1 Abstract.....</b>	<b>77</b>
<b>2.4.2 Introduction.....</b>	<b>77</b>
<b>2.4.3 Computational Methods.....</b>	<b>80</b>
<b>2.4.4 Results and Discussion.....</b>	<b>81</b>
<b>2.4.4.1 Ambimodal reactions .....</b>	<b>81</b>
<b>2.4.4.2 Correlation between ambimodal TS geometries and product ratio.....</b>	<b>87</b>
<b>2.4.4.3 Application.....</b>	<b>91</b>

## TABLE OF CONTENTS

<b>2.4.5 Conclusion .....</b>	<b>93</b>
<b>2.4.6 Reference .....</b>	<b>93</b>
<b>Chapter 3. Energetics and Reaction Dynamics in Condensed Media: Methodology and Application .....</b>	<b>97</b>
<b>3.1 Solvent-Perturbed Transition State Sampling and Application to Water-Accelerated Diels-Alder Reaction .....</b>	<b>97</b>
<b>3.1.1 Abstract.....</b>	<b>97</b>
<b>3.1.2 Introduction.....</b>	<b>98</b>
<b>3.1.3 Computational Methods.....</b>	<b>101</b>
<b>3.1.4 Results and discussion .....</b>	<b>103</b>
<b>3.1.5 Conclusion .....</b>	<b>111</b>
<b>3.1.6 Reference .....</b>	<b>112</b>
<b>3.2 QM/QM' Direct Molecular Dynamics of Water-Accelerated Diels-Alder Reaction.....</b>	<b>118</b>
<b>3.2.1 Abstract.....</b>	<b>118</b>
<b>3.2.2 Introduction.....</b>	<b>119</b>
<b>3.2.3 Computational Methods.....</b>	<b>121</b>
<b>3.2.4 Results and Discussion.....</b>	<b>122</b>
<b>3.2.5 Conclusion .....</b>	<b>127</b>

## TABLE OF CONTENTS

<b>3.2.6 Reference .....</b>	<b>128</b>
<b>3.3 Chronology of C-H···O Hydrogen Bonding of the Phosphoric Acid-Catalyzed Allylboration of Benzaldehyde .....</b>	<b>131</b>
<b>3.3.1 Abstract.....</b>	<b>131</b>
<b>3.3.2 Introduction.....</b>	<b>131</b>
<b>3.3.3 Computational Methods.....</b>	<b>133</b>
<b>3.3.4 Results and Discussion.....</b>	<b>134</b>
<b>3.3.5 Conclusion .....</b>	<b>142</b>
<b>3.3.6 Reference .....</b>	<b>143</b>
<b>3.4 Environment-Perturbed Transition State Sampling and Application to SpnF-catalyzed Diels-Alder .....</b>	<b>145</b>
<b>3.4.1 Abstract.....</b>	<b>145</b>
<b>3.4.2 Introduction.....</b>	<b>145</b>
<b>3.4.3 Computational Methods.....</b>	<b>148</b>
<b>3.4.4 Results and Discussion.....</b>	<b>150</b>
<b>3.4.4.1 Conformational ensembles for reactant, ambimodal TS-A and Diels–Alder TS-B</b>	<b>150</b>
<b>3.4.4.2 Computed free energies of activation.....</b>	<b>153</b>
<b>3.4.4.3 Reaction dynamics simulations.....</b>	<b>156</b>



TABLE OF CONTENTS

**3.4.5 Conclusion ..... 162**

**3.4.6 References ..... 163**

**Chapter 4. Summary ..... 167**

**REFERENCE ..... 170**

## LIST OF FIGURES

## LIST OF FIGURES

<b>Figure 1.1</b> Representative trajectories in the reaction. <sup>8</sup> .....	3
<b>Figure 1.2.</b> Caldera surface and the illustration of “dynamic matching” effects. ....	7
<b>Figure 1.3.</b> Model potential energy surface with bifurcation. ....	7
<b>Figure 1.4.</b> Transition structures in cyclopentadiene dimerization. ....	8
<b>Figure 1.5.</b> Representative ambimodal pericyclic reactions. ....	9
<b>Figure 1.6.</b> Dynamics simulation for the Diels–Alder reaction between butadiene and ethylene at 298K. a) the transition structure; b) the transition state (overlay of normal mode sampling); c) distribution of forming bond lengths in b); d) 256 trajectories plotted on the two forming C-C bond lengths. ....	11
<b>Figure 1.7.</b> Snapshots from dynamics simulations of water-accelerated Diels-Alder reaction between cyclopentadiene and methylvinylketone using the SPTSS method. ....	13
<b>Figure 1.8.</b> Snapshots from a dynamics simulation of the phosphoric acid-catalyzed allylboration of benzaldehyde (a) in the gas phase, and (b) in toluene. ....	14
<b>Figure 1.9.</b> Snapshots from dynamics simulations of the transannular Diels-Alder reactions in water and in enzyme SpnF. ....	15
<b>Figure 2.1.1.</b> Free energy diagram of isobutane oxidation by DMDO in the gas phase. <sup>20</sup> Energies reported are in kcal mol <sup>-1</sup> .....	28
<b>Figure 2.1.2.</b> Free energy diagram of isobutane oxidation by DMDO in implicit solvent (acetone). Electronic energies are given in parentheses. <b>TS-2</b> cannot be located with solvation so	

## LIST OF FIGURES

<p>that the energy reported in red is a single point based on the gas phase <b>TS-2</b> geometry. All energies reported are in kcal mol<sup>-1</sup>. .....</p> <p><b>Figure 2.1.3.</b> Snapshots of two typical reactive trajectories for the hydroxylation of isobutane by DMDO in implicit acetone. (a) An oxygen-rebound trajectory, in which DMDO hydroxylation of isobutane gives <i>tert</i>-butanol and acetone through oxygen rebound mechanism. (b) A radical pair separation pathway, in which <i>tert</i>-butyl and 2-oxidanylpropan-2-ol separate after C–H abstraction. The 0 fs panels correspond to the transition state geometry where trajectories are initiated. ....</p> <p><b>Figure 2.1.4.</b> (a) A typical oxygen-rebound and recrossing trajectory represented by the O<sub>D</sub>–H<sub>B</sub> and O<sub>D</sub>–C<sub>B</sub> bond lengths. The labels are consistent with <b>Figure 2.1.3</b>. (b) Distribution of 100 reactive trajectories propagated in the gas phase. (c) Distribution of 100 reactive trajectories propagated in implicit acetone. (d) Distribution of time gap between formation of the O<sub>D</sub>–H<sub>B</sub> and O<sub>D</sub>–C<sub>B</sub> bond. The time gap is extracted from the oxygen-rebound trajectories propagated in implicit acetone solvent. The criteria for O<sub>D</sub>–H<sub>B</sub> and O<sub>D</sub>–C<sub>B</sub> bond formation are set as 1.2 and 1.6 Å, respectively. (e) An oxygen-rebound trajectory with 45 fs time gap. (f) An oxygen-rebound trajectory with 115 fs time gap. Blues dots labeled in (a–c), (e), and (f) are sampled transition state used to initiate trajectories. ....</p> <p><b>Figure 2.1.5.</b> Computed gas phase energetics of DMDO hydroxylation of <i>trans</i>-1-phenyl-2-ethylcyclopropane (Newcomb’s radical clock experiment). Energies reported are in kcal mol<sup>-1</sup>. ....</p> <p><b>Figure 2.2.1.</b> (U)M06-2X/6-311+G(d,p)-optimized transition structures for the concerted and</p>	<p>32</p> <p>33</p> <p>34</p> <p>37</p>
---	---

## LIST OF FIGURES

stepwise DA and DDA reactions. Enthalpies and free energies of activation are in kcal/mol. .... 49

**Figure 2.2.2.** Plot of activation energies versus distortion energies for six concerted reactions.

Energies are in kcal/mol..... 51

**Figure 2.2.3.** Snapshots for two typical reactive trajectories of butadiyne–acetylene cycloadditions in (a) concerted pathway where butadiyne and acetylene lead to benzyne and in (b) stepwise pathway in which butadiyne and acetylene give a diradical intermediate after one C–C bond formation. The intermediate does not give the benzyne intermediate within 500 fs. Time 0 fs corresponds to the transition state geometry where trajectories are initiated. .... 52

**Figure 2.2.4.** (a) Distribution of 300 reactive trajectories, 150 for the concerted pathway and 150 for the stepwise pathway. Blue dots are starting points from normal mode sampling used to initiate trajectories. Contour plots were calculated with UM06-2X/6-31G(d). Energies are in kcal/mol relative to separated reactants. The energy scale is shown on the right. (b) The averaged trajectory generated from 150 quasiclassical trajectories represented by bending angle versus time in the concerted butadiyne–acetylene reactions. (c) The averaged trajectory generated from 150 quasiclassical trajectories represented by bending angle versus time in the stepwise butadiyne–acetylene reactions. Bending angles are labeled in red on each TS structure. .... 54

**Figure 2.3.1.** (a) Cycloaddition transition structure, and (b) Cope rearrangement transition structure involved in the dimerization of cyclopentadiene, reported by Caramella et al. using B3LYP/6-31G(d) method. Bond 1, 2 and 3 are labeled on the graph. .... 64

**Figure 2.3.2.** Transition structures of cyclopentadiene dimerization, optimized under (a) B3LYP/6-31G(d), (b) B3LYP-D3/6-31G, (c)  $\omega$ B97X-D/6-31G(d), (d) M06-2X/6-31G(d)

## LIST OF FIGURES

methods. (e) Second-order saddle point located by M06-2X/6-31G(d). <b>Bond 1, 2 and 3</b> are labeled in (a). .....	68
<b>Figure 2.3.3.</b> (a) Trajectories that lead to <b>bonds 2</b> or <b>3</b> formation. (See <b>Fig. 1</b> for definition) The red dots that are circled in black are transition zones for cycloaddition TS and Cope TS. (b) and (c) are the overlays of transition state geometries for the cycloaddition TS and Cope TS, while (e) and (f) are averages of transition state geometries for trajectories that lead exclusively to the formation of <b>bonds 2</b> and <b>3</b> , respectively. ....	70
<b>Figure 2.3.4.</b> (a) Two typical trajectories from dynamics simulation with different time gap between formation of two bonds. The trajectory representing the dashed line has a time gap of 11 fs, and that with a solid line is 130 fs. (b) and (c) show representative snapshots involved in the dashed, and the solid trajectories respectively. The time zero corresponds to the transition state geometries that initiate the trajectories in both directions. ....	72
<b>Figure 2.3.5.</b> Time gap distributions for trajectories propagated at (a) 298 K, and (b) 1000 K. The cutoff time gap ( $t_{\text{cut}}$ ) for dynamically concerted versus stepwise trajectories is defined based on the pre-exponential factor in Eyring's equation ( $h/k_{\text{B}}T$ ), which is 60 fs at 298 K, and 18 fs at 1000 K.....	73
<b>Figure 2.3.6.</b> Snapshots for a typical deep-recrossing trajectory. ....	74
<b>Figure 2.4.1.</b> Ambimodal reactions for [4+2]/[2+4] bifurcation.....	83
<b>Figure 2.4.2.</b> Ambimodal reactions for [4+2]/[6+4] bifurcation.....	85
<b>Figure 2.4.3.</b> Other ambimodal reactions.....	87
<b>Figure 2.4.4.</b> Plot of the yield of product A vs. the TS bond length difference. ....	89

## LIST OF FIGURES

<b>Figure 2.4.5.</b> Correlation between logarithm of the product ratio $\ln(B:A)$ and bond length difference bond3-bond2.....	91
<b>Figure 2.4.6.</b> Transition structures of cyclopentadiene and $\alpha$ -keto- $\beta,\gamma$ -unsaturated phosphonates with and without Lewis acid catalysts.....	92
<b>Figure 3.1.1.</b> Four solvent configurations after the equilibration with fixed $TS_w$ in step 3. Hydrogen bond lengths are shown (Black solid lines).....	105
<b>Figure 3.1.2.</b> (a) Distribution of forming bond lengths of 20 SPTSs of the endo Diels-Alder reaction between CP and MVK according to step 4. Forming bonds are shown as blue and red dotted lines on the Figure. (b) Transition zones for the forming bonds, i.e., the most probable 98% of the distribution of forming bond lengths of 200 sampled transition states according to step 5. Inset: 200 superimposed sampled structures.....	105
<b>Figure 3.1.3.</b> Test for statistical convergence. Protocol steps 2-5 are carried out with box sizes of 10, 12 and 13 Å and $N_{SPTS} = 15, 20, 25$ ; transition zones are plotted for each combination. Statistical convergence occurs with a 12 Å box and $N_{SPTS} = 20$ .....	106
<b>Figure 3.1.4.</b> Transition zones of endo-CP-MVK reaction at 300 K in the gas phase, with SMD implicit water solvation and with explicit water (12 Å box, $N_{SPTS} = 20$ ). Insets at upper right show 200 superimposed sampled structures.....	107
<b>Figure 3.1.5.</b> C-C bond lengths for sampled TS points in gas phase, SMD, QM/MM and QM/MM+QM. 150 points are plotted for each.....	107
<b>Figure 3.1.6.</b> Distribution of (a) hydrogen bonding length (O(carbonyl)-H(water) distance), and (b) hydrogen bonding angle (O(carbonyl)-H(water)-O(water) angle) in transition states (in green,	

## LIST OF FIGURES

<p>at 0 fs), reactants (in blue, at -150 fs), and products (in pink, at 150 fs). 150 reactive trajectories are used for the analysis. (c) 3D representation of distribution of hydrogen bonding length and angle in the transition states, reactants and products. ....</p> <p><b>Figure 3.1.7.</b> Snapshots taken at -150fs, -75 fs, 0 fs and 150 fs of a typical trajectory with three water molecules added into the QM region. ....</p> <p><b>Figure 3.2.1.</b> Distribution of forming bond lengths of 200 SPTSs of the endo Diels-Alder reaction between CP and MVK, sampled using (a) QM/MM, (b) QM/MM+3QM water, and (c) QM/QM' method. Forming bonds are shown as blue and red dotted lines on the Figure. ....</p> <p><b>Figure 3.2.2.</b> Distribution of hydrogen bonding lengths (O(carbonyl)-H(water) distance) and hydrogen bonding angles (O(carbonyl)-H(water)-O(water) angle) in transition states (in green, at 0 fs), reactants (in blue, at -150 fs), and products (in pink, at 150 fs). (a), (b), and (c) are distributions of H-bond lengths in QM/MM, QM/MM+3QM water, and QM/QM' methods. (d), (e), and (f) are distributions of H-bonding angles in QM/MM, QM/MM+3QM water, and QM/QM' methods. 200 reactive trajectories from QM/MM and QM/QM', and 150 reactive trajectories from QM/MM+3 QM waters are used for the analysis. ....</p> <p><b>Figure 3.3.1.</b> Snapshots for typical reactive trajectories in the catalyzed allylboration of benzaldehyde (a) in the gas phase, and (b) in toluene. ....</p> <p><b>Figure 3.3.2.</b> Distribution of (a) benzaldehyde formyl hydrogen bond (CH<math>\cdots</math>O) distances and (b) phosphoric acid hydrogen bond (OH<math>\cdots</math>O) distances in the gas phase at reactants, transition states, and products. In each trajectory, the transition state is at 0 fs, and the reactants and products are defined as structures at -150 fs, and 150 fs, respectively. H-bond cutoff is set as 2.25 Å. ....</p>	<p>110</p> <p>111</p> <p>123</p> <p>126</p> <p>136</p> <p>137</p>
---	---

## LIST OF FIGURES

- Figure 3.3.3.** Distribution of (a) benzaldehyde formyl hydrogen bond ( $\text{CH}\cdots\text{O}$ ) distances and (b) phosphoric acid hydrogen bond ( $\text{OH}\cdots\text{O}$ ) distances in toluene at reactants, transition states, and products. In each trajectory, the transition state is at 0 fs, and the reactants and products are defined as structures at -150 fs, and 150 fs, respectively. H-bond cutoff is set as 2.25 Å..... 138
- Figure 3.3.4.** Dynamics of averaged  $\text{CH}\cdots\text{O}$  and  $\text{OH}\cdots\text{O}$  distances in the gas phase. One hundred and forty two product trajectories were averaged..... 140
- Figure 3.3.5.** Evolution of percentage of trajectories possessing  $\text{CH}\cdots\text{O}$  hydrogen bonds in the gas phase and in toluene. The H-bond criteria is defined as 2.25 Å..... 141
- Figure 3.3.6.** Catalyst-aldehyde interaction energies for TS-1 (aldehyde = benzaldehyde) and TS-2 (aldehyde = ethanal). M06-2X/def2-TZVPP//B3LYP/6-31G(d). All energies in  $\text{kcal mol}^{-1}$ .  
..... 142
- Figure 3.4.1.** SpnF-catalyzed transannular Diels–Alder reaction of **1** to form **2**. This is a step in the biosynthesis of spinosyn A..... 148
- Figure 3.4.2.** Ensembles of reactants from classical MD in water and in the enzyme. Water molecules and enzyme residues are not displayed. R-A and R-B are two representative conformations optimized in the gas phase. The dihedral angle used for discriminating between the two conformations is highlighted..... 152
- Figure 3.4.3.** Ensembles of ambimodal TS-A and Diels-Alder TS-B in enzyme. Ambimodal TS-A and Diels-Alder TS-B are representative conformations for their corresponding ensembles. The dihedral angle used for discriminating two conformations is highlighted. The intramolecular H-bond is the first case stabilizes a conformation suitable for the ambimodal TS-A. .... 152



## LIST OF FIGURES

- Figure 3.4.4.** Distribution of bonds 2 and 3 in 240 transition state geometries for (a) Diels-Alder TS-B in water, (b) ambimodal-A TS in the gas phase, (c) ambimodal TS-A in water, and (d) ambimodal TS-A in the enzyme. Bond 2 in blue leads to the [4+2] adduct, while bond 3 in red leads to the [6+4] adduct. For (a), (c), and (d), transition state geometries were sampled by using normal mode sampling on 60 transition structures optimized in various snapshots of enzyme or of water..... 157
- Figure 3.4.5.** Typical trajectories for the formation of (a) [4+2] adduct in water, (b) [6+4] adduct in water, (c) [4+2] adduct in enzyme, (b) [6+4] adduct in enzyme. We define 1.6 Å as the criterion for C-C bond formation..... 159
- Figure 3.4.6.** Distributions of reactive trajectories initiated from Diels-Alder TS in water, ambimodal TS in the gas phase, in water, and in enzyme. One hundred randomly chosen trajectories were plotted in each case. Trajectories leading to [4+2] adduct are shown in blue, and those leading to [6+4] adduct are shown in red. .... 160
- Figure 3.4.7.** (a) Hydrophobic interactions in SpnF-TS complex. The distance is measured from the closest H on V26 or L30 (depending which residue is closer in the snapshot) to C4 or C2, and the angle is the closest H-C4-C14 or H-C2-C14. Framed are the strong hydrophobic contacts, defined as the angle larger than 150° and the distance shorter than 2.9 Å. (b) Average of potential energy, kinetic energy and total energy of the substrate versus time. (c) Average of kinetic energy for residues V26, L30 and L198 versus time. Energies are averaged from 159 trajectories leading to the [4+2] adduct. The energy at 0 fs are set as zero..... 162

## LIST OF SCHEMES

## LIST OF SCHEMES

<b>Scheme 2.1.2.</b> Ultrafast Radical Clock Experiment. ....	29
<b>Scheme 2.2.1.</b> Diels–Alder (DA) and Dehydro-Diels–Alder (DDA) Reactions.....	44
<b>Scheme 2.3.1.</b> Dimerization of cyclopentadiene. ....	63
<b>Scheme 2.4.1.</b> A potential energy surface with ambimodal transition state and a post-TS bifurcation surface. ....	79
<b>Scheme 3.1.1.</b> Second-order rate constants and endo/exo product ratios for the CP + MVK Diels-Alder reaction in several solvents. <sup>32b</sup> .....	100
<b>Scheme 3.2.1.</b> Second-order rate constants and endo/exo product ratio for the CP + MVK Diels-Alder reaction in water at room temperature. ....	121
<b>Scheme 3.3.1.</b> Asymmetric Allylboration of Benzaldehyde. ....	132

## LIST OF TABLES

## LIST OF TABLES

<b>Table 2.2.1.</b> Activation, Distortion, Interaction, and Reaction Energies (in kcal/mol) Calculated with M06-2X/6-311+G(d,p) for Concerted Reactions.....	49
<b>Table 2.2.2.</b> Activation, Distortion, and Interaction Energies (in kcal/mol) Calculated with (U)M06-2X/6-311+G(d,p) for Stepwise Reactions <sup>a</sup> .....	49
<b>Table 2.4.1.</b> Summary of forming bond lengths in the transition structures and product ratios for ambimodal reactions. ....	88
<b>Table 3.1.1.</b> Time gaps (fs) for bond formation, and the percent of time gaps > 35 fs. <sup>a</sup> .....	107
<b>Table 3.2.1.</b> Time gaps (fs) for bond formation, and maximum gap. <sup>a</sup> .....	124
<b>Table 3.4.1.</b> Free energy barriers for cycloadditions of <b>1</b> in water and SpnF enzyme. ....	154
<b>Table 3.4.2.</b> Percentage of structures that have H-bond interactions with enzyme residues in ensembles of Reactant, TS-A, and TS-B after QM/MM optimizations. An H-bond is defined as having an H–O bond length shorter than 2.25 Å and an O–H–O bond angle greater than 150°.155	

## ACKNOWLEDGEMENT

## ACKNOWLEDGEMENT

This thesis can not be possibly finished without the help from the following people. I would like to start by expressing my gratitude to my parents, who in the first place supported me to pursue graduate study in the United States. I'm honored to be a graduate student in the Department of Chemistry and Biochemistry at UCLA, which has a glorious history in the chemistry program. My supervisor, Dr. Kendall N. Houk, is arguably the best computational chemist in the world, a true authority in physical organic chemistry, a wise mentor, and a nice friend. Not only is he prolific in science, but also incredible in guiding students to achieve academic growth. He inspires us to find the unsolved important problems, and works on improving our skills of reading, writing and presenting, which are essential for a good researcher. Prof. Houk also thinks ahead for his students by enthusiastically recommending us to apply fellowships and other opportunities, actively reinforcing our package of getting academic or industrial positions before most of our peers. He is so sharp as a scientist that can easily recognize the logical problem in one's presentation, but the way he expressed his opinion is always gentle and acceptable, melting people's embarrassment momentarily with his great sense of humor. I really enjoyed my four years as a graduate student in his lab, and am grateful for what he has taught me and helped me on my way up to be a good scientist. Besides, I also want to thank my collaborators, Charles Doubleday, Daniel Singleton, Dina Merrer, Heather Maynard, and Ohyun Kwon. Last but not least, I want to thank my labmates and good friends Jason Fell, Brian Levandowski, Ashay Patel, Steven Lopez, Joel Mackey, Matthew Grayson, Marc Garcia

## ACKNOWLEDGEMENT

Borràs, Peng Liu, Yong Liang, Xin Hong, Yunfang Yang, Peiyuan Yu, Song Yang, Cyndi He, Xiaofei Dong, Jeong Hoon Ko, Lingchao Cai, and Yanwei Li for their collaborations or discussions during my graduate study.

## Vita

### VITA

In 2009, I went to Nankai University as a college student, majoring in chemistry. Back then, Nankai University holds the best chemistry program in China, along with Peking University. In 2010, I was selected to Po-Ling program, which is designed to cultivate students with outstanding potentials in scientific research. In 2013, I graduated from Nankai University with a top undergraduate thesis award, and was accepted as a graduate student in the chemistry and biochemistry department at UCLA, working with Prof. Kendall Houk on theoretical and computational chemistry. My thesis mainly focuses on the development of method for quasiclassical trajectory simulation in condensed media, and the application of molecular dynamics in the mechanistic elucidation of important chemical and enzymatic reactions.

I was involved in collaborations with Charles Doubleday from Columbia University, Matthias Brewer from University of Vermont, Dina Merrer from Barnard College, Daniel Singleton from Texas A&M, Dean Tantillo from UC Davis, Xuefeng Guo from Peking University, and Yong Liang from Nanjing University. I also served as a mentor for many undergraduate students, graduate students and visiting students and professors. My Ph. D. research has generated 16 publications so far, and 2 in revision, and 6 in preparation.

I will be graduating in December, 2017, but continue to work on the field of computational chemistry with Prof. Heather Kulik at MIT.

## **Chapter 1. The Dynamics of Chemical Reactions: Atomistic Visualizations of Organic Reactions, and Homage to Van't Hoff**

### **1.1 Abstract**

Jacobus Henricus Van't Hoff was the first Nobel Laureate in Chemistry. He pioneered in the study of chemical dynamics, which referred at that time to chemical kinetics and thermodynamics. The term has evolved in modern times to refer to the exploration of chemical transformations in a time-resolved fashion. Chemical dynamics has been driven by the development of molecular dynamics trajectory simulations, which provide atomic visualization of chemical processes and illuminate how dynamic effects influence chemical reactivity and selectivity. In homage to the legend of Van't Hoff, we review the development of the chemical dynamics of organic reactions, our area of research. We then discuss our trajectory simulations of pericyclic reactions, and our development of dynamic criteria for concerted and stepwise reaction mechanisms. We also describe a method that we call environment-perturbed transition state sampling, which enables trajectory simulations in condensed-media using quantum mechanics and molecular mechanics (QM/MM). We apply the method to reactions in solvent and in enzyme.

### **1.2 Introduction**

Jacobus Henricus Van't Hoff is arguably the greatest chemist in 19<sup>th</sup> century, the founding father of physical chemistry along with Ostwald and Arrhenius. In his epoch-making publication, "*Voorstel tot Uitbreiding der Tegenwoordige in de Scheikunde gebruikte*

## BACKGROUND

*Structuurformules in de Ruimte*” (*A Suggestion Looking to the Extension into Space of the Structural Formula at Present Used in Chemistry*),<sup>1</sup> he developed the concept of the three-dimensional chemical structural formula, particularly the tetrahedral structure of carbon in molecules.<sup>2</sup> The concept renders possible the emergence of stereochemistry, which is an indispensable component of modern chemistry. In 1884, he published his ground-breaking research on chemical kinetics, “*Études de Dynamique chimique*” (*Studies in Chemical Dynamics*),<sup>3</sup> in which he describes a new way of obtaining the order of reaction. He also proposed what we call the Van’t Hoff equation (1),<sup>2</sup> which relates the equilibrium constant,  $K_{eq}$ , to the change in temperature,  $T$ , by the standard enthalpy change,  $\Delta H^\ominus$ , of a chemical reaction.

$$\frac{d \ln K_{eq}}{d (1/T)} = - \frac{\Delta H^\ominus}{R} \quad (1)$$

The seminal research of Van’t Hoff in 19<sup>th</sup> century revealed the governing principle of kinetics and thermodynamics in chemical reactions, enlightening the intrinsic properties of chemical transformation.<sup>4,5</sup> He was awarded Nobel Prize in Chemistry in 1901 “*in recognition of the extraordinary services he has rendered by the discovery of the laws of chemical dynamics and osmotic pressure in solutions.*” In 1935, Eyring,<sup>6</sup> Evans and Polanyi,<sup>7</sup> pioneered in the development of the thermodynamics picture of transition state theory (TST), which sets up a statistical mechanical foundation for chemical kinetics. TST may overestimate the rate of a reaction because of the one-way reactive flux postulate, which assumes that molecules entering into the transition state region always lead to the formation of product. In reality, however,



## BACKGROUND

dynamic motions or collisions may cause the reacting molecules to recross back to the reactant, as shown in **Figure 1.1**.

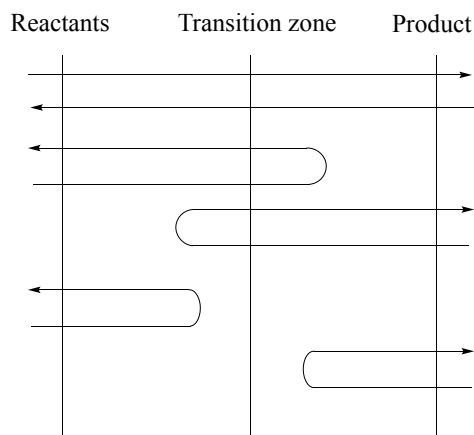


**Figure 1.1** Representative trajectories in the reaction.<sup>8</sup>

In 1938, Wigner developed the dynamical picture of TST,<sup>9</sup> and insightfully pointed out that the true transition state dividing surface should be variationally determined to minimize recrossing. The theory later evolves to be variational transition state theory, as extensively developed by Truhlar.<sup>10</sup> Keck<sup>11</sup> and Anderson<sup>8</sup> utilized the modern reaction trajectory simulation to estimate the ratio of recrossing trajectories and reactive trajectories. This gives the parameter  $\kappa$ , originally introduced by Eyring<sup>2</sup> as an *ad hoc* fudge, later called the transmission coefficient.

These theoretical advances highlighted the importance of molecular dynamics in elucidation of chemical transformations. In the 1960s-1980s, the technological developments of molecular beam and spectroscopic techniques, pioneered by Herschbach, Polanyi and Y.-T. Lee, boosted the explorations of time-resolved mechanisms of reaction.<sup>12</sup> Further advancements were made by Zewail by the establishment of femtosecond chemistry.<sup>13</sup> Molecular reaction dynamics

## BACKGROUND

emerged to be a powerful weapon for exploring the microscopic world, providing an atomic level understanding of the chronology of chemical processes.

On the theoretical side, the rapid development of computational power in the second half of the twentieth century enabled chemists to explore the nature of a reaction through simulation, which can rationalize chemical phenomena and even predict new chemistry.<sup>14</sup> Time-resolved simulations, or molecular dynamics, have been used to investigate the reactions in the femtosecond time scale and on the single-molecule level.<sup>15,16,17</sup> These simulations reveal how the motion and momenta of molecules influence the reactivity and selectivity of chemical transformations.<sup>18</sup> We now briefly review how molecular dynamics simulations have reshaped our knowledge of organic reactions. We also review a new methodology of molecular dynamics that we developed, environment-perturbed transition state sampling, which enables more quantitative understanding of pericyclic and other reactions in condensed-media.

### 1.3 Organic reaction dynamics

Molecular dynamics trajectory simulations can be performed either with a previously constructed analytical potential energy surface, or alternatively, with a direct chemical dynamics method.<sup>19,20,21,22</sup> Direct dynamics allows the trajectory simulations by integrating numerically the Newtonian equation of motion through energy, force and Hessian calculated on-the-fly using semi-empirical or *ab initio* quantum mechanical methods.<sup>23</sup> Computer programs have been developed that interface chemical dynamics to electronic structure calculations. For example, Hase's reaction dynamics code, VENUS,<sup>24</sup> has been coupled with both Gaussian<sup>25</sup> and the

## BACKGROUND

NWChem code.<sup>26</sup> In addition, Doubleday's VMG (VENUS, MOPAC, and Gaussian),<sup>27</sup> Singleton's Progdyn/Gaussian,<sup>28</sup> and Truhlar's Polyrate<sup>29</sup>/Gaussrate<sup>30</sup> were also developed to execute direct dynamics simulations.

Direct dynamics simulations have been employed to elucidate the time-resolved mechanisms of organic and bioorganic reactions. Karplus pioneered in the study of organic reaction dynamics, beginning with the atomically simple, but mechanistically complex,  ${}^1\text{CH}_2 + \text{H}_2 \rightarrow \text{CH}_4$  reaction with the CNDO method,<sup>31</sup> while Leforestier performed the first *ab initio* direct dynamics on a reaction  $\text{H}_2 + \text{CH}_3^-$  or  $\text{H}^- + \text{CH}_4$  using Hartree-Fock, minimal basis set, STO-3G calculations.<sup>32</sup> Dynamics simulations are essential when non-statistical behaviors dominate the chemical transformation.<sup>17,33,34,35,36,37</sup> These calculations reveal the dynamical processes of bonding,<sup>38</sup> such as bifurcations,<sup>39,40</sup> and avoidance of shallow intermediates that are beyond the scope of transition state theory and Rice–Ramsperger–Kassel–Marcus (RRKM) theory.<sup>41,42,43,44</sup> Carpenter showed that non-statistical dynamics control the selectivity of organic reactions involving a broad flat region of the PES, like transformations involving singlet biradicals, or zwitterionic intermediates.<sup>35,36</sup> One typical example is the vinylcyclopropane-cyclopentene rearrangement,<sup>45,46,47</sup> which involves what Doering called a “caldera” surface.<sup>48</sup> The species residing on the caldera are singlet diradicals, with little excess internal energy comparable to  $k_{\text{B}}T$ , and large geometric flexibility, as exemplified in **Figure 1.2** with the degenerate rearrangement of bicyclo[3.1.0]hex-2-ene studied by Doubleday and Houk.<sup>49,50</sup> The caldera surface is also involved in reactions like stereomutation of

## BACKGROUND

cyclopropane,<sup>51</sup> the degenerate rearrangement of bicyclo[3.1.0]hex-2-ene,<sup>49</sup> or 5-methylenebicyclo[2.1.0]pentane.<sup>52</sup>

Carpenter elucidated the dynamic origin of the stereoselectivity by trajectory simulations on the [1,3]-sigmatropic migration of bicyclo[3.2.0]hept-2-ene with the PM3 method.<sup>53</sup> Despite the existence of a 5 kcal/mol local minimum for a biradical intermediate, trajectories were found that directly connect the entrance and exit channels of the biradical, leading to the inversion of stereochemistry. These reactions can hardly be classified as either concerted or stepwise, because of the involvement of a diradical intermediate, and a certain degree of selectivity.<sup>54</sup> Carpenter proposed the concept of “dynamic matching” to rationalize this effect, which indicate that the energized vibrational modes in the transition state likely lead to a product that rests closer to its momentum vector.<sup>35</sup> This can be interpreted as a result of momentum conservation, or vibrational mode-specific chemical activation. Instead of being equilibrated through intramolecular vibrational energy redistribution, the singlet diradical carries the “memory” of bond breaking as it enters into the caldera surface all the way to the product formation. Houk proposed that some elements of orbital symmetry control the stereochemistry of bond cleavage to the diradical in the vinylcyclobutene-cyclohexene rearrangement.<sup>55</sup> A similar situations was later observed by Doubleday and Houk from the direct dynamics simulations on the [1,3]-sigmatropic rearrangement of vinylcyclopropane and of bicyclo[3.1.0]hex-2-ene using the AM1 method parameterized to fit ab initio calculations.<sup>50</sup> The concept of “dynamic matching” was also found applicable in reactions involving shallow intermediates, including deazetization of 2,3-diazabicyclo[2.2.1]hept-2-ene (DBH) by Carpenter group,<sup>56</sup> and the intermediate formed

## BACKGROUND

from tetrazine Diels–Alder reactions with alkenes by the Houk group.<sup>57</sup> In both cases, the selectivity largely deviates from the predictions of TST.

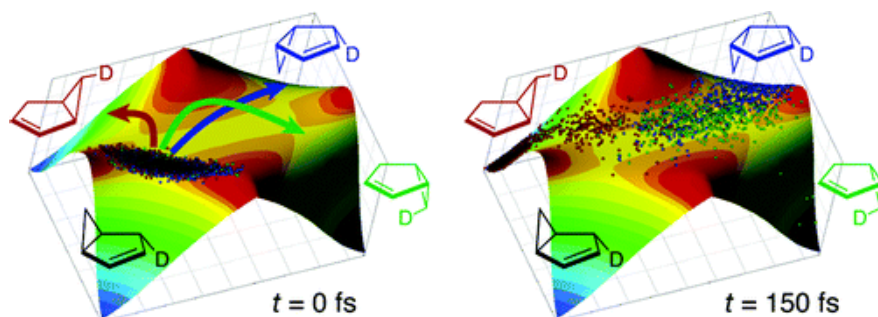


**Figure 1.2.** Caldera surface and the illustration of “dynamic matching” effects.

Trajectory simulations have been applied to predict quantitatively the product ratios for reactions with PES bifurcations, where multiple products were generated from one single transition state without a barrier.<sup>58,59</sup> The concept was initially proposed for reactions involving symmetry-breaking along the reaction path, (as shown in **Figure 1.3**) like  $\text{H}_3^+$  dissociation,<sup>60</sup> the ring opening of cyclopropylidene to allene,<sup>61</sup> 1,2-hydrogen shift in  $\text{H}_3\text{CO}$  radical,<sup>62</sup> conformational changes in cyclooctatetraene,<sup>63,64</sup> as well the other cases.<sup>65,66,67</sup>

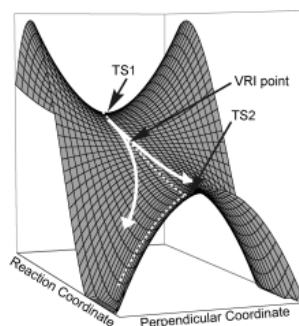


**Figure 1.3.** Model potential energy surface with bifurcation.

Cyclopentadiene dimerization was the first organic pericyclic reaction that was found to involve post-transition state bifurcation.<sup>68</sup> The  $\text{C}_2$  symmetric transition state shown in **Figure 1.4** is defined as a bispericyclic TS, or ambimodal TS, with three forming bonds that represent a

## BACKGROUND

merging of [4+2] and [2+4] reactions. They differ by which cyclopentadiene serves as the diene and which as the dienophile. Trajectory simulations show that the transition state leads to equal amounts of bond 2 and bond 3 formation to give identical products.<sup>69,70</sup> The IRC initiated from the TS proceeds to a Cope rearrangement transition state with a preserved C<sub>2</sub> symmetry, and then gives either one of the product with symmetry breaking.

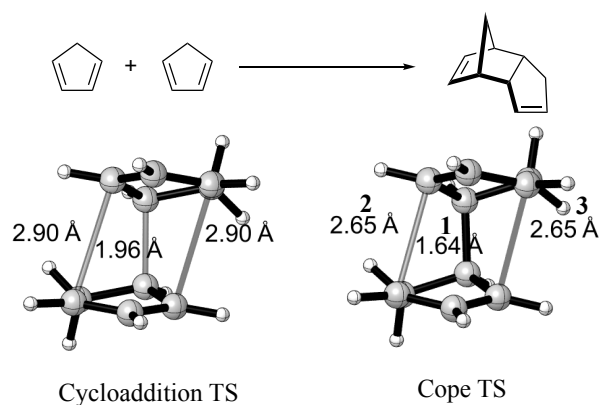


**Figure 1.4.** Transition structures in cyclopentadiene dimerization.

Unsymmetrical bifurcating reactions were later reported in which different products originate from one same TS.<sup>58,59</sup> In such cases, the ratio of the two products is determined by various factors including initial geometry,<sup>71</sup> momenta<sup>53</sup> and the shape of the PES.<sup>72,73</sup> These reactions were largely of interest to organic community because of the new source of selectivity it provides. This is widely observed in pericyclic reactions,(shown in **Figure 1.5**) including [4+2]/[2+4] bifurcation as reported by Singleton in the cycloaddition of acrolein with methylvinylketone,<sup>74</sup> and of 3-methoxycarbonylcyclopentadienone to different dienes;<sup>71</sup> [4+2]/[6+4] bifurcation reported by Houk in the biosynthesis of Heronamide and SpnF-catalyzed Diels–Alder reactions;<sup>75,76</sup> [6+4]/[4+6] bifurcations in the cycloadditions of tropone to

## BACKGROUND

dimethylfulvene;<sup>77</sup> [4+2]/[2+2] in the cycloadditions of cyclopentadiene with diphenylketene,<sup>28</sup> and others.<sup>78,79,80,81</sup>

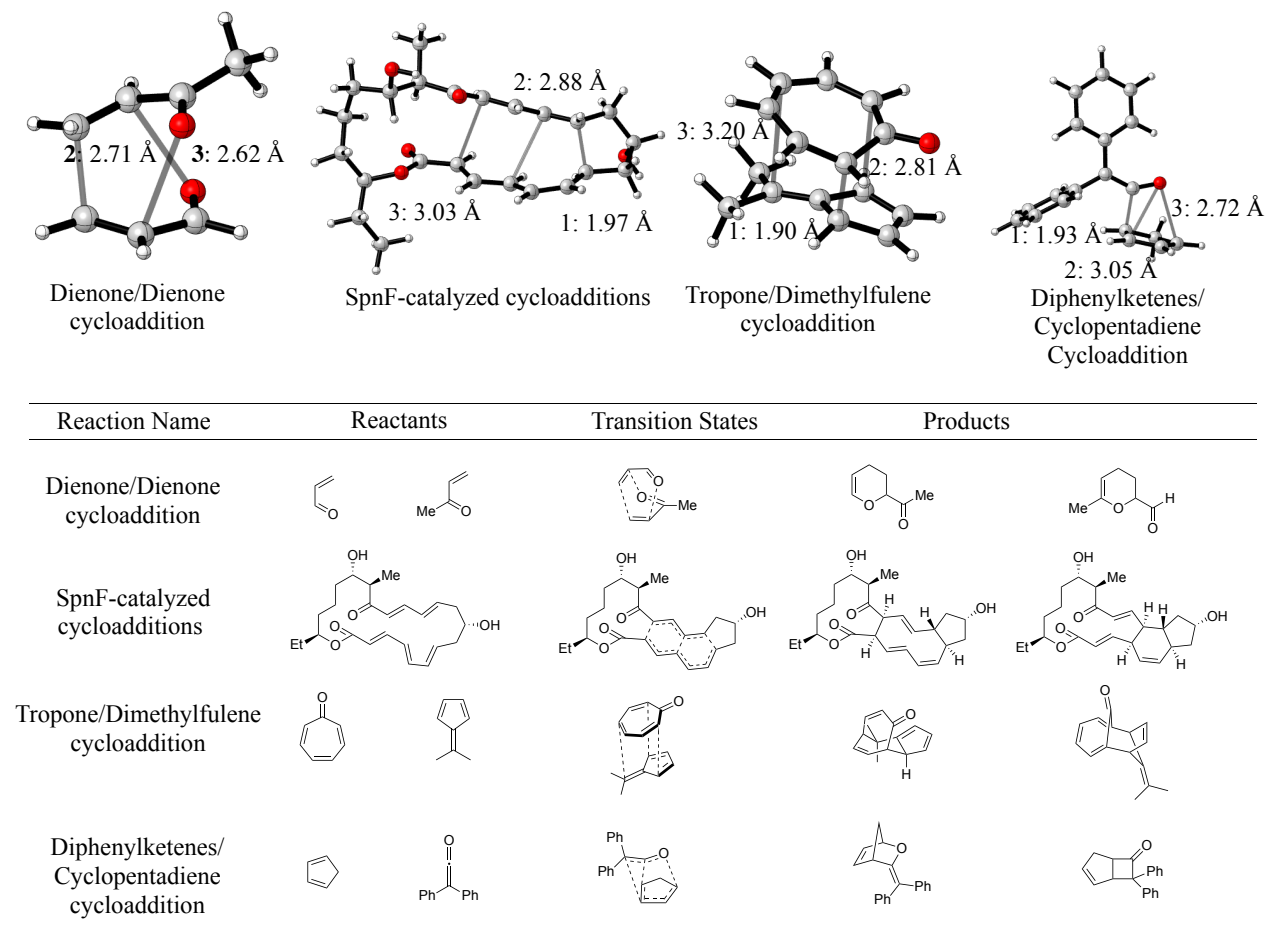


**Figure 1.5.** Representative ambimodal pericyclic reactions.

In addition, bifurcation phenomena have also been found important in other organic reactions,<sup>72</sup> biosynthetic reactions,<sup>82</sup> and organometallic reactions<sup>83,84</sup> as well. These were reviewed thoroughly by Houk,<sup>58</sup> Carpenter<sup>85</sup> and Tantillo.<sup>59</sup> The ambimodal reactions were even discovered in enzymatic reactions, as exemplified experimentally by Tang and Houk, in the SAM-dependent LprI-catalyzed Diels-Alder reaction.<sup>86</sup> Trajectory simulations have been essential to elucidate the ambimodal selectivity in these reactions.

#### 1.4 Dynamics of Pericyclic Reactions in the Gas Phase, Solution and Enzyme

We have applied molecular dynamics simulations to investigate pericyclic reactions, primarily cycloadditions<sup>38,87,88,89,90</sup> and Cope rearrangements.<sup>91</sup> This work established systematic dynamical criteria to differentiate concerted versus stepwise mechanisms at a single-molecule level. The criteria are complementary to the classic dichotomy based on potential energy (one or two barriers) or bonding simultaneous or sequential.<sup>92,93</sup> For reactions forming two bonds under ambient conditions, we defined a chemical transformation as dynamically concerted when the time gap between formation of two bonds smaller than 60 fs,<sup>94,6</sup> the lifetime of transition state derived from Eyring's equation for zero activation free energy. ( $h/k_B T$  with  $T=298K$ ) The reactive trajectories collectively provide us the distribution of time gaps, enabling classification of a chemical reaction as exclusively dynamically concerted or stepwise, or a mixture of both.

In the quasiclassical trajectory simulation of eight Diels–Alder reactions at 298K,<sup>38</sup> we showed that the average time gaps for symmetrical Diels–Alder reactions of butadiene, (**Figure 1.6**) cyclopentadiene, and cyclohexadiene with ethylene or acetylene are around 5 fs; these are dynamically concerted mechanisms. This feature also holds for the unsymmetrical reaction of butadiene and cyanoacetylene. Dynamically stepwise pathways with the formation of diradicals were observed in 2% of the trajectories for the reaction of butadiene with ethylene at 1,000 K, and 3% of the trajectories for the reaction of 2-hydroxybutadiene with cyanoacetylene at 298 K.



## BACKGROUND

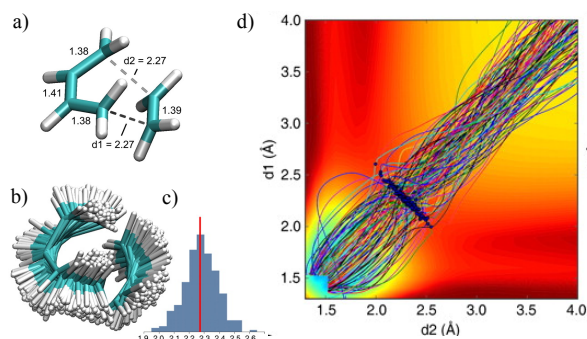


**Figure 1.6.** Dynamics simulation for the Diels–Alder reaction between butadiene and ethylene at 298K. a) the transition structure; b) the transition state (overlay of normal mode sampling); c) distribution of forming bond lengths in b); d) 256 trajectories plotted on the two forming C–C bond lengths.

Dynamics simulations were also performed for eighteen 1,3-dipolar cycloadditions.<sup>87,88</sup> The average time gap for the cycloaddition of nitrous oxide, fulminic acid, and methylene nitrene to acetylene range from 6–12 fs, again indicating dynamically concerted mechanism. The trajectory simulations also reveal how bending and vibrational excitations were involved in the reaction.

The dynamics of carbene cycloadditions to ethylene were investigated with trajectory simulations with B3LYP/6-31G(d) for  $\text{CCl}_2$ , and B3LYP/6-31G(d) with adjusted HF component (to 12%) for  $\text{CF}_2$ .<sup>89</sup> The average time gap for  $\text{CCl}_2$  is 50 fs, representing a dynamically concerted mechanism. The time gap distribution for  $\text{CF}_2$  involves biexponential decays of short and long time constants, representing a mixture of dynamically concerted and stepwise pathways. Diradical intermediates were observed from the  $\text{CF}_2$  cycloaddition trajectories in a region with no potential energy minimum, suggestive of the existence of an entropic intermediate. The

## BACKGROUND

entropic intermediate is commonly seen from dynamically stepwise trajectories, as demonstrated in the dynamics of dimethyldioxirane C-H oxidation,<sup>95</sup> Cope rearrangement,<sup>91</sup> cyclopentadiene dimerization,<sup>70</sup> and triplet di- $\pi$ -methane rearrangement.<sup>96</sup>

Solvents, the most common media for organic reactions, influence the reactions by either altering the potential energy surface in an ensemble-average fashion, or participating dynamically in the chemical transformation.<sup>97,98</sup> Elucidation of solvent effects represents one of the most challenging tasks in computational organic chemistry.<sup>99</sup> Implicit solvent models have been developed, but cannot reflect how solvent relaxation influences chemical dynamics.<sup>100,101,102</sup> To overcome this limitation, we developed the solvent-perturbed transition state sampling (SPTSS) method,<sup>103</sup> which enables the simulation of direct dynamics trajectories in explicit solvent with QM/MM methods. Similar approaches have been proposed previously by Hase and Doubleday,<sup>104</sup> Chandler,<sup>105</sup> Glowacki,<sup>106</sup> and Singleton.<sup>107</sup> Our approach integrates conformational sampling for solvent molecules and quasiclassical sampling for reacting molecules, inspired originally from Truhlar and Gao's ensemble average-variational transition state theory (EA-VTST) approach.<sup>108</sup> SPTSS method has been applied to probe the dynamical process of water-accelerated Diels–Alder reactions.<sup>103</sup> The phenomenon was first observed in the 1980s by the Breslow group.<sup>109</sup> For the reaction between cyclopentadiene and methylvinylketone, the rate is almost 100-fold faster in water than in non-polar solvent. QM/MM Monte Carlo simulations by Jorgensen group<sup>110</sup> showed that the origin of rate-enhancement primarily lies in the enhanced hydrogen bonding in the transition state relative to the reactant, and hydrophobic effects proposed by Breslow contributes to a less extent. The dynamics

## BACKGROUND

simulations clearly reveal that water molecules dynamically reorient and form a stronger hydrogen bonding network with the carbonyl group at the transition state, as shown in **Figure 1.7**. Statistically, the average hydrogen bond length O(carbonyl)-H(water) is 0.14 Å shorter, and the O(carbonyl)-H(water)-O(water) is 10° larger in the TS. The average time gap between formation of two C-C bonds varies from 11 fs in the gas phase, to 17 fs in Truhlar's implicit solvent model (SMD),<sup>102</sup> and to 25 fs in QM/MM calculations, indicative of the stabilization of dynamical zwitterionic species by explicit water molecules. We further tested the reaction with QM/QM'(PM3),<sup>111</sup> which also shows the hydrogen bonding enhancement effects.

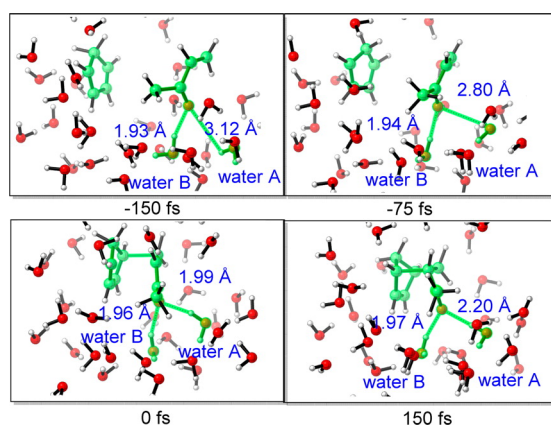


**Figure 1.7.** Snapshots from dynamics simulations of water-accelerated Diels-Alder reaction between cyclopentadiene and methylvinylketone using the SPTSS method.

The SPTSS method was also applied to study the chronology of CH $\cdots$ O and OH $\cdots$ O hydrogen bonding in the phosphoric acid-catalyzed allylboration of benzaldehyde.<sup>112</sup> (**Figure 1.8**) The simulations suggest that both hydrogen bonds are enhanced from reactants to transition states in the gas phase, while in toluene, the trend of H-bond enhancement is observed with a smaller magnitude because of solvent caging.

## BACKGROUND

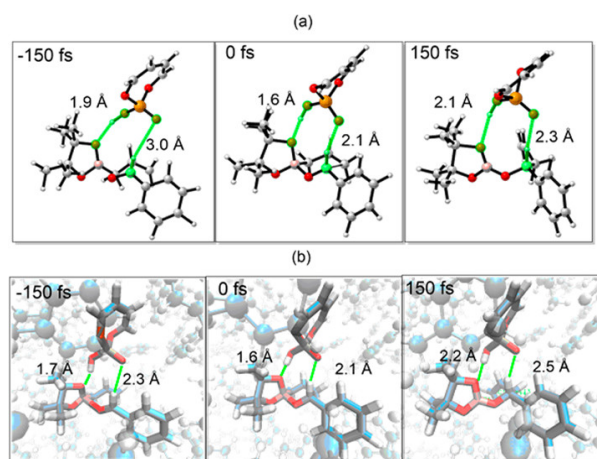


**Figure 1.8.** Snapshots from a dynamics simulation of the phosphoric acid-catalyzed allylboration of benzaldehyde (a) in the gas phase, and (b) in toluene.

We further developed a direct dynamics protocol to explore enzymatic reactions with QM/MM. The method is named environment-perturbed transition state sampling (EPTSS),<sup>113</sup> an extension of our previous SPTSS protocol. We applied the method to study the time-resolved mechanism of SpnF-catalyzed Diels-Alder reaction. SpnF is the first stand-alone Diels-Alderase reported by Hung-wen Liu at UT-Austin.<sup>114</sup> Trajectory simulations were performed in the gas phase by our group in collaboration with Singleton, which shows an ambimodal TS that leads to both [4+2] and [6+4] adducts with a ratio of 1 to 2.5 using the B3LYP-D2 method, and 1 to 1.1 using the M06-2X method. Hess et al.<sup>115</sup> and Medvedev et al.<sup>116</sup> show that both the Diels-Alder TS and the ambimodal TS conformation were potentially involved in the reaction. The EPTSS method was performed to understand how water and enzyme modify the nature of the TS and dynamically alter the product ratio. The results show that the Diels-Alder TS is favored in water with a maximum formation of intermolecular H-bonds, while the ambimodal TS is favored in the enzyme because of the hydrophobic active site that makes this conformation most stabilized by

## BACKGROUND

the intramolecular H-bonds; this is similar to the gas phase calculation. The EPTSS method also reproduces the activation free energies in both cases with a computational time that is  $\sim 10$  times faster than the traditional Umbrella Sampling method. Trajectory simulations (**Figure 1.9**) initiated from the ambimodal TS show that the product ratio of [4+2] and [6+4] adducts is 1 to 1.1 in the gas phase, 1.6 to 1 in water, and 11 to 1 in enzyme with M06-2X method. The EPTSS method is also being applied to investigate the time-resolved mechanism of other Diels-Alderases including PyrI4,<sup>117</sup> and AbyU.<sup>118</sup>

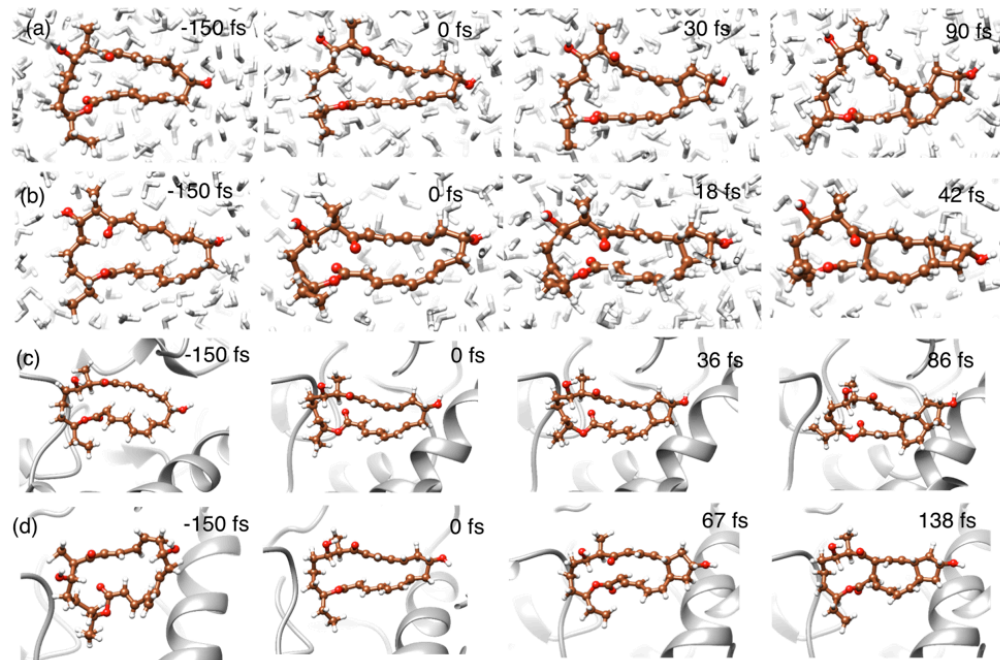


**Figure 1.9.** Snapshots from dynamics simulations of the transannular Diels-Alder reactions in water and in enzyme SpnF.

### 1.5 Conclusion

The development of organic reaction dynamics reshapes about knowledge about the origins of reactivity and selectivity in chemical transformations. Molecular dynamics simulations allow

## BACKGROUND

an atomic visualization into the detail of molecular reactions on a femtosecond time scale. Our work on the dynamics of pericyclic reactions establishes a new criterion for the classification of dynamically concerted versus stepwise pathways based on the timing of bond formation. This definition is complementary to the classic dichotomy based on energetics or bonding. The dynamical complexity of mechanisms for many important organic reactions have been presented, including Diels–Alder reactions, 1,3-dipolar cycloadditions, carbene cycloadditions, cyclopentadiene dimerization, Cope rearrangements, and dimethyldioxirane C-H oxidations. We have developed a new method, environment-perturbed transition state sampling that enables quasiclassical trajectory simulations in solvent and in enzyme. The EPTSS method has been applied to explore how solvent molecules or enzymatic residues dynamically influence the reaction dynamics, as exemplified in the water-accelerated Diels-Alder reactions, the phosphoric acid-catalyzed allylboration of benzaldehyde, and SpnF-catalyzed Diels-Alder reactions. The methodology has the potential of informing more dynamical features in condensed-phase reactions. The atomic visualization elucidated from molecular trajectory simulations largely advance our knowledge into the nature of chemical dynamics, which has been the pursuit of Van't Hoff and chemists for many generations after Van't Hoff.

### 1.6 Reference

1. Van't Hoff, J. H. Voorstel. Utrecht, **1874**. This work was revised, expanded and reprinted in French as *La Chimie dans l'Espace*. Pairs, **1875**.
2. Meijer, E.W. *Angew. Chem. Int. Ed.* **2001**, 40, 3783-3789.

## BACKGROUND

3. Van't Hoff, J. H. *Etudes de dynamique chimique*, Muller, Amsterdam, **1884**.
4. Nobelprize.org., Jacobus H. Van 't Hoff - Biographical. Nobel Media AB 2014, web. 8th Dec **2017**. <[http://www.nobelprize.org/nobel\\_prizes/chemistry/laureates/1901/hoff-bio.html](http://www.nobelprize.org/nobel_prizes/chemistry/laureates/1901/hoff-bio.html)>
5. Steinfeld, J. I.; Francisco, J. S.; Hase, W. L. *Chemical kinetics and dynamics* Vol. 3, Englewood Cliffs (New Jersey): Prentice Hall, **1989**.
6. Eyring, H. *J. Chem. Phys.* **1935**, 3, 107.
7. Evans, M. G.; Polanyi, M. *Trans. Faraday Soc.* **1935**, 31, 875.
8. Anderson, J. B. *J. Chem. Phys.* **1973**, 58, 4684.
9. Hirschfelder, J. O.; Wigner, E. *J. Chem. Phys.* **1939**, 7, 616.
10. Truhlar, D. G.; Garrett, B. C. *Annu. Rev. Phys. Chem.* **1984**, 35, 159-189.
11. Mansbach, P.; Keck, J. *Phys. Rev.* **1969**, 181, 275.
12. Levine, R.D. *Molecular reaction dynamics*. Cambridge University Press, Cambridge, **2009**.
13. Khundkar, L. R.; Zewail, A. H. *Annu. Rev. Phys. Chem.* **1990**, 41, 15-60.
14. von Ragué Schleyer, P.; Schreiner, P. R.; Schaefer III, H. F.; Jorgensen, W. L.; Thiel, W.; Glen, R. C.; Allinger, L. N.; Clark, T.; Gasteiger, J.; Chandler, D.; Handy, N. C. *Encyclopedia of Computational Chemistry*. John Wiley and Sons, **1998**.
15. Truhlar, D. G.; Hase, W. L.; Hynes, J. T. *J. Phys. Chem.* **1983**, 87, 2664-2682.
16. Hynes, J. T. *Annu. Rev. Phys. Chem.* **1985**, 36, 573-597.
17. Pratihar, S.; Ma, X.; Homayoon, Z.; Barnes, G. L.; Hase, W. L. *J. Am. Chem. Soc.* **2017**, 139, 3570-3590.
18. Carpenter, B. K. *Annu. Rev. Phys. Chem.* **2005**, 56, 57-89.

## BACKGROUND

19. Truhlar, D. G.; Muckermann, J. T. In *Atom-Molecule Collision Theory*. **1979**, Bernstein, R. B., Ed.; Plenum: New York.
20. Bunker, D. L. *J. Chem. Phys.* **1962**, *37*, 393–403.
21. Bunker, D. L. *J. Chem. Phys.* **1964**, *40*, 1946–1957.
22. Karplus, M.; Porter, R. N.; Sharma, R. D. *J. Chem. Phys.* **1965**, *43*, 3259–3287.
23. Sun, L.; Hase, W. L. *Rev. Comput. Chem.* **2003**, *19*, 79-128.
24. Hase, W. L.; Duchovic, R. J.; Hu, X.; Komornicki, A.; Lim, K.; Lu, D. H.; Peslherbe, G. H.; Swamy, K. N.; Linde, S. V.; Wang, H.; and Wolf, R. J. **1996**, *QCPE*, *16*, 671.
25. Gaussian 09, Revision E.01, Frisch, M. J.; Trucks, G. W.; Schlegel, H. B.; Scuseria, G. E.; Robb, M. A.; Cheeseman, J. R.; Scalmani, G.; Barone, V.; Mennucci, B.; Petersson, G. A.; Nakatsuji, H.; Caricato, M.; Li, X.; Hratchian, H. P.; Izmaylov, A. F.; Bloino, J.; Zheng, G.; Sonnenberg, J. L.; Hada, M.; Ehara, M.; Toyota, K.; Fukuda, R.; Hasegawa, J.; Ishida, M.; Nakajima, T.; Honda, Y.; Kitao, O.; Nakai, H.; Vreven, T.; Montgomery, J. A., Jr.; Peralta, J. E.; Ogliaro, F.; Bearpark, M.; Heyd, J. J.; Brothers, E.; Kudin, K. N.; Staroverov, V. N.; Kobayashi, R.; Normand, J.; Raghavachari, K.; Rendell, A.; Burant, J. C.; Iyengar, S. S.; Tomasi, J.; Cossi, M.; Rega, N.; Millam, J. M.; Klene, M.; Knox, J. E.; Cross, J. B.; Bakken, V.; Adamo, C.; Jaramillo, J.; Gomperts, R.; Stratmann, R. E.; Yazyev, O.; Austin, A. J.; Cammi, R.; Pomelli, C.; Ochterski, J. W.; Martin, R. L.; Morokuma, K.; Zakrzewski, V. G.; Voth, G. A.; Salvador, P.; Dannenberg, J. J.; Dapprich, S.; Daniels, A. D.; Farkas, Ö.; Foresman, J. B.; Ortiz, J. V.; Cioslowski, J.; Fox, D. J. Gaussian, Inc., Wallingford CT, 2009.



## BACKGROUND

26. Lourderaj, U.; Sun, R.; Kohale, S. C.; Barnes, G. L.; de Jong, W. A.; Windus, T. L.; Hase, W. L. *Comput. Phys. Comm.* **2014**, 185, 1074-1080.
27. Doubleday, C.; Boguslav, M.; Howell, C.; Korotkin, S. D.; Shaked, D. *J. Am. Chem. Soc.* **2016**, 138, 7476-7479.
28. Ussing, B. R.; Hang, C.; Singleton, D. A. Dynamic effects on the periselectivity, rate, isotope effects, and mechanism of cycloadditions of ketenes with cyclopentadiene. *J. Am. Chem. Soc.* **2006**, 128, 7594-7607.
29. Lu, D. H.; Truong, T. N.; Melissas, V. S.; Lynch, G. C.; Liu, Y. P.; Garrett, B. C.; Steckler, R.; Isaacson, A. D.; Rai, S. N.; Hancock, G. C.; Lauderdale, J. G. *Comput. Phys. Comm.* **1992**, 71, 235-262.
30. Corchado, J. C.; Chuang, Y. Y.; Coitino, E. L.; Truhlar, D. G.; GAUSSRATE-version 8.5/P8. 5-G94. Minneapolis, MN: University of Minnesota, based on POLYRATE-version, 8, **1999**.
31. Wang, I. S. Y.; Karplus, M. Dynamics of organic reactions. *J. Am. Chem. Soc.* **1973**, 95, 8160-8164.
32. Leforestier, C. Classical trajectories using the full ab initio potential energy surface  $\text{H}^+ + \text{CH}_4 \rightarrow \text{CH}_4 + \text{H}^+$ . *J. Chem. Phys.* **1978**, 68, 4406-4410.
33. Rehbein, J.; Carpenter, B. K. Do we fully understand what controls chemical selectivity? *Phys. Chem. Chem. Phys.* **2011**, 13, 20906-20922.
34. Carpenter, B. K. Energy disposition in reactive intermediates. *Chem. Rev.* **2013**, 113, 7265-7286.

## BACKGROUND

35. Carpenter, B. K. *Annu. Rev. Phys. Chem.* **2005**, 56, 57-89.
36. Collins, P.; Kramer, Z. C.; Carpenter, B. K.; Ezra, G. S.; Wiggins, S. *J. Chem. Phys.* **2014**, 141, 034111.
37. Yamataka, H. *Adv. Phys. Org. Chem.* **2010**, 44, 173.
38. Black, K.; Liu, P.; Xu, L.; Doubleday, C.; Houk, K. N. *Proc. Natl. Acad. Sci. USA* **2012**, 109, 12860-12865.
39. Kraus, W. A.; DePristo, A. E. *Theor. Chim. Acta* **1986**, 69, 309-322.
40. Valtazanos, P.; Ruedenberg, K. *Theor. Chim. Acta* **1986**, 69, 281-307.
41. Bunker, D. L.; Hase, W. L. *J. Chem. Phys.* **1973**, 59, 4621-4632.
42. Marcus, R. A.; Hase, W. L.; Swamy, K. *J. Phys. Chem.* **1984**, 88, 6717-6720.
43. Lourderaj, U.; Hase, W. L. *J. Phys. Chem. A* **2009**, 113, 2236-2253.
44. Hase, W. L. *Acc. Chem. Res.* **1998**, 31, 659-665.
45. Baldwin, J. E. *Chem. Rev.* **2003**, 103, 1197-1212.
46. Goldschmidt, Z.; Crammer, B. *Chem. Soc. Rev.* **1988**, 17, 229-267.
47. Doubleday, C.; Nendel, M.; Houk, K. N.; Thweatt, D.; Page, M. *J. Am. Chem. Soc.* **1999**, 121, 4720-4721.
48. Doering, W. V. E.; Cheng, X.; Lee, K.; Lin, Z. *J. Am. Chem. Soc.* **2002**, 124, 11642-11652.
49. Doubleday, C.; Nendel, M.; Houk, K. N.; Thweatt, D.; Page, M. *J. Am. Chem. Soc.* **1999**, 121, 4720-4721.
50. Doubleday, C.; Suhrada, C. P.; Houk, K. N. *J. Am. Chem. Soc.* **2006**, 128, 90-94.
51. Doubleday, C.; Bolton, K.; Hase, W. L. *J. Am. Chem. Soc.* **1997**, 119, 5251-5252.

## BACKGROUND

52. Reyes, M. B.; Lobkovsky, E. B.; Carpenter, B. K. *J. Am. Chem. Soc.* **2002**, 124, 641-651.
53. Carpenter, B. K. *J. Am. Chem. Soc.* **1995**, 117, 6336-6344.
54. Carpenter, B. K. *J. Am. Chem. Soc.* **1996**, 118, 10329-10330.
55. Northrop, B. H.; O'Malley, D. P.; Zografos, A. L.; Baran, P. S.; Houk, K. N. *Angew. Chem. Int. Ed.* **2006**, 118, 4232-4236.
56. Reyes, M. B.; Carpenter, B. K. *J. Am. Chem. Soc.* **2000**, 122, 10163-10176.
57. Törk, L.; Jiménez-Osés, G.; Doubleday, C.; Liu, F.; Houk, K. N. *J. Am. Chem. Soc.* **2015**, 137, 4749-4758.
58. Ess, D. H.; Wheeler, S. E.; Iafe, R. G.; Xu, L.; Çelebi-Ölçüm, N.; Houk, K. N. *Angew. Chem. Int. Ed.* **2008**, 47, 7592-7601.
59. Hare, S. R.; Tantillo, D. J. *Pure Appl. Chem.* **2017**, 89, 679-698.
60. Chajia, M.; Levine, R.D. *Phys. Chem. Chem. Phys.* **1999**, 1, 1205-1212.
61. Valtazanos, P.; Elbert, S. T.; Ruedenberg, K. *J. Am. Chem. Soc.* **1986**, 108, 3147-3149.
62. Kumeda, Y.; Taketsugu, T. *J. Chem. Phys.* **2000**, 113, 477-484.
63. Hrovat, D. A.; Borden, W. T. *J. Am. Chem. Soc.* **1992**, 114, 5879-5881.
64. Kato, S.; Lee, H. S.; Gareyev, R.; Wenthold, P. G.; Lineberger, W. C.; DePuy, C. H.; Bierbaum, V. M. *J. Am. Chem. Soc.* **1997**, 119, 7863-7864.
65. Windus, T. L.; Gordon, M. S. *Theor. Chim. Acta* **1992**, 83, 21-30.
66. Windus, T. L.; Gordon, M. S.; Burggraf, L. W.; Davis, L. P. *J. Am. Chem. Soc.* **1991**, 113, 4356-4357.
67. Yanai, T.; Taketsugu, T.; Hirao, K. *J. Chem. Phys.* **1997**, 107, 1137-1146.

## BACKGROUND

68. Caramella, P.; Quadrelli, P.; Toma, L. *J. Am. Chem. Soc.* **2002**, 124, 1130-1131.
69. Kelly, K. K.; Hirschi, J. S.; Singleton, D. A. *J. Am. Chem. Soc.* **2009**, 131, 8382-8383.
70. Yang, Z.; Zou, L.; Liu, F.; Yu, Y.; Dong, X.; Houk, K. N. Submitted to *Chem. Phys.* in honor of Prof. Raphael Levine for his 80th birthday.
71. Thomas, J. B.; Waas, J. R.; Harmata, M.; Singleton, D. A. *J. Am. Chem. Soc.* **2008**, 130, 14544-14555.
72. Bogle, X. S.; Singleton, D. A. *Org. Lett.* **2012**, 14, 2528-2531.
73. Hare, S. R.; Pemberton, R. P.; Tantillo, D. J. *J. Am. Chem. Soc.* **2017**, 139, 7485-7493
74. Wang, Z.; Hirschi, J. S.; Singleton, D. A. *Angew. Chem. Int. Ed.* **2009**, 48, 9156-9159.
75. Yu, P.; Patel, A.; Houk, K. N. *J. Am. Chem. Soc.* **2015**, 137, 13518-13523.
76. Patel, A.; Chen, Z.; Yang, Z.; Gutiérrez, O.; Liu, H. W.; Houk, K. N.; Singleton, D. A. *J. Am. Chem. Soc.* **2016**, 138, 3631-3634.
77. Yu, P.; Chen, T. Q.; Yang, Z.; He, C. Q.; Patel, A.; Lam, Y. H.; Liu, C. Y.; Houk, K. N. *J. Am. Chem. Soc.* **2017**, 139, 8251-8258
78. Singleton, D. A.; Hang, C.; Szymanski, M. J.; Meyer, M. P.; Leach, A. G.; Kuwata, K. T.; Chen, J. S.; Greer, A.; Foote, C. S.; Houk, K. N. *J. Am. Chem. Soc.* **2003**, 125, 1319-1328.
79. Biswas, B.; Collins, S. C.; Singleton, D. A. *J. Am. Chem. Soc.* **2014**, 136, 3740-3743.
80. Pham, H. V.; Houk, K. N. *J. Org. Chem.* **2014**, 79, 8968-8976.
81. Glowacki, D. R.; Marsden, S. P.; Pilling, M. J. *J. Am. Chem. Soc.* **2009**, 131, 13896-13897.
82. Hong, Y. J.; Tantillo, D. J. *Nat. Chem.* **2009**, 1, 384-389.
83. Hare, S. R.; Tantillo, D. J. *Chem. Sci.* **2017**, 8, 1442-1449.

## BACKGROUND

84. Zhang, L.; Wang, Y.; Yao, Z. J.; Wang, S.; Yu, Z. X. *J. Am. Chem. Soc.* **2015**, 137, 13290-13300.
85. Collins, P.; Carpenter, B. K.; Ezra, G. S.; Wiggins, S. *J. Chem. Phys.* **2013**, 139, 154108.
86. Ohashi, M.; Liu, F.; Hai, Y.; Chen, M.; Tang, M. C.; Yang, Z.; Sato, M.; Watanabe, K.; Houk, K. N.; Tang, Y. *Nature*, **2017**, 549, 502-506.
87. Xu, L.; Doubleday, C. E.; Houk, K. N. *J. Am. Chem. Soc.* **2010**, 132, 3029-3037.
88. Xu, L.; Doubleday, C. E.; Houk, K. E. *Angew. Chem.* **2009**, 121, 2784-2786.
89. Xu, L.; Doubleday, C. E.; Houk, K. N. *J. Am. Chem. Soc.* **2011**, 133, 17848-17854.
90. Yu, P.; Yang, Z.; Liang, Y.; Hong, X.; Li, Y.; Houk, K. N. *J. Am. Chem. Soc.* **2016**, 138, 8247-8252.
91. Mackey, J. L.; Yang, Z.; Houk, K. N. *Chem. Phys. Lett.* **2017**, 683, 253-257.
92. Baldwin, J. E.; Fleming M. *Fortsch Chem. Forschung.* **1970**, 15, 281.
93. Firestone, R. A. *J. Org. Chem.* **1968**, 33, 2285-2290.
94. Horn, B. A.; Herek, J. L.; Zewail, A. H. *J. Am. Chem. Soc.* **1996**, 118, 8755-8756.
95. Yang, Z.; Yu, P.; Houk, K. N. *J. Am. Chem. Soc.* **2016**, 138, 4237-4242.
96. Jiménez-Osés, G.; Liu, P.; Matute, R. A.; Houk, K. N. *Angew. Chem. Int. Ed.* **2014**, 53, 8664-8667.
97. Reichardt, C.; Welton, T. John Wiley & Sons, **2011**.
98. Carpenter, B. K.; Harvey, J. N.; Orr-Ewing, A. J. *J. Am. Chem. Soc.* **2016**, 138, 4695-4705.
99. Houk, K. N.; Liu, F. *Acc. Chem. Res.* **2017**, 50, 539-543.
100. Roux, B.; Simonson, T. *Biophys. Chem.* **1999**, 78, 1-20.

## BACKGROUND

101. Cramer, C. J.; Truhlar, D. G. *Chem. Rev.* **1999**, 99, 2161-2200.
102. Marenich, A. V.; Cramer, C. J.; Truhlar, D. G. *J. Phys. Chem. B* **2009**, 113, 6378-6396.
103. Yang, Z.; Doubleday, C.; Houk, K. N. *J. Chem. Theory Comput.* **2015**, 11, 5606-5612.
104. Bolton, K.; Hase, W. L.; Doubleday, C. *J. Phys. Chem. B* **1999**, 103, 3691-3698.
105. Bolhuis, P. G.; Chandler, D.; Dellago, C.; Geissler, P. L. *Annu. Rev. Phys. Chem.* **2002**, 53, 291-318.
106. Booth, J.; Vazquez, S.; Martinez-Nunez, E.; Marks, A.; Rodgers, J.; Glowacki, D. R.; Shalashilin, D. V. *Phil. Trans. R. Soc. A.* **2014**, 372, 20130384.
107. Chen, Z.; Nieves-Quinones, Y.; Waas, J. R.; Singleton, D. A. *J. Am. Chem. Soc.* **2014**, 136, 13122-13125.
108. Gao, J.; Truhlar, D. G. *Annu. Rev. Phys. Chem.* **2002**, 53, 467-505.
109. Rideout, D. C.; Breslow, R. *J. Am. Chem. Soc.* **1980**, 102, 7816-7817.
110. Chandrasekhar, J.; Shariffskul, S.; Jorgensen, W. L. *J. Phys. Chem. B* **2002**, 106, 8078-8085.
111. Liu, F.; Yang, Z.; Mei, Y.; Houk, K. N. *J. Phys. Chem. B.* **2016**, 120, 6250-6254.
112. Grayson, M. N.; Yang, Z.; Houk, K. N. *J. Am. Chem. Soc.* **2017**, 139, 7717-7720.
113. Yang, Z.; Yang, S.; Yu, P.; Li, Y.; Park, J.; Patel, A.; Doubleday, C.; Houk, K. N. Enzymatic Control of Reaction Dynamics (Submitted to Proc. Natl. Acad. Sci. U. S. A. In revision)
114. Kim, H. J.; Ruszczycky, M. W.; Choi, S. H.; Liu, Y. N.; Liu, H. W. *Nature* **2011**, 473, 109-112.

## BACKGROUND

115. Hess, B. A.; Smentek, L. *Org. & Biomol. Chem.* **2012**, 10, 7503-7509.
116. Medvedev, M. G.; Zeifman, A. A.; Novikov, F. N.; Bushmarinov, I. S.; Stroganov, O. V.; Titov, I. Y.; Chilov, G. G.; Svitanko, I. V. *J. Am. Chem. Soc.* **2017**, 139, 3942–3945.
117. Zheng, Q.; Guo, Y.; Yang, L.; Zhao, Z.; Wu, Z.; Zhang, H.; Liu, J.; Cheng, X.; Wu, J.; Yang, H.; Jiang, H.; Pan, L.; Liu, W. *Cell Chem. Bio.* **2016**, 23, 352-360.
118. Byrne, M. J.; Lees, N. R.; Han, L. C.; van der Kamp, M.W.; Mulholland, A. J.; Stach, J. E.; Willis, C. L.; Race, P. R. *J. Am. Chem. Soc.* **2016**, 138, 6095-6098.

## Chapter 2. Molecular Reaction Dynamics in the Gas Phase

### 2.1 Molecular Dynamics of Dimethyldioxirane C-H Oxidation

#### 2.1.1 Abstract

We report molecular dynamics simulations of the reaction of dimethyldioxirane (DMDO) with isobutane. The reaction involves hydrogen atom abstraction in the transition state, and trajectories branch to the oxygen rebound pathway, which gives *tert*-butanol and acetone, or a separated radical pair. In the gas phase, only 10% of the reactive trajectories undergo the oxygen rebound pathway, but this increases to 90% in simulations in an implicit acetone solvent (SMD) because the oxygen rebound becomes barrierless in solution. Short-lived diradical species were observed in the oxygen rebound trajectories. The time gap between C–H bond-breaking and C–O bond formation ranges from 30 to 150 fs, close to the <200 fs lifetime of radical pairs from DMDO hydroxylation of *trans*-1-phenyl-2-ethylcyclopropane measured by Newcomb.

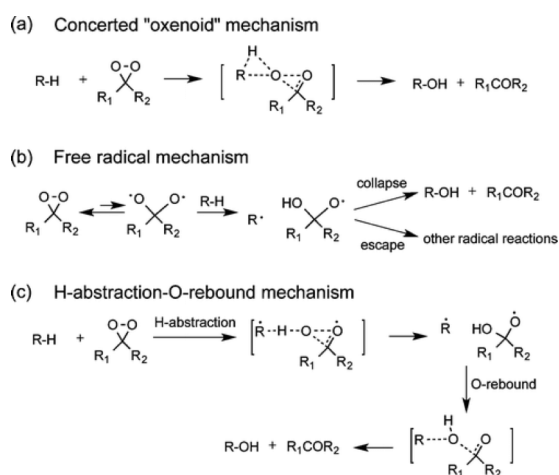
#### 2.1.2 Introduction

Dioxiranes afford efficient and stereospecific oxyfunctionalizations of unactivated C–H bonds of alkanes under extremely mild conditions and without metal catalysts.<sup>1-5</sup> Three mechanisms have been proposed to rationalize the high efficiency and stereospecificity of dioxirane C–H oxidation. Murray and Curci suggested a concerted “oxenoid” mechanism (shown in **Scheme 2.1.1a**) based on kinetics, H/D isotope effects, selectivity, and stereochemical evidence.<sup>2, 5-8</sup> This mechanism was challenged by Minisci, who showed that free radicals (shown in **Scheme 2.1.1b**) are involved in the reactions by trapping with BrCCl<sub>3</sub> or by conducting the



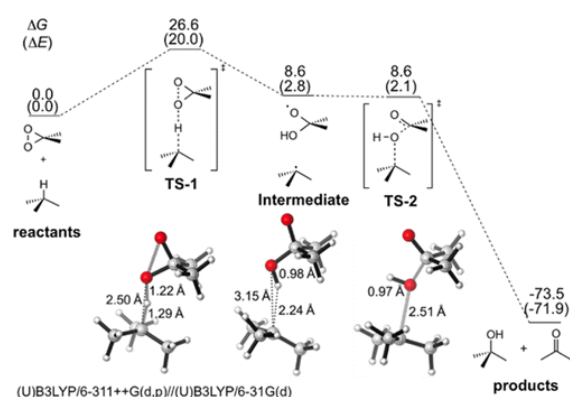
experiment under an argon atmosphere.<sup>9-11</sup> Others argued against the free radical mechanism, citing stereospecific and stereoselective hydroxylations of *cis*- and *trans*-1,2-dimethylcyclohexane,<sup>2</sup> the lack of ring opening in hydroxylation of isopropylcyclopropane,<sup>10</sup> and ultrafast radical clock experiments.<sup>12, 13</sup> This evidence, however, does not directly prove whether hydroxylation occurs by an oxenoid insertion reaction or by singlet radical pair formation and subsequent collapse (H-abstraction-O-rebound mechanism shown in **Scheme 2.1.1c**).

**Scheme 2.1.1.** Possible Mechanisms of Hydroxylation of Alkanes by Dioxirane



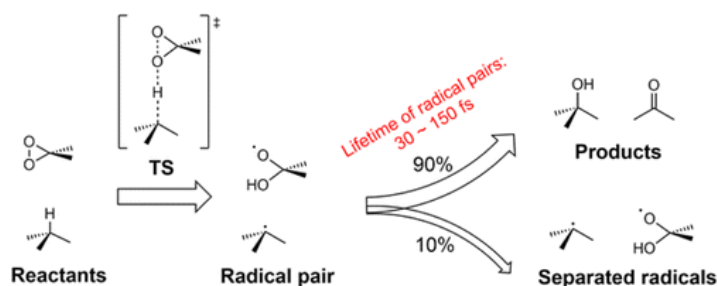
Bach, Fokin, Schreiner, Cremer, Sarzi-Amade, and Houk have all studied computationally a prototype of dimethyldioxirane (DMDO) C–H oxidations: the hydroxylation of isobutane.<sup>14-21</sup> The H-abstraction-O-rebound mechanism (**Scheme 2.1.1c**) was shown to be most favorable with an open-shell singlet TS in the rate-determining step (i.e., C–H abstraction). The diradical character of the TS originates from homolytic O–O bond cleavage of DMDO. It is noteworthy that in 1978, Goddard insightfully suggested that the dioxy radical form, dioxymethane (OCH<sub>2</sub>O), could make a contribution to the chemistry of the parent dioxirane.<sup>22</sup> As shown

in **Figure 2.1.1**,<sup>20</sup> C–H abstraction results in a radical pair, which leads to the hydroxyl product through a no-barrier O-rebound transition state. Bach proposed a 7.3 kcal/mol barrier based on G4 calculations.<sup>21</sup> After the C–H abstraction, oxygen rebound has to be rapid enough to prevent radical pair diffusion; otherwise, stereoretention would be unlikely. Therefore, the time scale of oxygen rebound, or the lifetime of radical pair, is key to understanding the mechanism of DMDO hydroxylation.



**Figure 2.1.1.** Free energy diagram of isobutane oxidation by DMDO in the gas phase.<sup>20</sup> Energies reported are in kcal mol<sup>-1</sup>.

Newcomb conducted the DMDO hydroxylation of *trans*-1-phenyl-2-ethyl-cyclopropane to estimate the lifetime of radical pair. This ultrafast radical clock experiment, illustrated in **Scheme 2.1.2**, is based on the fact that C–H abstraction would give a radical known to rearrange with a rate constant of 10<sup>11</sup> s<sup>-1</sup>. The experiment gave very small amount of products identified as **3a–c**, giving a ratio of unrearranged to rearranged products of at least 40 at ambient temperature. This indicates that the rate constant for radical collapse is at least 4 × 10<sup>12</sup> s<sup>-1</sup>. Thus, it was proposed that the maximum lifetime of a putative radical pair is 200 fs,<sup>12</sup> a time scale only 3–4 times longer than that of a transition state (~60 fs).<sup>23a–23d</sup>

**Scheme 2.1.2.** Ultrafast Radical Clock Experiment.

Free radicals were clearly excluded by radical clock experiment, but whether and how short-lived radical pairs are involved in the DMDO oxidation remains unknown. Many assumptions were proposed for the oxygen rebound process. On one hand, solvent-caging effects,<sup>24-28</sup> consisting of steric hindrance and dipole stabilization, were generally assumed to facilitate rapid oxygen rebound. Steric hindrance could effectively inhibit radical pair dissociation, and solvent polarity might stabilize the dynamical species during the transformation from a moderately polar radical pair to very polar products (*tert*-butyl alcohol and acetone). On the other hand, nonstatistical effects might be involved in the reaction, making the nascent radical pair carry dynamical memory, thus resulting in the products with stereoretention.<sup>29-35</sup> To explore how solvent effects and dynamics effects influence the oxygen rebound, we performed direct molecular dynamics (MD) simulations<sup>36-39</sup> on the DMDO C–H oxidation of isobutane in the gas phase and in implicit acetone. The solvent effect discussed here is only limited to solvent polarization because of the lack of explicit solvent molecules in implicit model.

### 2.1.3 Computational Method

MD simulations were performed both in the gas phase and in implicit acetone solvent. For the gas phase MD studies, the open-shell singlet transition state (**TS-1** shown in **Figure 2.1.1**) for the reaction was located by QM method in Gaussian 09.<sup>40</sup> UB3LYP/6-31G(d) with HOMO–LUMO mixing for the initial guess was used in both transition state optimization and dynamics simulation. (U)B3LYP/6-311++G(d,p) single point energies were computed on the (U)B3LYP/6-31G(d)-optimized structures. We have previously shown that this method gives similar energetics compared to the multiconfigurational second-order perturbation method CASPT2 for this reaction.<sup>20</sup> The Cramer-Truhlar SMD solvation model was used for the implicit solvent calculations.<sup>41</sup> Quasiclassical direct-dynamics simulations were then initialized within the region of the potential energy surface near **TS-1**, adding zero-point energy for each real normal mode in **TS-1**, plus a Boltzmann sampling of thermal energy available at 300 K with a random phase. The trajectories were propagated forward and backward until the emergence of the final products (*tert*-butanol and acetone) ( $O_D-H_B < 1.15 \text{ \AA}$  and  $O_D-C_B < 1.59 \text{ \AA}$ , where D stands for DMDO and B stands for isobutane), radical pairs ( $O_D-H_B \text{ bond} < 1.15 \text{ \AA}$  and  $O_D-C_B \text{ bond} > 3.00 \text{ \AA}$ ), or separated reactants ( $O_D-H_B \text{ bond} > 5.00 \text{ \AA}$ ). The classical equations of motion were integrated with a velocity-Verlet algorithm using Singleton's program Progdyn,<sup>42</sup> with the energies and derivatives computed on the fly by the UB3LYP method using Gaussian 09. The step length for integration was 1 fs. The MD simulations in implicit solvent followed the same protocol as the gas-phase MD studies, except that the location of the reaction

saddle point and the propagation of trajectories were carried out in conjunction with a continuum solvation model.

### 2.1.4 Results and Discussion

The free energy profile of DMDO C–H oxidation of isobutane with implicit acetone solvation (shown in **Figure 2.1.2**) was obtained to compare to that in the gas phase (**Figure 2.1.1**). Implicit solvation has only a minor effect on the barrier of reaction ( $\Delta\Delta G^\ddagger = 0.6$  kcal/mol) and does not change the geometries of **TS-1** and **Intermediate** significantly. The oxygen-rebound transition state **TS-2** found in the gas phase (**Figure 2.1.1**) cannot be located with solvation. Unrestricted single-point calculations with implicit solvent on the gas phase optimized **TS-2** geometry result in a substantially lower energy than that of **Intermediate** (~10 kcal/mol). In addition, its stable wave function shows no diradical character ( $\langle S^2 \rangle = 0$ ). The estimated ~10 kcal/mol energy difference likely reflects an overestimate of the solvent stabilization, but the solvent effect is likely to be quite large. These results indicate that the oxygen rebound is barrierless in implicit acetone solvent. This originates from a crossover from singlet diradical character to zwitterionic character, which is better stabilized by polar solvation.

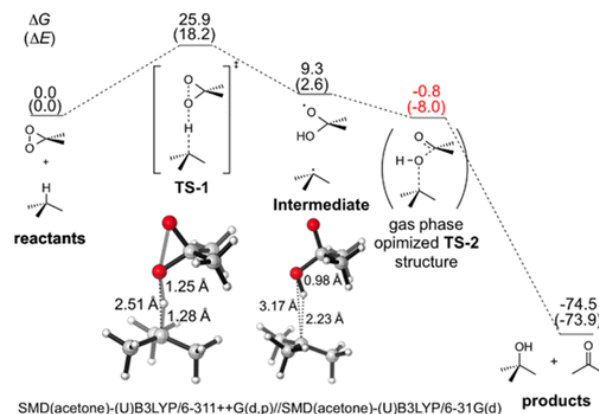


**Figure 2.1.2.** Free energy diagram of isobutane oxidation by DMDO in implicit solvent (acetone). Electronic energies are given in parentheses. **TS-2** cannot be located with solvation so that the energy reported in red is a single point based on the gas phase **TS-2** geometry. All energies reported are in kcal mol<sup>-1</sup>.

**Figure 2.1.3** shows snapshots of two typical reactive trajectories for the hydroxylation of isobutane by DMDO in implicit acetone. **Figure 2.1.3a** is an oxygen-rebound trajectory, and **Figure 2.1.3b** is one in which the radical pair separates. The bond lengths of the O<sub>D</sub>-H<sub>B</sub> and O<sub>D</sub>-C<sub>B</sub> bonds are labeled on the graph, where the subscript D stands for DMDO and B stands for isobutane. Both trajectories involve similar transition states with H transfer from C to O, and O-O bond breaking. At 0 fs, the starting point for the trajectories in both directions, the forming O<sub>D</sub>-H<sub>B</sub> bond length is 0.98 Å for the oxygen-rebound trajectory, and 1.10 Å for the radical pair separation trajectory. The O<sub>D</sub>-C<sub>B</sub> bond length for the oxygen-rebound trajectory is 2.50 Å at 0 fs, 2.45 Å at 31 fs, and 1.58 Å at 80 fs. This shows that the oxygen on DMDO rebounds immediately after C-H abstraction and gives the final products, *tert*-butanol and acetone. We have defined “dynamically concerted” as reactions in which formation of two bonds in less than 60 fs, the time it takes to pass through a transition state.<sup>23a-23d</sup> In the radical pair separation trajectory, the O<sub>D</sub>-C<sub>B</sub> bond length increases from 2.51 Å at 0 fs, to 2.61 Å at 35 fs, and to 3.55 Å at 200 fs; there is clear separation of the radicals.<sup>43</sup>

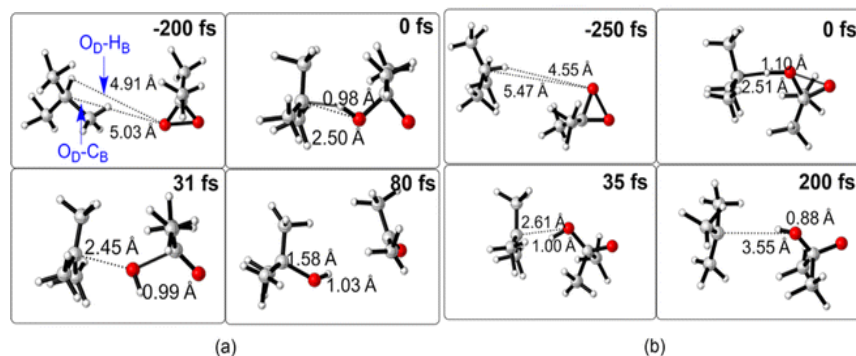


**Figure 2.1.3.** Snapshots of two typical reactive trajectories for the hydroxylation of isobutane by DMDO in implicit acetone. (a) An oxygen-rebound trajectory, in which DMDO hydroxylation of isobutane gives *tert*-butanol and acetone through oxygen rebound mechanism. (b) A radical pair separation pathway, in which *tert*-butyl and 2-oxidanylpropan-2-ol separate after C–H abstraction. The 0 fs panels correspond to the transition state geometry where trajectories are initiated.

Results for DMDO C–H oxidation of isobutane trajectories are summarized in **Figure 2.1.4**.<sup>44</sup> **Figure 2.1.4a** shows typical oxygen-rebound and radical pair separation trajectory represented by the O<sub>D</sub>–H<sub>B</sub> and O<sub>D</sub>–C<sub>B</sub> bond lengths. In the gas phase, 10% of the reactive trajectories directly lead to the alcohol (**Figure 2.1.4b**), while in implicit acetone solvent, the percentage increases to 90% (**Figure 2.1.4c**). Since oxygen rebound is barrierless in implicit acetone solvation, trajectories tend to propagate downhill to give the final product subsequent to the generation of the radical pair intermediate. In contrast, gas-phase trajectories propagate on a relatively flat potential energy surface. They will give final product only after crossing the **TS-2**. Or even more likely, radical pair may drift apart during the propagation. Noticeably, spin contamination is significant when the radical pair separates. This might be another reason for the

high proportion of radical-separation trajectories observed in the gas phase. Even so, the oxygen rebound trajectory observed in the gas phase does indicate a very rapid rebound, much faster than the rotational motion of the alkyl radical that would be needed to erode stereoselectivity

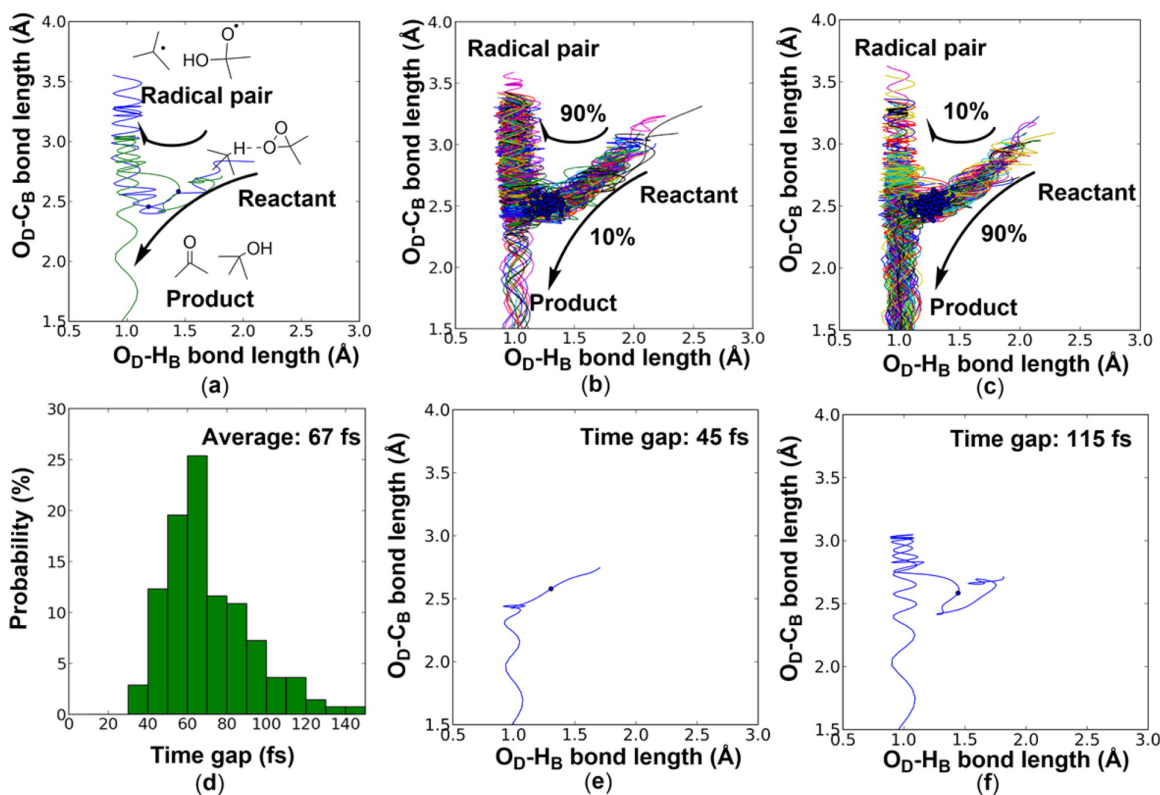


**Figure 2.1.4.** (a) A typical oxygen-rebound and recrossing trajectory represented by the  $O_D-H_B$  and  $O_D-C_B$  bond lengths. The labels are consistent with **Figure 2.1.3**. (b) Distribution of 100 reactive trajectories propagated in the gas phase. (c) Distribution of 100 reactive trajectories propagated in implicit acetone. (d) Distribution of time gap between formation of the  $O_D-H_B$  and  $O_D-C_B$  bond. The time gap is extracted from the oxygen-rebound trajectories propagated in implicit acetone solvent. The criteria for  $O_D-H_B$  and  $O_D-C_B$  bond formation are set as 1.2 and 1.6 Å, respectively. (e) An oxygen-rebound trajectory with 45 fs time gap. (f) An



oxygen-rebound trajectory with 115 fs time gap. Blues dots labeled in (a–c), (e), and (f) are sampled transition state used to initiate trajectories.

**Figure 2.1.4d** displays the distribution of time gaps between the formation of  $O_D-H_B$  and  $O_D-C_B$  bonds in the oxygen-rebound trajectories propagated in implicit acetone solvent. We have previously defined two terms, “*dynamically concerted*” (time gap of formation of two bonds  $\tau \leq 60$  fs) and “*dynamically stepwise*” (time gap of formation of two bonds  $\tau > 60$  fs), to describe reaction mechanisms in a time-resolved fashion. Unlike the traditional concept of “*concerted*” and “*stepwise*”, which focus on the existence of an intermediate on the PES, the new definitions are concerned about the involvement of fleeting intermediates in reactions based on dynamics.<sup>45-47, 23</sup> The oxygen-rebound process is dynamically concerted ( $\tau \leq 60$  fs) and stepwise ( $\tau > 60$  fs). Only 35% of the time gaps are shorter than 60 fs, and 65% are longer than 60 fs. This duality of mechanism is exemplified in **Figure 2.1.4e,f**. **Figure 2.1.4e** shows a 45 fs-time-gap trajectory in which, subsequent to the formation of  $O_D-H_B$  bond,  $O_D-C_B$  bond oscillates around 2.5 Å for about one vibrational period of  $O_D-H_B$  bond and then decreases to 1.6 Å. This dynamical behavior indicates that no well-defined radical pair intermediate is generated along the trajectory, suggesting a dynamically concerted mechanism. **Figure 2.1.4f** displays a 115 fs-time-gap trajectory where, subsequent to the formation of  $O_D-H_B$  bond, the  $O_D-C_B$  bond increases to about 3.0 Å and undergoes several vibrational motions of the  $O_D-H_B$  bond before the formation of  $O_D-C_B$  bond. This trajectory involves a fleeting radical pair, which geometrically resembles the **Intermediate** shown in **Figure 2.1.2**, suggestive of a dynamically stepwise mechanism.

The implicit acetone model provides qualitative understanding of how solvent polarity influences oxygen rebound. However, the model has some limitations. The model intrinsically treats dynamical species using a fully adiabatically optimized equilibrium continuum surrounding. In reality, however, solvent reorientation and relaxation may take several picoseconds or even longer.<sup>48-52</sup> On the time scale of oxygen rebound, the solvent will be approximately stationary, which is inconsistent with the adiabatic behavior assumed by implicit solvation. In addition, the implicit solvation does not account for the steric hindrance with solvent cage. These facts highlight the necessity of dynamics simulations with explicit solvent, which is ongoing work in our group.

In Newcomb's radical clock experiment (**Scheme 2.1.2**), the substrate (**1**) generates the more complex secondary radical. We have computed the energetics of the reaction with DMDO. The results are shown in **Figure 2.1.5**. In the gas phase, the H-abstraction step has a free energy of activation of 26.2 kcal/mol, very close to that of isobutane oxidation (**Figure 2.1.1**, 26.6 kcal/mol). Once the radical pair forms, it may collapse (O-rebound) to form alcohol **2a**, or rearrange to form radical pair **Int-3a** (as well as its *cis* isomer, not shown).

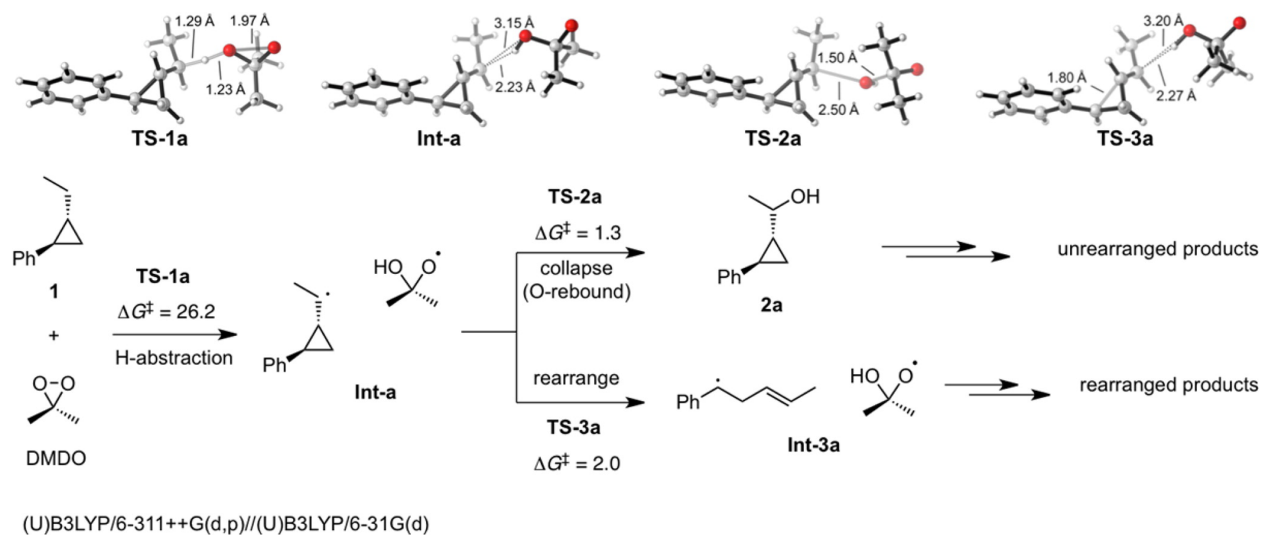


**Figure 2.1.5.** Computed gas phase energetics of DMDO hydroxylation of *trans*-1-phenyl-2-ethylcyclopropane (Newcomb's radical clock experiment). Energies reported are in kcal mol<sup>-1</sup>.

The O-rebound has a barrier of 1.3 kcal/mol in the gas phase, but the barrier disappears with implicit acetone solvent, similar to the isobutane case. The radical rearrangement has a barrier of 2.0 kcal/mol, in good agreement with the rate constant measured by Newcomb ( $10^{11}$  s<sup>-1</sup>) based on transition state theory. The experimental ratio of unrearranged to rearranged products is greater than 40:1,<sup>12</sup> which indicates that the energy barrier of O-rebound is 2.2 kcal/mol lower than that of rearrangement at ambient temperature. This further supports that the O-rebound step has no barrier in solvent. The lifetimes of radical pairs computed for the isobutane case are shown in **Figure 2.1.4d**; the time spans of radical pairs involved in DMDO C–H oxidation of isobutane are between 30 and 150 fs. These are consistent with the lifetime of radical pairs measured by Newcomb from DMDO C–H oxidation of *trans*-1-phenyl-2-ethylcyclopropane (<200 fs).<sup>12</sup>

### 2.1.5 Conclusion

We have studied the molecular dynamics of DMDO C–H oxidation of isobutane. The free energy profile of the reaction was calculated, and indicates that the oxygen rebound is barrierless in acetone solvation. In MD simulations, oxygen-rebound and radical pair separation pathways were identified. The percentage of oxygen-rebound trajectories is 10% in the gas phase and 90% in implicit acetone solvent. This indicates that the solvent influences the oxygen rebound, by response to the polarity change during hydroxyl group transfer. Analysis of oxygen rebound trajectories indicates that both dynamically concerted and stepwise mechanisms are observed. The time gaps of oxygen rebound (i.e., the lifetime of radical pairs) from DMDO C–H oxidation of isobutane range from 30 to 150 fs. For comparison, Newcomb estimated the lifetime of the radical pair to be <200 fs in his radical clock experiment involving DMDO C–H oxidation of *trans*-1-phenyl-2-ethylcyclopropane.<sup>12</sup>

### 2.1.6 Reference

1. Murray, R. W.; Jeyaraman, R. *J. Org. Chem.* **1985**, 50, 2847
2. Murray, R. W.; Jeyaraman, R.; Mohan, L. *J. Am. Chem. Soc.* **1986**, 108, 2470
3. Adam, W.; Curci, R.; Edwards, J. O. *Acc. Chem. Res.* **1989**, 22, 205
4. (a) Chen, K.; Eschenmoser, A.; Baran, P. S. *Angew. Chem., Int. Ed.* **2009**, 48, 9705 (b) Chen, K.; Baran, P. S. *Nature* **2009**, 459, 824 (c) Gaich, T.; Baran, P. S. *J. Org. Chem.* **2010**, 75, 4657 (d) Michaudel, Q.; Journot, G.; Regueiro-Ren, A.; Goswami, A.; Guo, Z.; Tully, T. P.; Zou, L.; Ramabhadran, R. O.; Houk, K. N.; Baran, P. S. *Angew. Chem., Int. Ed.* **2014**, 53, 12091

## CHAPTER 2.1

5. Curci, R.; Dinoi, A.; Rubino, M. F. *Pure Appl. Chem.* **1995**, 67, 811
6. Mello, R.; Fiorentino, M.; Fusco, C.; Curci, R. *J. Am. Chem. Soc.* **1989**, 111, 6749
7. Adam, W.; Asensio, G.; Curci, R.; Gonzaleznunez, M. E.; Mello, R. *J. Org. Chem.* **1992**, 57, 953
8. Murray, R. W.; Singh, M.; Jeyaraman, R. *J. Am. Chem. Soc.* **1992**, 114, 1346
9. Minisci, F.; Zhao, L.; Fontana, F.; Bravo, A. *Tetrahedron Lett.* **1995**, 36, 1697
10. Vanni, R.; Garden, S. J.; Banks, J. T.; Ingold, K. U. *Tetrahedron Lett.* **1995**, 36, 7999
11. Bravo, A.; Bjorsvik, H.-R.; Fontana, F.; Minisci, F.; Serri, A. *J. Org. Chem.* **1996**, 61, 9409
12. Simakov, P. A.; Choi, S.-Y.; Newcomb, M. *Tetrahedron Lett.* **1998**, 39, 8187
13. Curci, R.; D'Accolti, L.; Fusco, C. *Tetrahedron Lett.* **2001**, 42, 7087
14. Cremer, D.; Kraka, E.; Szalay, P. G. *Chem. Phys. Lett.* **1998**, 292, 97
15. Shustov, G. V.; Rauk, A. *J. Org. Chem.* **1998**, 63, 5413
16. Bach, R. D.; Andres, J. L.; Su, M. D.; McDouall, J. J. W. *J. Am. Chem. Soc.* **1993**, 115, 5768
17. Bach, R. D.; Su, M. D. *J. Am. Chem. Soc.* **1994**, 116, 10103
18. Fokin, A. A.; Tkachenko, B. A.; Korshunov, O. I.; Gunchenko, P. A.; Schreiner, P. R. *J. Am. Chem. Soc.* **2001**, 123, 11248
19. Freccero, M.; Gandolfi, R.; Sarzi-Amade, M.; Rastelli, A. *J. Org. Chem.* **2003**, 68, 811
20. Zou, L.; Paton, R. S.; Eschenmoser, A.; Newhouse, T. R.; Baran, P. S.; Houk, K. N. *J. Org. Chem.* **2013**, 78, 4037
21. Bach, R. D. *J. Phys. Chem. A* **2016**, 120, 840
22. Harding, L. B.; Goddard, W. A. *J. Am. Chem. Soc.* **1978**, 100, 7180

## CHAPTER 2.1

23. (a) Black, K.; Liu, P.; Xu, L.; Doubleday, C.; Houk, K. N. *Proc. Natl. Acad. Sci. U. S. A.* **2012**, 109, 12860 (b) Xu, L.; Doubleday, C. E.; Houk, K. N. *Angew. Chem., Int. Ed.* **2009**, 48, 2746 (c) Xu, L.; Doubleday, C. E.; Houk, K. N. *J. Am. Chem. Soc.* **2010**, 132, 3029 (d) Xu, L.; Doubleday, C. E.; Houk, K. N. *J. Am. Chem. Soc.* **2011**, 133, 17848
24. Yang, H.; Snee, P. T.; Kotz, K. T.; Payne, C. K.; Harris, C. B. *J. Am. Chem. Soc.* **2001**, 123, 4204
25. Koneshan, S.; Rasaiah, J. C.; Lynden-Bell, R. M.; Lee, S. H. *J. Phys. Chem. B* **1998**, 102, 4193
26. Wan, C.; Gupta, M.; Baskin, J. S.; Kim, Z. H.; Zewail, A. H. *J. Chem. Phys.* **1997**, 106, 4353
27. Liu, Q.; Wang, J.-K.; Zewail, A. H. *Nature* **1993**, 364, 427
28. Van Der Zwan, G.; Hynes, J. T. *Chem. Phys. Lett.* **1983**, 101, 367
29. Bogle, X. S.; Singleton, D. A. *Org. Lett.* **2012**, 14, 2528
30. Oyola, Y.; Singleton, D. A. *J. Am. Chem. Soc.* **2009**, 131, 3130
31. Collins, P.; Kramer, Z. C.; Carpenter, B. K.; Ezra, G. S.; Wiggins, S. *J. Chem. Phys.* **2014**, 141, 034111
32. Carpenter, B. K. *Chem. Rev.* **2013**, 113, 7265
33. Litovitz, A. E.; Keresztes, I.; Carpenter, B. K. *J. Am. Chem. Soc.* **2008**, 130, 12085
34. Glowacki, D. R.; Marsden, S. P.; Pilling, M. J. *J. Am. Chem. Soc.* **2009**, 131, 13896
35. Glowacki, D. R.; Liang, C. H.; Marsden, S. P.; Harvey, J. N.; Pilling, M. J. *J. Am. Chem. Soc.* **2010**, 132, 13621
36. Doubleday, C.; Suhrada, C. P.; Houk, K. N. *J. Am. Chem. Soc.* **2006**, 128, 90

## CHAPTER 2.1

37. Suhrada, C. P.; Houk, K. N. *J. Am. Chem. Soc.* **2002**, 124, 8796
38. Houk, K. N.; Nendel, M.; Wiest, O.; Storer, J. W. *J. Am. Chem. Soc.* **1997**, 119, 10545
39. Carpenter, B. K. *J. Am. Chem. Soc.* **1995**, 117, 6336
40. Frisch, M. J.; Trucks, G. W.; Schlegel, H. B.; Scuseria, G. E.; Robb, M. A.; Cheeseman, J. R.; Scalmani, G.; Barone, V.; Mennucci, B.; Petersson, G. A.; Nakatsuji, H.; Caricato, M.; Li, X.; Hratchian, H. P.; Izmaylov, A. F.; Bloino, J.; Zheng, G.; Sonnenberg, J. L.; Hada, M.; Ehara, M.; Toyota, K.; Fukuda, R.; Hasegawa, J.; Ishida, M.; Nakajima, T.; Honda, Y.; Kitao, O.; Nakai, H.; Vreven, T.; Montgomery, Jr., J. A.; Peralta, J. E.; Ogliaro, F.; Bearpark, M. J.; Heyd, J.; Brothers, E. N.; Kudin, K. N.; Staroverov, V. N.; Kobayashi, R.; Normand, J.; Raghavachari, K.; Rendell, A. P.; Burant, J. C.; Iyengar, S. S.; Tomasi, J.; Cossi, M.; Rega, N.; Millam, N. J.; Klene, M.; Knox, J. E.; Cross, J. B.; Bakken, V.; Adamo, C.; Jaramillo, J.; Gomperts, R.; Stratmann, R. E.; Yazyev, O.; Austin, A. J.; Cammi, R.; Pomelli, C.; Ochterski, J. W.; Martin, R. L.; Morokuma, K.; Zakrzewski, V. G.; Voth, G. A.; Salvador, P.; Dannenberg, J. J.; Dapprich, S.; Daniels, A. D.; Farkas, Ö.; Foresman, J. B.; Ortiz, J. V.; Cioslowski, J.; Fox, D. J.; Gaussian, Inc.: Wallingford, CT, **2009**.
41. Marenich, A. V.; Cramer, C. J.; Truhlar, D. G. *J. Phys. Chem. B* **2009**, 113, 6378
42. Singleton, D. A.; Wang, Z. H. *J. Am. Chem. Soc.* **2005**, 127, 6679
43. Propagation of the trajectory for even longer time (~500 fs) leads to the further separation of the radical pair.
44. In **Figure 2.1.4b,c**, we show the distribution of the reactive trajectories, which are defined as trajectories starting from reactants and lead to rebound product or radical pair. In the dynamics

## CHAPTER 2.1

simulations, we obtained reactive trajectories, recrossing trajectories, and product-to-radical pair trajectories. The percentage for these three types are around 60%, 35%, and 5%, respectively.

45. Patel, A.; Chen, Z.; Yang, Z.; Gutierrez, O.; Liu, H.-w.; Houk, K. N.; Singleton, D. A. *J. Am. Chem. Soc.* **2016**, 138, 3631-3634.

46. Yang, Z.; Doubleday, C.; Houk, K. N. *J. Chem. Theory Comput.* **2015**, 11, 5606

47. Hong, X.; Bercovici, D. A.; Yang, Z.; Al-Bataineh, N.; Srinivasan, R.; Dhakal, R. C.; Houk, K. N.; Brewer, M. *J. Am. Chem. Soc.* **2015**, 137, 9100

48. Nandi, N.; Bhattacharyya, K.; Bagchi, B. *Chem. Rev.* **2000**, 100, 2013

49. Bagchi, B.; Biswas, R. *Adv. Chem. Phys.* **1999**, 109, 207

50. Hamm, P.; Lim, M.; Hochstrasser, R. M. *J. Chem. Phys.* **1997**, 107, 10523

51. Voth, G. A.; Hochstrasser, R. M. *J. Phys. Chem.* **1996**, 100, 13034

52. Chen, Z.; Nieves-Quinones, Y.; Waas, J. R.; Singleton, D. A. *J. Am. Chem. Soc.* **2014**, 136, 13122



## 2.2 Distortion-Controlled Reactivity and Molecular Dynamics of Dehydro-Diels–Alder Reactions

### 2.2.1 Abstract

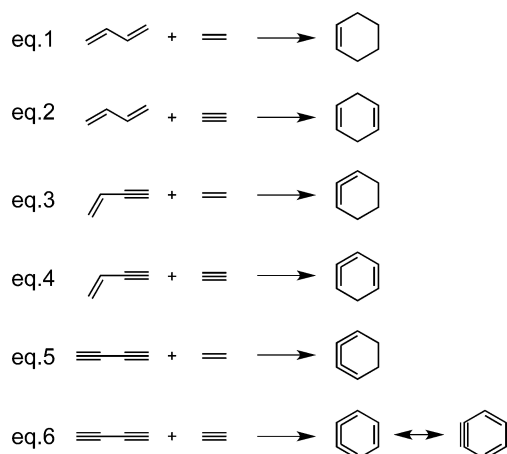
We report density functional theory (M06-2X) studies of a series of dehydro-Diels–Alder (DDA) reactions. For these and the parent reaction, the stepwise mechanisms have similar barriers, whereas the barriers of the concerted mechanisms differ significantly. The reactivity of DDA reactions is controlled by distortion energy. The concerted and stepwise mechanisms of the hexadehydro-Diels–Alder (HDDA) reaction are competitive with activation barriers of ~36 kcal/mol. This is because a large distortion energy (~43 kcal/mol) is required to achieve the concerted transition state geometry. MD simulations reveal that productive concerted trajectories display a strong angle bending oscillation (~25° oscillation amplitude), while the stepwise trajectories show only a chaotic pattern and less pronounced bending vibrations.

### 2.2.2 Introduction

The Diels–Alder (DA) reaction between a diene and a dienophile (alkene or alkyne) represents one of the most widely utilized and well-studied synthetic transformations in organic chemistry (**Scheme 2.2.1**, eqs 1 and 2).<sup>1-5</sup> This (4 + 2) cycloaddition is particularly useful for constructing six-membered rings with up to four stereogenic centers in a single step, often with good regio- and stereocontrol. Various aspects of the DA reactions, such as mechanism,<sup>6</sup> dynamics,<sup>7</sup> selectivity,<sup>8</sup> asymmetric catalysis,<sup>9</sup> and industrial applications,<sup>10</sup> have attracted generations of theoretical and synthetic chemists ever since its original discovery in

1928.<sup>1</sup> Specific types or variants of DA reactions, such as intramolecular (IMDA) and transannular (TADA) reactions,<sup>11-14</sup> and hetero-Diels–Alder (HDA) reactions,<sup>15,16</sup> have been categorized. Novel utilities and new aspects of DA reactions are still emerging. The development of the tetrazine ligation<sup>17-19</sup> (an inverse electron demand HDA reaction<sup>20</sup> widely used for bioorthogonal applications) and the search for enzymes that catalyze DA reactions (Diels–Alderase)<sup>21-23</sup> are recent examples.

**Scheme 2.2.1.** Diels–Alder (DA) and Dehydro-Diels–Alder (DDA) Reactions



In 2008, Wessig et al. described another important variant of the DA reaction, the dehydro-Diels–Alder (DDA) reaction<sup>24</sup> (**Scheme 2.2.1**, eqs 3–6). If one or both double bonds in the diene component of a DA reaction are replaced by a triple bond, the product must contain cumulated double bonds (i.e., cyclic allenes).<sup>25</sup> Due to high strain, these initially formed species usually undergo further reactions such as hydrogen migration or dimerization to generate more stable final products.<sup>24</sup> The trapping of these reactive intermediates in a controlled fashion was the key to harnessing the synthetic power of DDA reactions. Over the past few years, various research groups have demonstrated the synthetic utility of DDA reactions.<sup>26-29</sup> One prominent

example of these achievements is the development of the intramolecular version of eq 6 (**Scheme 2.2.1**), the hexadehydro-Diels–Alder (HDDA) reaction.<sup>30</sup>

Mechanistically, thermal DA reactions are symmetry allowed pericyclic transformations according to Woodward–Hoffmann rules.<sup>31</sup> In most cases, they are concerted processes, although stepwise mechanisms via diradical intermediates operate in some special cases.<sup>24</sup> However, for HDDA reactions, whether the reactions are concerted or stepwise has engendered some controversy recently. Schaefer et al. studied the thermal fragmentation of *ortho*-benzyne (a retro-HDDA reaction), a process that is believed to play an important role in the combustion of aromatic compounds.<sup>32</sup> According to *ab initio* calculations, the concerted mechanism is consistent with experimental observations. However, it was pointed out “there may also be a competitive, nonconcerted route through an open-chain singlet diradical intermediate, a problem that awaits elucidation”.<sup>32</sup> In 2011, Johnson et al. reported (U)CCSD(T)//M05-2X computational results on the concerted and stepwise pathways for all six reactions shown in **Scheme 2.2.1**.<sup>33</sup> It was found that a concerted reaction is favored in every case, but the difference between the barriers of the two mechanisms is only 0.5 kcal/mol for the last reaction (eq 6).<sup>33</sup> Recently, Cramer, Hoye, and Kuwata reported a combined experimental and computational study of intramolecular HDDA reactions.<sup>34</sup> They found that the stepwise transition states are lower in energy than the corresponding concerted ones, and the computed barriers of reaction are in good agreement with experimentally measured kinetics. While the stepwise mechanism is most likely involved in the intramolecular HDDA reactions of substituted reactants, there is competition between concerted and stepwise mechanisms for the parent reaction (eq 6). Johnson et al.

showed that for the series of DA and DDA reactions in **Scheme 2.2.1**, the advantage of the concerted mechanism diminishes as the substrate becomes more unsaturated.<sup>33</sup> Our group has studied computationally the mechanism of bimolecular HDDA reactions involving substituted substrates.<sup>35</sup> We found that the accelerating effect of alkynyl substituents on the reaction rate is due to the decrease in distortion energy required to achieve the stepwise transition states. Very recently, Hoye and co-workers reported another intriguing type of DDA reactions, the pentadehydro-Diels–Alder (PDDA) reaction.<sup>36</sup> The PDDA reactions are also likely involving stepwise mechanisms according to density functional theory (DFT) calculations.<sup>36</sup>

These results prompted us to ask how distortion energies contribute to the increase in concerted barriers for DA and DDA reactions. We have now conducted DFT studies and performed distortion/interaction analyses on the 6 DA and DDA reactions shown in **Scheme 2.2.1**. We also performed direct molecular dynamics (MD) simulations on HDDA reactions, to illuminate how reactants distort into transition state geometries in both concerted and stepwise trajectories.

### 2.2.3 Computational Methods

All density functional theory (DFT) computations were performed using Gaussian09.<sup>37</sup> Geometry optimizations were carried out at the (U)M06-2X/6-311+G(d,p) level of theory.<sup>38</sup> HOMO–LUMO mixing for the initial guess was used for open-shell singlet calculations. Normal vibrational mode analysis at the same level confirmed that optimized structures were minima or transition states (TS). The distortion/interaction analysis is based on “electronic energies ( $E$ )”,

which are the energies of hypothetically rigid molecules. This is used, instead of  $H$  or  $G$ , because the distorted separated fragments are not stationary points and no harmonic frequency analysis can be performed to obtain  $H$  and  $G$ .

(U)M06-2X/6-31G(d) was found to give qualitatively the same conclusions about the relative energetics of the reactions studied. Therefore, molecular dynamics (MD) simulations were performed at the (U)M06-2X/6-31G(d) level of theory. Direct molecular dynamics (MD) simulations were performed for the concerted and stepwise reactions of diyne-yne (**Scheme 2.2.1**, eq 6) in the gas phase. Quasiclassical trajectories (QCTs) were initialized in the region of the potential energy surface near the TS. Normal mode sampling involved adding zero-point energy for each real normal mode in the TS, and performing a Boltzmann sampling of geometries to afford the thermal energy available at 300 K with a random phase. The trajectories were propagated forward and backward, 500 fs in each direction. The classical equations of motion were integrated with a velocity-Verlet algorithm using Singleton's program ProgDyn,<sup>39</sup> with the energies and derivatives computed on the fly by the UM06-2X method using Gaussian 09. The step length for integration was 1 fs.

#### 2.2.4 Results and Discussion

The top row of **Figure 2.2.1** shows the six transition structures TS-1c–6c for the concerted reactions. For the stepwise reactions, the transition structures TS-1s–6s for the formation of diradical intermediates are shown in the bottom row of **Figure 2.2.1**. The enthalpies and free energies of activation for the concerted and stepwise reactions are shown below the

corresponding TS. The concerted mechanisms are energetically favored over the stepwise mechanisms for eqs 1–4. In contrast, TS-5s and TS-6s are lower in energy than TS-5c and TS-6c, respectively. The detailed energetics for all six reactions are summarized in **Tables 2.2.1** and **2.2.2**. These are electronic energies, including no ZPE or thermal corrections, so that the distortion energies can be evaluated. The activation energies and reaction energies agree qualitatively with Johnson's results.<sup>33</sup> For the concerted pathways (**Table 2.2.1**), the barriers of reaction ( $E_{\text{act}}$ ) range from 19.6 to 36.0 kcal/mol for the six reactions. In contrast, for the stepwise pathways (**Table 2.2.2**), transition states TS-1s–6s are very close in energy relative to the corresponding reactants (34.2–35.4 kcal/mol). The first steps are rate-determining except for the reaction between diyne and ene (entry 5), where the second TS (37.8 kcal/mol) is 3.6 kcal/mol higher in energy than the first TS (34.2 kcal/mol). This might be due to the instability of the product of ring closure, the cyclic cumulene ( $E_{\text{rxn}} = -4.4$  kcal/mol, Table 2.2.1, entry 5). In fact, the diradical would prefer to form a cyclobutene (in a [2 + 2] cycloaddition) instead of cyclic cumulene. Comparing the  $E_{\text{act}}$  values in Table 2.2.1 to those of Table 2.2.2 for all six reactions, it is clear that the preference for concerted mechanism diminishes as the reaction goes from DA (eq 1) to HDDA (eq 6). For the HDDA reaction, TS-6s is 0.8 kcal/mol lower in energy than that of TS-6c.

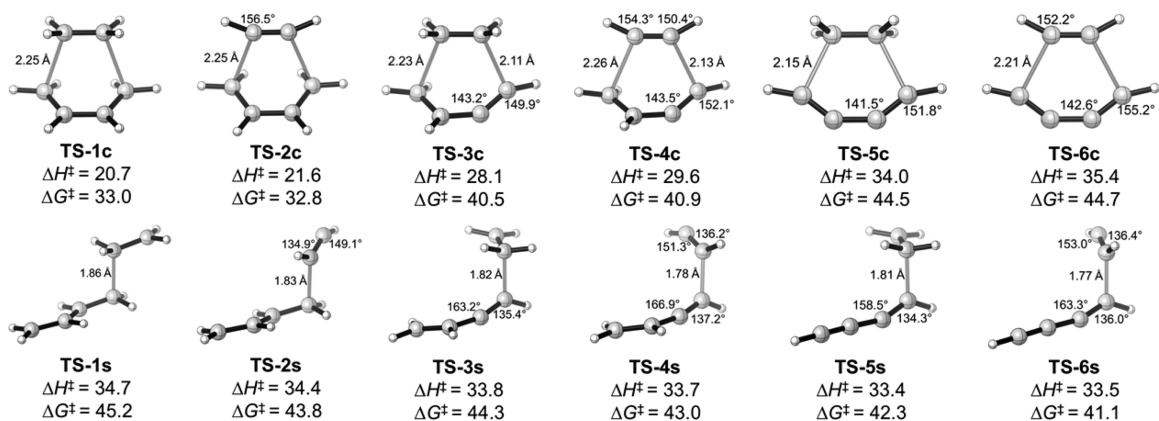


**Figure 2.2.1.** (U)M06-2X/6-311+G(d,p)-optimized transition structures for the concerted and stepwise DA and DDA reactions. Enthalpies and free energies of activation are in kcal/mol.

**Table 2.2.1.** Activation, Distortion, Interaction, and Reaction Energies (in kcal/mol) Calculated with M06-2X/6-311+G(d,p) for Concerted Reactions.

entry	TS	$E_{\text{act}}$	$E_{\text{dist-}4\pi}$	$E_{\text{dist-}2\pi}$	$E_{\text{dist}}$	$E_{\text{int}}$	$E_{\text{rxn}}$
1	TS-1c	19.6	18.8	7.4	26.1	-6.5	-47.6
2	TS-2c	21.2	17.1	10.3	27.4	-6.2	-61.8
3	TS-3c	27.3	24.3	10.6	34.9	-7.6	-18.6
4	TS-4c	29.5	22.2	14.0	36.2	-6.7	-30.0
5	TS-5c	33.9	32.8	11.4	44.3	-10.4	-4.4
6	TS-6c	36.0	29.2	14.0	43.2	-7.2	-57.3

**Table 2.2.2.** Activation, Distortion, and Interaction Energies (in kcal/mol) Calculated with (U)M06-2X/6-311+G(d,p) for Stepwise Reactions<sup>a</sup>

entry	TS	$E_{\text{act}}$	$E_{\text{dist-}4\pi}$	$E_{\text{dist-}2\pi}$	$E_{\text{dist}}$	$E_{\text{int}}$	$E_{\text{(DR)}}$	$E_{\text{(TSs2)}}$
1	TS-1s	35.4	12.6	12.2	24.9	10.5	28.5	32.1
2	TS-2s	35.4	10.9	16.5	27.4	8.0	27.0	29.1
3	TS-3s	34.5	13.5	11.2	24.7	9.8	27.8	32.9
4	TS-4s	35.0	11.9	15.1	27.0	8.0	25.0	28.3
5	TS-5s	34.2	14.8	11.0	25.8	8.4	29.5	37.8
6	TS-6s	35.2	13.0	14.6	27.5	7.7	25.7	30.8

<sup>a</sup>Energies of diradical intermediates (DR) and second transition state (TSs2) are also shown.

Both concerted and stepwise transition states (TS-1c–6c and TS-1s–6s) were analyzed using the distortion/interaction model,<sup>40</sup> also known as the activation strain model.<sup>41</sup> For each reaction, the

transition structure is separated into two fragments (diene/enyne/diyne and ene/yne), followed by single-point energy calculations on each fragment. The difference in energy between the distorted fragments and optimized ground-state geometries is the distortion energy of diene/enyne/diyne ( $E_{\text{dist-}4\pi}$ ) and ene/yne ( $E_{\text{dist-}2\pi}$ ), respectively. The difference between the activation energy ( $E_{\text{act}}$ ) and the total distortion energy ( $E_{\text{dist}} = E_{\text{dist-}4\pi} + E_{\text{dist-}2\pi}$ ) is the interaction energy ( $E_{\text{int}}$ ). The results are also shown in **Tables 2.2.1** and **2.2.2**.

For concerted reactions (**Table 2.2.1**), distortion energies are the main contributors (26–44 kcal/mol) to the activation barriers, while the favorable (negative) interaction energies are relatively small (–6 to –10 kcal/mol). For each reaction, the distortion energy of the  $4\pi$  component ( $E_{\text{dist-}4\pi}$ ) is the main contributor to the total distortion energy, because significant bending distorts the planar or linear molecule into the concerted transition state geometry, where both termini of the diene/enyne/diyne overlap with the termini of the ene/yne. In contrast, for the stepwise reactions (**Table 2.2.2**), the  $E_{\text{dist-}4\pi}$  and  $E_{\text{dist-}2\pi}$  are similar in magnitude and approximately constant at 11–16 kcal/mol each. In the stepwise transition states, the  $4\pi$  components distort much less than in the concerted transition states. Nevertheless, the total distortion energies are still the controlling factors of activation barriers, whereas the unfavorable (positive) interaction energies are relatively small as well (8–10 kcal/mol). We previously demonstrated that alkynyl substituents accelerate the HDDA reaction by ~5 orders of magnitude, mainly by decreasing the distortion energy required to achieve the diradical transition state.<sup>35</sup> In the present study, the distortion energy still predominantly influences the reactivity of unsubstituted DA and DDA reactions. Most notably, the great difference in activation energies



( $E_{\text{act}}$ ) for the six concerted reactions is associated with the dramatic change in distortion energies ( $E_{\text{dist}}$ ). Generally, reaction with a higher  $E_{\text{dist}}$  tends to have a higher  $E_{\text{act}}$ , except for the reaction between diyne and ene (**Table 2.2.1**, entry 5), in which the interaction energy ( $-10.4$  kcal/mol) partially offsets the highest distortion energy (44.3 kcal/mol). This trend is illustrated in **Figure 2.2.2**, which is a plot of  $E_{\text{act}}$  versus  $E_{\text{dist}}$  for the six concerted reactions. One manifestation of this trend is that, for the HDDA reaction, the stepwise mechanism becomes competitive, whereas for DA reactions, the concerted mechanisms are energetically favored. The high barrier of the concerted mechanism for the HDDA reaction is attributed to the high distortion energy required to distort the reactants into transition state geometries.

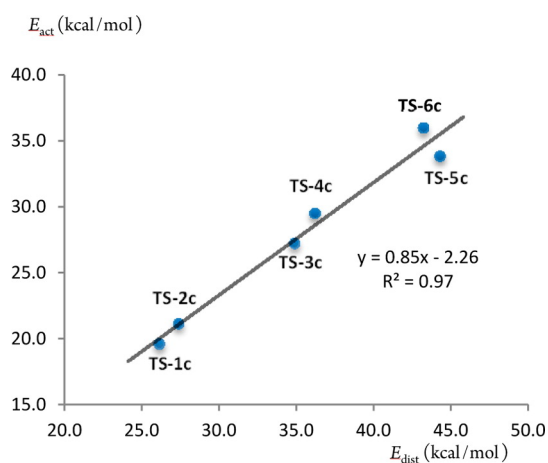


**Figure 2.2.2.** Plot of activation energies versus distortion energies for six concerted reactions. Energies are in kcal/mol.

We performed direct molecular dynamics (MD) simulations for the concerted and stepwise mechanisms of the diyne–yne (HDDA) reaction to study how reactants distort into transition state geometries in a time-resolved fashion. In particular, the vibrations that must be excited for reaction to occur are of special interest. **Figure 2.2.3** shows snapshots of two typical reactive

trajectories in butadiyne–acetylene cycloadditions, a prototype of HDDA reactions. **Figure 2.2.3a, b** are two trajectories, one for a concerted and the other for a stepwise pathway, respectively. The bond angles and time at which each snapshot is taken are shown for eight snapshots of each trajectory. As shown in **Figure 2.2.3a**, a strong bending motion is observed for butadiyne before it reaches the transition state. The bending angle of butadiyne is  $151^\circ$  at  $-250$  fs,  $177^\circ$  at  $-200$  fs,  $154^\circ$  at  $-100$  fs,  $175^\circ$  at  $-50$  fs, and  $143^\circ$  at  $0$  fs. This vibration displays a large bending angle oscillation ( $\sim 25^\circ$  oscillation amplitude). The first C–C bond of benzyne forms at  $30$  fs. We consider bond formation to occur when the first C–C distance reaches  $1.6 \text{ \AA}$ . The time gap between formation of the two bonds is  $3$  fs. This is a highly dynamically concerted trajectory, since we have defined a dynamically concerted trajectory as one with a time gap of  $60$  fs or less.<sup>7</sup>

<sup>42</sup> In comparison, the period of vibration for a fully formed C–C bond is  $30$  fs.<sup>42</sup>

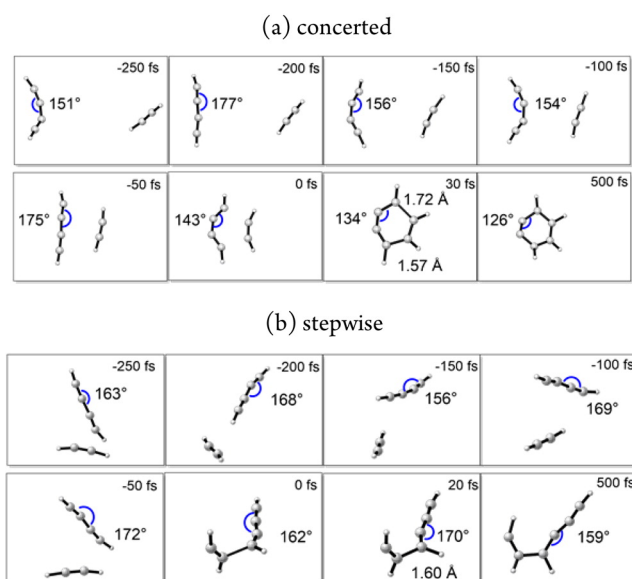


**Figure 2.2.3.** Snapshots for two typical reactive trajectories of butadiyne–acetylene cycloadditions in (a) concerted pathway where butadiyne and acetylene lead to benzyne and in (b) stepwise pathway in which butadiyne and acetylene give a diradical intermediate after one C–C

bond formation. The intermediate does not give the benzyne intermediate within 500 fs. Time 0 fs corresponds to the transition state geometry where trajectories are initiated.

**Figure 2.2.3b** shows a stepwise trajectory. From  $-250$  to  $0$  fs, the bending angle ranges from  $156^\circ$  to  $172^\circ$  ( $\sim 16^\circ$ ). The oscillation pattern of the stepwise trajectory is not as severe as the concerted one. Notably, butadiyne and acetylene mutually rotate as they approach the transition state. The first bond forms at  $20$  fs, which is comparable to the timing of first bond formation in the concerted pathway. The second bond does not form during the full  $500$  fs simulation, indicating the formation of a relatively long-lived diradical intermediate.

Results for 300 butadiyne–acetylene cycloaddition molecular dynamics trajectories are summarized in **Figure 2.2.4**. **Figure 2.2.4a** shows the 150 concerted and 150 stepwise trajectories, plotted with respect to two forming bond lengths, Bond 1 and Bond 2 labeled on the graph. Trajectories are initiated from the transition state (blue dots shown on the graph). The 98% confidence interval of the forming bond lengths in the transition state was defined as the transition zone. The transition zones in the concerted trajectories are  $2.24 \pm 0.29$  Å for both bonds, and those in the stepwise trajectories are  $5.54 \pm 0.32$  Å for Bond 1 and  $1.80 \pm 0.05$  Å for Bond 2. The concerted and stepwise trajectories largely overlap on the upper right corner of the graph, ( $4$ – $6$  Å for both bonds), which is the region of separated reactants. The trajectories on the concerted pathway move diagonally on the two-dimensional PES, because both bond lengths must decrease together to pass the concerted reaction barrier. The stepwise trajectories move vertically, because only Bond 2 forms in crossing the first barrier. Bond 2 is about  $1.5$  Å in the intermediates, while Bond 1 is  $4$ – $6$  Å, indicating the random rotation of the newly formed Bond

2. During the time of passage beyond **TS-6s**, only intermediates are formed, and none of the diradicals traverse the second transition state region marked by a green oval in **Figure 2.2.4a**. The intermediate is 5 kcal/mol below the second TS (**Table 2.2.2**, entry 6), and both rotation about Bond 2 and vibrational excitation is required before the second bond can form. This takes picoseconds, not femtoseconds.

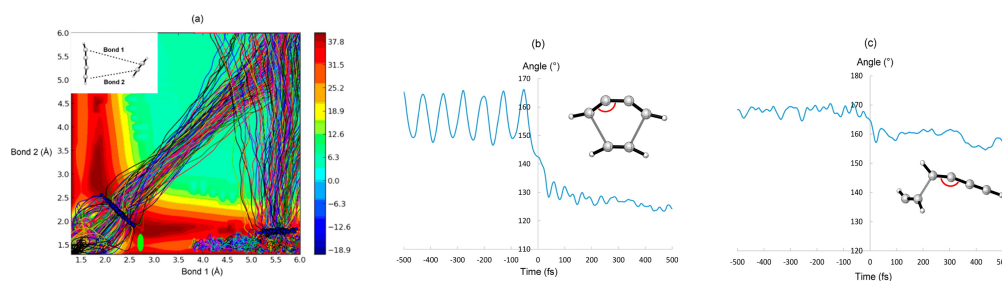


**Figure 2.2.4.** (a) Distribution of 300 reactive trajectories, 150 for the concerted pathway and 150 for the stepwise pathway. Blue dots are starting points from normal mode sampling used to initiate trajectories. Contour plots were calculated with UM06-2X/6-31G(d). Energies are in kcal/mol relative to separated reactants. The energy scale is shown on the right. (b) The averaged trajectory generated from 150 quasiclassical trajectories represented by bending angle versus time in the concerted butadiyne–acetylene reactions. (c) The averaged trajectory generated from 150 quasiclassical trajectories represented by bending angle versus time in the stepwise butadiyne–acetylene reactions. Bending angles are labeled in red on each TS structure.

**Figure 2.2.4b** shows a single trajectory generated from averaging the 150 trajectories initiated from the concerted butadiyne–acetylene cycloaddition TS. The averaged trajectory shows a strong oscillation pattern from  $-500$  to  $-50$  fs. A concerted single trajectory was conducted to investigate how activation energy is partitioned into translational, rotational, and

vibrational motions in reactants.<sup>43, 44</sup> The single trajectory was propagated using UM06-2X/6-31G(d) method with no ZPE or thermal energy and with 0.6 kcal/mol kinetic energy in the direction of the reaction coordinate. The 33.9 kcal/mol barrier plus 0.6 kcal/mol kinetic energy is released in these reactants as 15.9 kcal/mol translational energy, 0 kcal/mol rotational energy, and 18.4 kcal/mol vibrational energy.<sup>45</sup> This result shows the bending excitation in the HDDA reactions as the linear diyne reactants distort to form the TS geometries. The oscillation pattern was previously reported in fluoroethane decomposition to hydrofluoride and ethene,<sup>46</sup> 1,2,6-heptatriene rearrangement to 3-methylenehexa-1,5-diene,<sup>47</sup> and several 1,3-dipolar cycloadditions.<sup>43</sup> In these papers, the oscillation was attributed to a significant bending vibrational excitation that must occur in productive trajectories, and this is the case here, as well. After  $-50$  fs, the bending angle of the averaged trajectory decreases to about  $130^\circ$  to form benzyne product. The oscillation amplitude after forming the product largely decreases.

In contrast, the averaged trajectory for the stepwise reaction displayed in Figure 2.2.4c does not show a significant oscillation pattern from  $-500$  to  $0$  fs. Energy partition of the stepwise single trajectory shows that the 32.4 kcal/mol barrier plus 0.6 kcal/mol kinetic energy is partitioned to 14.4 kcal/mol translational energy, 11.2 kcal/mol rotational energy, and 7.5 kcal/mol vibrational energy in the reactants.<sup>45</sup> The stepwise mechanism involves considerable rotational excitation, and a moderate degree of vibrational excitation during the formation of the first C–C bond. A diradical intermediate is formed after the first bond formation, and the intermediate still survives after 500 fs. The chaotic pattern after  $0$  fs is suggestive of intramolecular vibrational energy relaxation.

### 2.2.5 Conclusion

We report details of the concerted and stepwise mechanisms of six Diels–Alder (DA) and dehydro-Diels–Alder (DDA) reactions. While the stepwise mechanisms have similar barriers for the six prototype reactions studied, the energies of concerted transition states differ significantly in the series. Distortion/interaction analyses reveal that this difference originates from the distortion energy required to achieve the transition states. One manifestation of this distortion-controlled reactivity of DDA reactions is that the stepwise HDDA reaction is competitive with the concerted mechanism.

Direct molecular dynamics (MD) simulations for the concerted and stepwise mechanisms of the HDDA reaction were conducted. From  $-500$  to  $0$  fs, the concerted trajectories display a strong bending angle oscillation ( $\sim 25^\circ$  oscillation amplitude), while the stepwise trajectories show a relatively chaotic pattern, and rotational motion instead. The concerted mechanism of the HDDA reaction involves high bending vibrational excitation, because linear diyne reactants need to be highly bent to form the TS geometries. In contrast, the stepwise mechanism requires less geometrical deformation to enable the first C–C bond formation.

The distortion/interaction analyses, based upon the transition structures computed for each reaction, reflect the observations from MD trajectory simulations. That is, the more highly distorted the transition state, the greater the necessity for excitation of the corresponding vibrational modes in order to achieve productive trajectories.

**2.2.6 Reference**

1. Diels, O.; Alder, K. *Justus Liebigs Annalen der Chemie* **1928**, 460, 98
2. Norton, J. A. *Chem. Rev.* **1942**, 31, 319
3. Martin, J. G.; Hill, R. K. *Chem. Rev.* **1961**, 61, 537
4. Winkler, J. D. *Chem. Rev.* **1996**, 96, 167
5. Nicolaou, K. C.; Snyder, S. A.; Montagnon, T.; Vassilikogiannakis, G. *Angew. Chem., Int. Ed.* **2002**, 41, 1668
6. Goldstein, E.; Beno, B.; Houk, K. N. *J. Am. Chem. Soc.* **1996**, 118, 6036
7. Black, K.; Liu, P.; Xu, L.; Doubleday, C.; Houk, K. N. *Proc. Natl. Acad. Sci. U. S. A.* **2012**, 109, 12860
8. Hoffmann, R.; Woodward, R. B. *J. Am. Chem. Soc.* **1965**, 87, 4388
9. Kagan, H. B.; Riant, O. *Chem. Rev.* **1992**, 92, 1007
10. Funel, J.-A.; Abele, S. *Angew. Chem., Int. Ed.* **2013**, 52, 3822
11. Brieger, G.; Bennett, J. N. *Chem. Rev.* **1980**, 80, 63
12. Juhl, M.; Tanner, D. *Chem. Soc. Rev.* **2009**, 38, 2983
13. Marsault, E.; Toró, A.; Nowak, P.; Deslongchamps, P. *Tetrahedron* **2001**, 57, 4243
14. (a) Yu, P.; Patel, A.; Houk, K. N. *J. Am. Chem. Soc.* **2015**, 137, 13518 (b) He, C. Q.; Chen, T. Q.; Patel, A.; Karabiyikloglu, S.; Merlic, C. A.; Houk, K. N. *J. Org. Chem.* **2015**, 80, 11039
15. Maruoka, K.; Itoh, T.; Shirasaka, T.; Yamamoto, H. *J. Am. Chem. Soc.* **1988**, 110, 310
16. Jørgensen, K. A. *Angew. Chem., Int. Ed.* **2000**, 39, 3558
17. Blackman, M. L.; Royzen, M.; Fox, J. M. *J. Am. Chem. Soc.* **2008**, 130, 13518

18. Devaraj, N. K.; Weissleder, R.; Hilderbrand, S. A. *Bioconjugate Chem.* **2008**, 19, 2297
19. (a) Yang, J.; Šečkutė, J.; Cole, C. M.; Devaraj, N. K. *Angew. Chem., Int. Ed.* **2012**, 51, 7476  
(b) Patterson, D. M.; Nazarova, L. A.; Xie, B.; Kamber, D. N.; Prescher, J. A. *J. Am. Chem. Soc.* **2012**, 134, 18638
20. Jiang, X.; Wang, R. *Chem. Rev.* **2013**, 113, 5515
21. Kim, H. J.; Ruszczycky, M. W.; Choi, S.-H.; Liu, Y.-N.; Liu, H.-W. *Nature* **2011**, 473, 109
22. Tian, Z.; Sun, P.; Yan, Y.; Wu, Z.; Zheng, Q.; Zhou, S.; Zhang, H.; Yu, F.; Jia, X.; Chen, D.; Mandi, A.; Kurtan, T.; Liu, W. *Nat. Chem. Biol.* **2015**, 11, 259
23. Klas, K.; Tsukamoto, S.; Sherman, D. H.; Williams, R. M. *J. Org. Chem.* **2015**, 80, 11672
24. Wessig, P.; Müller, G. *Chem. Rev.* **2008**, 108, 2051
25. A term “dehydropericyclic” has been used to describe the analogous variants of the more general pericyclic reactions. (a) Johnson, R. P. *J. Phys. Org. Chem.* **2010**, 23, 283 (b) Skraba-Joiner, S.; Johnson, R. P.; Agarwal, J. *J. Org. Chem.* **2015**, 80, 11779
26. Wessig, P.; Müller, G.; Herre, R.; Kühn, A. *Helv. Chim. Acta* **2006**, 89, 2694
27. Kocsis, L. S.; Kagalwala, H. N.; Mutto, S.; Godugu, B.; Bernhard, S.; Tantillo, D. J.; Brummond, K. M. *J. Org. Chem.* **2015**, 80, 11686
28. Brummond, K. M.; Kocsis, L. S. *Acc. Chem. Res.* **2015**, 48, 2320
29. Li, W.; Zhou, L.; Zhang, J. *Chem. - Eur. J.* **2016**, 22, 1558
30. (a) Hoye, T. R.; Baire, B.; Niu, D.; Willoughby, P. H.; Woods, B. P. *Nature* **2012**, 490, 208  
(b) Yun, S. Y.; Wang, K.-P.; Lee, N.-K.; Mamidipalli, P.; Lee, D. *J. Am. Chem. Soc.* **2013**, 135, 4668  
For earlier reports of this reaction, see: (c) Bradley, A. Z.; Johnson, R. P. *J. Am. Chem. Soc.*



- 1997, 119, 9917 (d) Miyawaki, K.; Suzuki, R.; Kawano, T.; Ueda, I. *Tetrahedron Lett.* **1997**, 38, 3943 For a review, see:(e) Holden née Hall, C.; Greaney, M. F. *Angew. Chem., Int. Ed.* **2014**, 53, 5746
31. Hoffmann, R.; Woodward, R. B. *J. Am. Chem. Soc.* **1965**, 87, 2046
32. Zhang, X.; Maccarone, A. T.; Nimlos, M. R.; Kato, S.; Bierbaum, V. M.; Ellison, G. B.; Ruscic, B.; Simmonett, A. C.; Allen, W. D.; Schaefer, H. F. *J. Chem. Phys.* **2007**, 126, 044312
33. Ajaz, A.; Bradley, A. Z.; Burrell, R. C.; Li, W. H. H.; Daoust, K. J.; Bovee, L. B.; DiRico, K. J.; Johnson, R. P. *J. Org. Chem.* **2011**, 76, 9320
34. Marell, D. J.; Furan, L. R.; Woods, B. P.; Lei, X.; Bendelsmith, A. J.; Cramer, C. J.; Hoye, T. R.; Kuwata, K. T. *J. Org. Chem.* **2015**, 80, 11744
35. Liang, Y.; Hong, X.; Yu, P.; Houk, K. N. *Org. Lett.* **2014**, 16, 5702
36. Wang, T.; Naredla, R. R.; Thompson, S. K.; Hoye, T. R. *Nature* **2016**, 532, 484
37. Frisch, M. J.; Trucks, G. W.; Schlegel, H. B.; Scuseria, G. E.; Robb, M. A.; Cheeseman, J. R.; Scalmani, G.; Barone, V.; Mennucci, B.; Petersson, G. A.; Nakatsuji, H.; Caricato, M.; Li, X.; Hratchian, H. P.; Izmaylov, A. F.; Bloino, J.; Zheng, G.; Sonnenberg, J. L.; Hada, M.; Ehara, M.; Toyota, K.; Fukuda, R.; Hasegawa, J.; Ishida, M.; Nakajima, T.; Honda, Y.; Kitao, O.; Nakai, H.; Vreven, T.; Montgomery, J. A., Jr.; Peralta, J. E.; Ogliaro, F.; Bearpark, M.; Heyd, J. J.; Brothers, E.; Kudin, K. N.; Staroverov, V. N.; Kobayashi, R.; Normand, J.; Raghavachari, K.; Rendell, A.; Burant, J. C.; Iyengar, S. S.; Tomasi, J.; Cossi, M.; Rega, N.; Millam, J. M.; Klene, M.; Knox, J. E.; Cross, J. B.; Bakken, V.; Adamo, C.; Jaramillo, J.; Gomperts, R.; Stratmann, R. E.; Yazyev, O.; Austin, A. J.; Cammi, R.; Pomelli, C.; Ochterski, J. W.; Martin, R. L.; Morokuma, K.;

- Zakrzewski, V. G.; Voth, G. A.; Salvador, P.; Dannenberg, J. J.; Dapprich, S.; Daniels, A. D.; Farkas, O.; Foresman, J. B.; Ortiz, J. V.; Cioslowski, J.; Fox, D. J. Gaussian 09, revision D.01; Gaussian, Inc.: Wallingford, CT, **2013**.
38. (a) Zhao, Y.; Truhlar, D. G. *Theor. Chem. Acc.* **2008**, 120, 215 (b) Zhao, Y.; Truhlar, D. G. *Acc. Chem. Res.* **2008**, 41, 157
39. Singleton, D. A.; Wang, Z. H. *J. Am. Chem. Soc.* **2005**, 127, 6679
40. (a) Ess, D. H.; Houk, K. N. *J. Am. Chem. Soc.* **2007**, 129, 10646 (b) Ess, D. H.; Houk, K. N. *J. Am. Chem. Soc.* **2008**, 130, 10187 The distortion/interaction model has been used to study the mechanism and reactivity of a variety of cycloaddition reactions. For relevant studies, see: (c) Liu, S.; Lei, Y.; Qi, X.; Lan, Y. *J. Phys. Chem. A* **2014**, 118, 2638 (d) Qi, X.; Li, Y.; Zhang, G.; Li, Y.; Lei, A.; Liu, C.; Lan, Y. *Dalton Trans.* **2015**, 44, 11165 (e) Li, Y.; Qi, X.; Lei, Y.; Lan, Y. *RSC Adv.* **2015**, 5, 49802
41. (a) van Zeist, W.-J.; Bickelhaupt, F. M. *Org. Biomol. Chem.* **2010**, 8, 3118 (b) Fernández, I.; Bickelhaupt, F. M. *Chem. Soc. Rev.* **2014**, 43, 4953
42. (a) Xu, L.; Doubleday, C. E.; Houk, K. N. *J. Am. Chem. Soc.* **2011**, 133, 17848 (b) Yang, Z.; Yu, P.; Houk, K. N. *J. Am. Chem. Soc.* **2016**, 138, 4237 (c) Patel, A.; Chen, Z.; Yang, Z.; Gutiérrez, O.; Liu, H.-w.; Houk, K. N.; Singleton, D. A. *J. Am. Chem. Soc.* **2016**, 138, 3631 (d) Yang, Z.; Doubleday, C.; Houk, K. N. *J. Chem. Theory Comput.* **2015**, 11, 5606 (e) Hong, X.; Bercovici, D. A.; Yang, Z.; Al-Bataineh, N.; Srinivasan, R.; Dhakal, R. C.; Houk, K. N.; Brewer, M. *J. Am. Chem. Soc.* **2015**, 137, 9100 (f) Liu, F.; Yang, Z.; Mei, Y.; Houk, K. N. *J. Phys. Chem. B* **2016**, DOI: 10.1021/acs.jpcc.6b02336

## CHAPTER 2.2

43. Xu, L.; Doubleday, C. E.; Houk, K. N. *J. Am. Chem. Soc.* **2010**, 132, 3029
44. Raff, L. M. *J. Chem. Phys.* **1988**, 89, 5680
45. The energy partition of single trajectory is detailed in the Supporting Information. The partition energies in reactants are averaged over 1000 fs in single trajectory after the reactants are separated by 5 Å. The error in average partition energy is about 0.2 kcal/mol, which causes the slight difference between the energy barrier and the sum of partition energies in the reactants.
46. Sun, L.; Park, K.; Song, K.; Setser, D. W.; Hase, W. L. *J. Chem. Phys.* **2006**, 124, 064313
47. Debbert, S. L.; Carpenter, B. K.; Hrovat, D. A.; Borden, W. T. *J. Am. Chem. Soc.* **2002**, 124, 7896

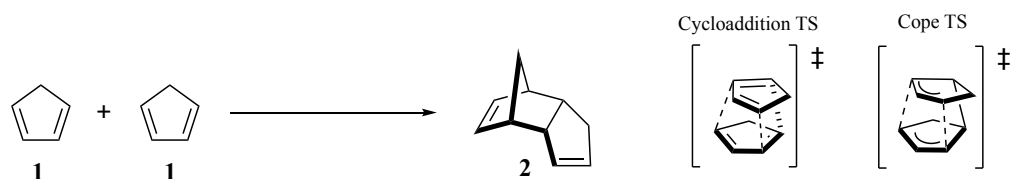
## **2.3 Molecular Dynamics of the Two-Stage Mechanism of Cyclopentadiene Dimerization: Concerted or Stepwise?**

### **2.3.1 Abstract**

In 1959, Woodward and Katz proposed a “two-stage” mechanism for the dimerization of cyclopentadiene, with a highly asynchronous transition state leading to the formation of a Cope rearrangement transition state and then to the dimeric product. This leaves an intriguing open question regarding the dynamical nature of the process. We report here the molecular dynamics studies of cyclopentadiene dimerization, following Singleton’s investigation of kinetic isotope effects in this reaction. Transition structures were re-optimized with different density functionals, which all give the ambimodal transition state (previously defined by Caramella as the bispericyclic transition state) for the reaction. Dynamics results show that 70% of the trajectories are dynamically-concerted, possessing a time gap between formation of two bonds smaller than 60 fs, which is the lifetime of transition state at room temperature from Eyring’s transition state theory equation. In these trajectories, the Cope TS is not sampled. A “Two-stage” mechanism was found in 13% of the trajectories, which follow the pathway through the Cope transition state hypothesized by Woodward and Katz in 1959. These are all categorized as dynamically-stepwise trajectories since there are multiple vibrations before the second bond formation is completed. These are 30% of the total trajectories. Dynamically-stepwise trajectories increase to 72% when the temperature of the simulation is set to 1000K. More deep-recrossing trajectories are also detected with an elevated temperature.

### 2.3.2 Introduction

In 1959, Woodward and Katz published a seminal paper, “*The Mechanism of Diels-Alder Reaction*”, describing the dimerization of cyclopentadiene as shown in **Scheme 2.3.1**.<sup>1</sup> The reaction gives only the *endo*-adduct **2** under mild conditions, leading to a suggestion of the “secondary attractive force” that determines the stereochemical specificity; this later became widely known as “secondary orbital interactions”.<sup>2</sup> Woodward and Katz<sup>1</sup> envisioned the resemblance between the transition state (TS) of cycloaddition and that of the Cope rearrangement, and proposed a two-stage mechanism for the reaction as an alternative to the usual description of concerted and stepwise mechanisms. The two-stage mechanism involves first the primary formation of the C-C bond through a highly asynchronous concerted transition state, leading to the Cope TS, and then second stage, the facile formation of the second bond to give the product. No intermediate was proposed.



**Scheme 2.3.1.** Dimerization of cyclopentadiene.

Considerable evidence was discovered later (primarily stereochemical) that supports the concertedness in most pericyclic reactions.<sup>3</sup> The Woodward-Hoffman rationalization through orbital symmetry of why both bonds could form at the same time in the Diels-Alder reactions, and their emphasis on the cyclic transition state caused the WK two-stage picture to be overlooked for decades, and most discussion was about concerted vs stepwise.<sup>3</sup>

In 2002, Caramella and co-workers studied computationally the dimerization of cyclopentadiene with DFT, and showed that the transition structure had C<sub>2</sub> symmetry (**Figure 2.3.1a**) that bifurcates to two indetical products on the potential energy surface (PES).<sup>4</sup> The intrinsic reaction coordinate (IRC) analysis shows that the cycloaddition TS leads to the Cope TS (**Figure 2.3.1b**) and then to product **2**, providing validation of the WK two-stage mechanism. The TS was called “bispericyclic”, referring to a merge of [4+2] and [2+4] pathways. The work of Caramella et al. initiated a fantastic adventure into the discovery of bifurcating reactions in the pericyclic reaction realm, and many more reactions with post-transition state bifurcations have been reported since that time.<sup>5,6</sup>

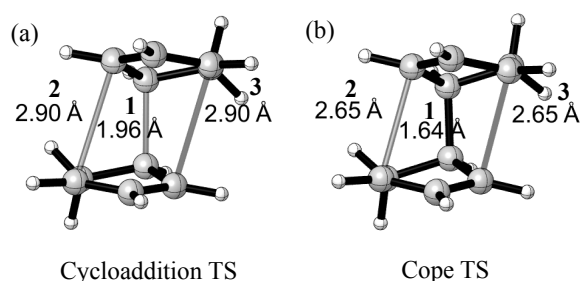


**Figure 2.3.1.** (a) Cycloaddition transition structure, and (b) Cope rearrangement transition structure involved in the dimerization of cyclopentadiene, reported by Caramella et al. using B3LYP/6-31G(d) method. Bond 1, 2 and 3 are labeled on the graph.

The dimerization of cyclopentadiene, and other bifurcating reactions in general, are highly asynchronous with the first forming bond around 2 Å, and the second bond around 3 Å. A fundamental question still exists, however, regarding the dynamic nature of the two-stage process. Woodward and Katz stated that “*the formation of the second bond could be opposed by a further relatively low barrier, since the change involves substantial geometrical*

*displacements*”,<sup>1</sup> indicating a potential dynamically-stepwise character of the two-stage process. On the other hand, the reduction in conformation space accompanying formation of the second bond might create a relatively long-lived “entropic intermediate”, which was first suggested conceptually by Zwanzig,<sup>7</sup> and were more thoroughly investigated by Singleton<sup>8</sup> and by our group.<sup>9</sup> A similar idea also emerge in Joel Bowman’s “roaming” mechanism,<sup>10</sup> or Cremer and Kraka’s hidden intermediate.<sup>11</sup> In addition, the dynamical complexity was also investigated by Levine in the [2+2] cycloaddition from nonbornadiene to quadricyclane.<sup>12</sup> These all leave the question open on whether the dimerization of cyclopentadiene is dynamically concerted or stepwise. As insightfully pointed out by Berson in 1961, “*the transition state structure and, in particular, the timing of the “changes of covalency” that result in formation of the two diene-dienophile bonds remain to be sharply defined*”.<sup>13</sup>

We have investigated the molecular dynamics of dimerization of cyclopentadiene, to unravel the time-resolved mechanism of the reaction. Singleton previously conducted dynamics on the reaction and proposed Newtonian kinetics isotope effects,<sup>14</sup> which is different from the scope of our paper. Specifically, we are interested in (1) the dynamically concerted versus stepwise pathways of the reaction, (2) the percentage of reactive trajectories that go through the Cope transition state, as proposed in the WK two-stage mechanism, (3) the distribution of time gaps between formation of two bonds, and (4) the influence of temperature on dynamics behavior. We have previously conducted molecular dynamics simulations on Diels-Alder reactions,<sup>15,16,17</sup> 1,3-dipolar cycloadditions,<sup>18</sup> and Cope rearrangements,<sup>19</sup> and utilized the time gap between formation of two bonds or time in the transition zone for the Cope rearrangement to

differentiate dynamically concerted from dynamically stepwise mechanisms of pericyclic reactions. Specifically, we invoked the lifetime of transition state from Eyring equation (60 fs at room temperature) as a cutoff, which was also applied by Zewail in the femtosecond experiments of the photochemical retro-Diels-Alder reaction.<sup>20</sup>

### 2.3.3 Computational Methods

Density functional theory (DFT) computations were performed using Gaussian09.<sup>21</sup> Geometry optimizations were mainly carried out at the B3LYP/6-31G(d) level of theory. Normal vibrational mode analysis at the same level confirmed that optimized structures were minima or transition states (TS). Benchmarks were performed with the other density functional methods, including  $\omega$ B97X-D and M06-2X, with 6-31G(d) basis set and 6-311+G(d, p) basis set. The Grimme D3 dispersion correction was tested. (shown in **Figure 2.3.1**) Direct molecular dynamics (MD) simulations were performed for the cyclopentadiene dimerization in the gas phase at 298.15 K and at 1000 K. Because of the thousands of quantum calculations required in the dynamics simulations, these were performed at the (U)B3LYP/6-31G(d) level of theory with guess=mix to capture the radical character of dynamical species. Quasiclassical trajectories (QCTs)<sup>22</sup> were initialized in the region of the potential energy surface near the TS with normal mode sampling method, which involves adding zero-point energy and thermal energy for each real normal mode in the TS, and then obtaining a Boltzmann distribution of energies by randomly sampling a set of geometries and velocities. No additional velocities were added other than vibrations along modes perpendicular to the reaction coordinate. The trajectories were propagated forward and backward



for 300fs in each direction. The classical equations of motion were integrated with a velocity-Verlet algorithm using Singleton's program Progdyn,<sup>23</sup> with the energies and derivatives computed on the fly by the UB3LYP method using Gaussian09. The step length for integration was 1 fs. We also conducted trajectory simulations at the M06-2X/6-31G(d) level at 298.15 K for comparison.

## 2.3.4 Results and Discussion

### 2.3.4.1 Transition state structure of cyclopentadiene dimerization

The transition state of cyclopentadiene dimerization was optimized with the B3LYP/6-31G(d) method. It is shown in **Figure 2.3.2a**. This geometry has C2 symmetry, involving three forming bonds labeled as **1**, **2**, and **3** with lengths of 1.96 Å, 2.90 Å, and 2.90 Å respectively. Our result reproduces the structure originally reported by Caramella et al. They called the TS "bispericyclic transition state" to indicate that the cycloadduct forms by completion of bond 1 and formation of either bond 2 or 3. We have proposed the more general term, "ambimodal transition state", to specify a saddle point leading to two or more multiple products, pericyclic or otherwise. The ambimodal transition state was also computed with other methods including B3LYP with Grimme's D3 correction (**Figure 2.3.2b**), Head-Gordon's  $\omega$ B97X-D (**Figure 2.3.2c**), and Truhlar's M06-2X method (**Figure 2.3.2d-e**). The transition state geometries are shown in **Figure 2.3.2a-c**. All have C2 symmetry with slight variations on the geometry. The TS optimized by M06-2X method, however, breaks the C2 symmetry with 2.55 Å for bond 2, and 3.02 Å for bond 3, similar to a normal Diels-Alder TS. Interestingly, the C2

symmetry structure is found to be a second-order saddle point as shown in **Figure 2.3.2e**. The second-order saddle is 0.2 kcal/mol higher in electronic energy than the TS, but is 0.2 kcal/mol lower in electronic energy plus zero-point energy. This indicates that M06-2X method gives a flat double-well potential energy surface near the saddle point region. It represents a “quasi-ambimodal TS”, because in the quasi-linear or quasi-planar molecules, the ZPE for the less symmetrized structure is greater than that for the symmetrized TS.<sup>24</sup> The geometries in **Figure 2.3.2d** and **2.3.2e** are interchangeable with thermal motion. Reaction dynamics trajectories were propagated from **2d** using M06-2X method, which bifurcates to the formation of bond **2** and **3** with a ratio of 7 to 1. From the mirror image TS, a 1:7 ratio would be obtained. Therefore, all the methods that we have tested support the existence of ambimodal (or quasi-ambimodal) transition state for the dimerization of cyclopentadiene. The optimization was also performed with the more complete basis set 6-311+G(d,p), which gives consistent results.

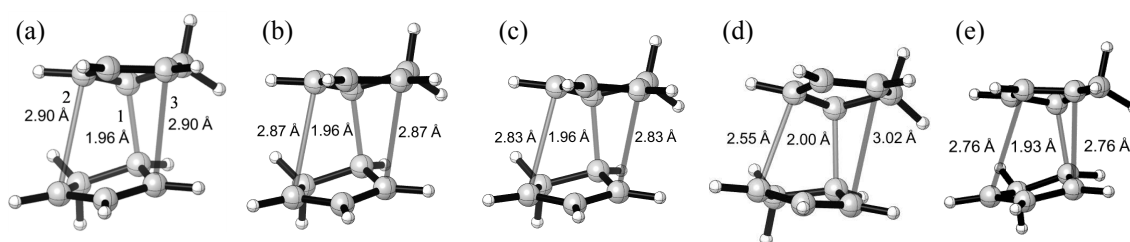


**Figure 2.3.2.** Transition structures of cyclopentadiene dimerization, optimized under (a) B3LYP/6-31G(d), (b) B3LYP-D3/6-31G, (c)  $\omega$ B97X-D/6-31G(d), (d) M06-2X/6-31G(d) methods. (e) Second-order saddle point located by M06-2X/6-31G(d). **Bond 1, 2** and **3** are labeled in (a).

### 2.3.4.2 Distribution of trajectories in the cyclopentadiene dimerization

Reaction trajectories were propagated using the (U)B3LYP/6-31G(d) method, and trajectories were initiated in the vicinity of the TS shown in **Figure 2.3.2a**. The distribution of 30 representative trajectories is shown in **Figure 2.3.3a**, along with the red dots that show transition state geometries for cycloaddition TS and Cope TS. The overlay of these geometries are shown in **Figure 2.3.3b** and **3c**, respectively. These TS geometries form a “transition zone” as labeled in the black ellipse. The trajectories bifurcate after passing the cycloaddition transition zone and give the same product via the formation of either bond **2** or **3** with equal probability. Dynamically, thirteen percent of the trajectories go through the Cope transition zone before forming the final product. These are truly consistent with what Woodward and Katz entitled a two-stage mechanism. The local PES from cycloaddition TS to Cope TS involves a valley-ridge inflection,<sup>25</sup> and most trajectories slide downhill after passing the TS before reaching the Cope TS region.

We identified the transition state geometries of trajectories that specifically lead to the formation of **bonds 2** or **3**. These are shown in **Figure 2.3.3e** and **3f**. The symmetry is broken in these two averaged structures, and the forming bond is slightly more favorable than the other. This suggests that an ambimodal transition state can be viewed as the merge of two hypothetical transition states that are identical energetically. When all the transition geometries are averaged, the TS shows a C<sub>2</sub> symmetry.

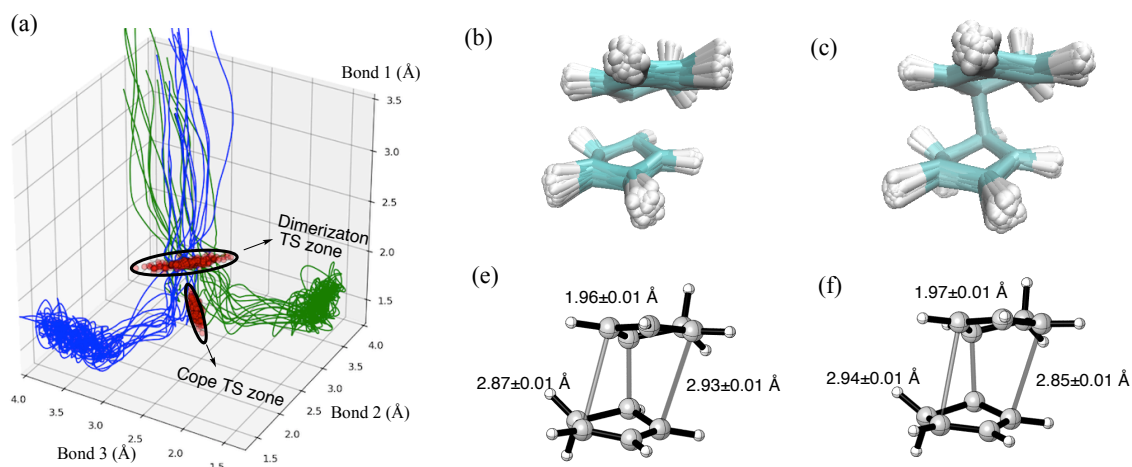


**Figure 2.3.3.** (a) Trajectories that lead to **bonds 2** or **3** formation. (See **Fig. 1** for definition) The red dots that are circled in black are transition zones for cycloaddition TS and Cope TS. (b) and (c) are the overlays of transition state geometries for the cycloaddition TS and Cope TS, while (e) and (f) are averages of transition state geometries for trajectories that lead exclusively to the formation of **bonds 2** and **3**, respectively.

### 2.3.4.3 Bond formation via dynamically concerted and dynamically stepwise fashion

We also monitored the timing of bond formation in the trajectories. Two typical trajectories are exemplified in **Figure 2.3.4a**. The dash-line trajectory directly gives the final product after passing the transition state, without exploring the Cope TS zone. The solid-line trajectory undergoes several vibrations before forming the final product, and it explores the Cope TS region during these vibrations. Typical snapshots are taken from the two trajectories. **Figure 2.3.4b** shows that two cyclopentadiene molecules approach mutually from -70 fs to 0 fs, and reach 2.01 Å for **bond 1** and 2.68 Å for **bond 3**. Here we define a distance for C-C bond formation of 1.6 Å. Both bonds are forming after 0 fs until **Bond 1** forms at 20 fs and **bond 3** at

31 fs, leading to a 11 fs time gap between formation of the two bonds. (Both are  $<1.6 \text{ \AA}$  because our time is 1 fs.) This is much shorter than the lifetime of a transition state calculated from Eyring equation (60 fs at room temperature), and presents typical dynamically-concerted character, as we discussed previously for Diels-Alder reactions<sup>14</sup> and the Cope rearrangement.<sup>18</sup> In contrast, **Figure 2.3.4c** shows that a dynamically stepwise trajectory (solid line) At -70 fs, the two reactants are separated (not shown), and at 0 fs, the trajectory gives 1.99  $\text{\AA}$  for **bond 1** and 3.07  $\text{\AA}$  for **bond 3**, a  $\sim 0.4 \text{ \AA}$  larger asynchronicity than the dashed one. After 20 fs, the first bond forms. **Bond 2** and **3** oscillate between 2.50  $\text{\AA}$  and 3.00  $\text{\AA}$  for about 90 fs (about three C-C vibrational periods). A typical snapshot at 100 fs shows a structure with 1.64  $\text{\AA}$  for **bond 1**, 2.62  $\text{\AA}$  for **bond 2**, and 2.68  $\text{\AA}$  for **bond 3**, which resembles the Cope TS shown in **Figure 2.3.1b**. We have taken some typical geometries from the trajectory in the vicinity of the Cope TS and calculated the stable wavefunction with guess=mix under the unrestricted method. It turns out that the  $\langle S^2 \rangle$  values are all zero, indicating no diradical character observed from the selected snapshot. The second bond finally forms at 150 fs, resulting in a time gap of 130 fs. This trajectory is what we call dynamically stepwise and what Woodward and Katz would call two-stage. The time gap is about twice as long as the lifetime of transition state ( $\sim 60$  fs), and is about four vibrational periods of C-C single bond stretching. This is a typical character of the dynamically-stepwise process. Such long-lived dynamical species have also been defined as “an entropic intermediate”.<sup>8,9</sup> We invoke the concept of “entropic intermediate” here because the formation of the second bond naturally results in a further decrease of conformational space, a process of decreasing entropy. It does not necessarily correspond to an actual entropic barrier

that can be computed from reaction path variational transition state theory (RP-VTST),<sup>26</sup> and Singleton reported that no entropic barrier is found for this reaction.<sup>13</sup>

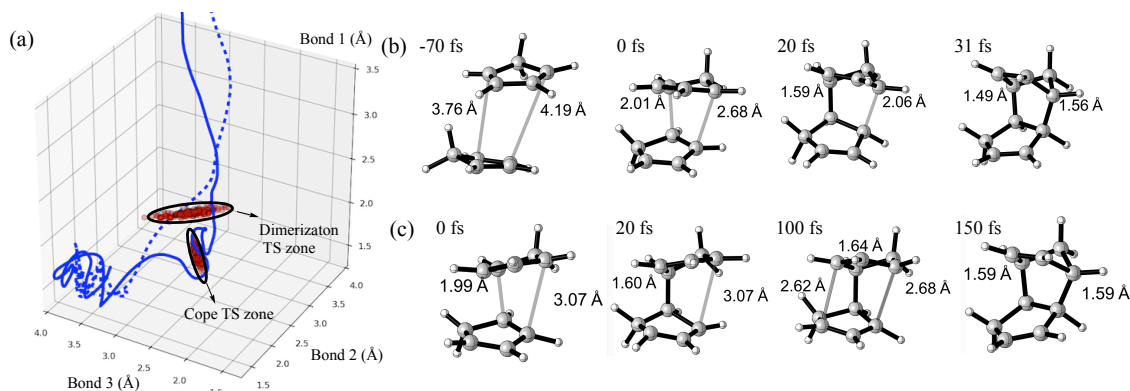


**Figure 2.3.4.** (a) Two typical trajectories from dynamics simulation with different time gap between formation of two bonds. The trajectory representing the dashed line has a time gap of 11 fs, and that with a solid line is 130 fs. (b) and (c) show representative snapshots involved in the dashed, and the solid trajectories respectively. The time zero corresponds to the transition state geometries that initiate the trajectories in both directions.

**Figure 2.3.5a** shows a statistical distribution of time gaps for 300 reactive trajectories at 298 K, ranging from 20 fs to 240 fs. We previously defined the border line between dynamically-concerted and -stepwise trajectories as 60 fs, the lifetime of transition state at 298 K, derived from Eyring's equation by using  $h/k_B T$ , where  $h$  is Planck constant,  $k_B$  is Boltzmann constant, and  $T$  is temperature. This enables a categorization of 30% dynamically-stepwise trajectories that involve entropic intermediates. When the temperature increases to 1000 K, the lifetime of TS decreases to 18 fs, and the percentage of dynamically-stepwise trajectories elevates to 70%. This is consistent with the idea that higher temperature results in more populations on higher vibrational energy levels and lead to more favorable entropies.

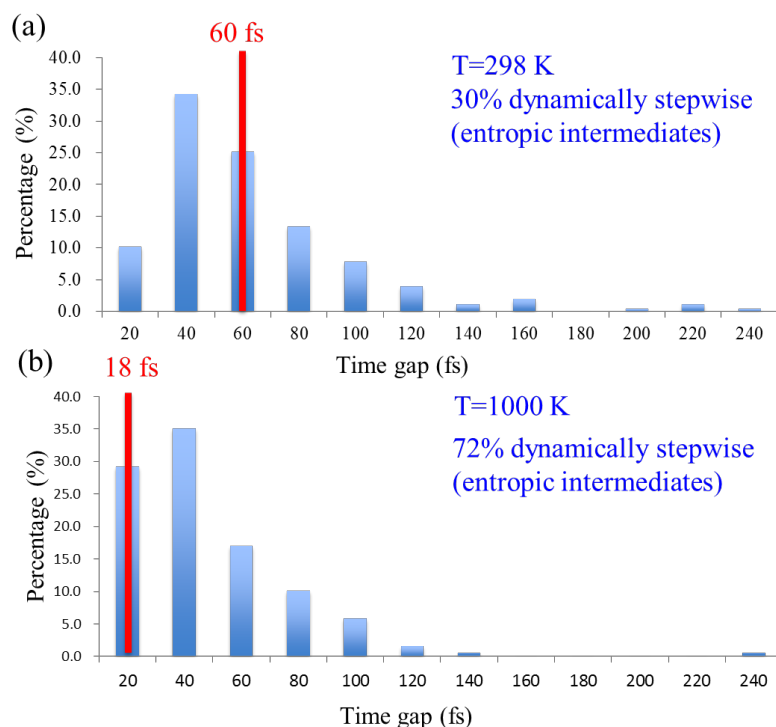


**Figure 2.3.5.** Time gap distributions for trajectories propagated at (a) 298 K, and (b) 1000 K. The cutoff time gap ( $t_{\text{cut}}$ ) for dynamically concerted versus stepwise trajectories is defined based on the pre-exponential factor in Eyring’s equation ( $h/k_{\text{B}}T$ ), which is 60 fs at 298 K, and 18 fs at 1000 K.

In addition, we observed “deep-recrossing” trajectories from our simulations, in which two molecules approach to form **bond 1**, but then bounce back to the reactants. As exemplified in **Figure 2.3.6**, the two cyclopentadiene molecules collide and form the first bond at about 20 fs, but the bond vibrates about 1.6 Å for around 60 fs, and then elongate to 2.0 Å. The molecules then move further apart back to the reactants. The percentage of recrossing trajectories increase from only 2% at 298 K, to about 20% at 1000 K. This indicates a shift of the dynamical bottleneck to a later bond formation stage, a way to compensate entropic penalty with higher temperature.

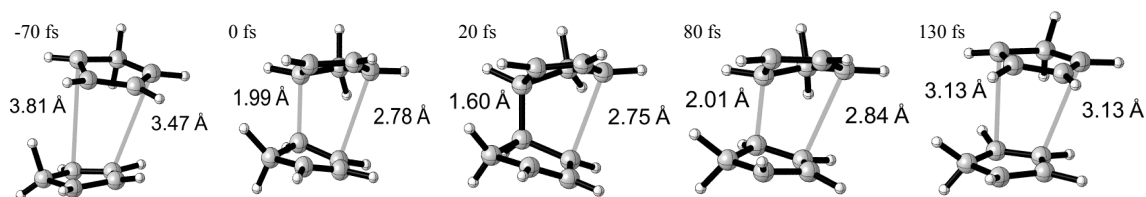


**Figure 2.3.6.** Snapshots for a typical deep-recrossing trajectory.

### 2.3.5 Conclusion

We report here the quasi-classical molecular dynamics simulations of cyclopentadiene dimerization. We showed that the ambimodality of the reaction is independent of the density functional used for the study. Both dynamically-concerted and -stepwise trajectories were observed from the simulation. The Woodward-Katz “two-stage” mechanism was found in 13% of the reactive trajectories, although the general features they envisioned are present in all trajectories. Increasing temperature favors the production of dynamically-stepwise trajectories.

### 2.3.6 Reference

1. Woodward, R. B. and Katz, T. J. *Tetrahedron*, **1959**, 5, 70-89.
2. Woodward, R. B. and Hoffmann, R. *Angew. Chem. Int. Ed.*, **1969**, 8, 781-853.
3. Houk, K. N., Gonzalez, J. and Li, Y. *Acc. Chem. Res.*, **1995**, 28, 81-90.
4. Caramella, P., Quadrelli, P. and Toma, L. *J. Am. Chem. Soc.*, **2002**, 124, 1130-1131.
5. Ess, D. H., Wheeler, S. E., Iafe, R. G., Xu, L., Çelebi-Ölçüm, N. and Houk, K. N. *Angew. Chem. Int. Ed.*, **2008**, 47, 7592-7601.
6. Hare, S. R. and Tantillo, D. J. *Pure Appl. Chem.*, **2017**, 89, 679-698.
7. Zwanzig, R., Diffusion past an entropy barrier. *J. Phys. Chem.*, **1992**, 96, 3926-3930.
8. Gonzalez-James, O. M., Kwan, E. E. and Singleton, D. A. *J. Am. Chem. Soc.*, **2012**, 134, 1914.



## CHAPTER 2.3

9. Patel, A., Chen, Z., Yang, Z., Gutiérrez, O., Liu, H.-w., Houk, K. N. and Singleton, D. A. *J. Am. Chem. Soc.*, **2016**, 138, 3631-3634.
10. Czakó, G. and Bowman, J. M. *Science*, **2011**, 334, 343-346.
11. Kraka, E. and Cremer, D. *Acc. Chem. Res.*, **2010**, 43, 591-601.
12. Raz, T. and Levine, R. D. *J. Phys. Chem.*, **1995**, 99, 13713-13715.
13. Berson, J. A. and Remanick, A. *J. Am. Chem. Soc.*, 1961, 83, 4947-4956.
14. Kelly, K. K., Hirschi, J. S. and Singleton, D. A. *J. Am. Chem. Soc.*, **2009**, 131, 8382.
15. Black, K., Liu, P., Xu, L., Doubleday, C. and Houk, K.N. *Proc. Natl. Acad. Sci.*, **2012**, 109, 12860-12865.
16. Yang, Z., Doubleday, C. and Houk, K. N. *J. Chem. Theory Comput.*, **2015**, 11, 5606-5612.
17. Yu, P., Yang, Z., Liang, Y., Hong, X., Li, Y. and Houk, K. N. *J. Am. Chem. Soc.*, **2016**, 138, 8247-8252.
18. Xu, L., Doubleday, C. E. and Houk, K. N. *J. Am. Chem. Soc.*, **2010**, 132, 3029-3037.
19. Mackey, J. L., Yang, Z. and Houk, K. N. *Chem. Phys. Lett.*, **2017**, 683, 253-257.
20. Horn, B. A., Herek, J. L. and Zewail, A. H. **1996**, 118, 8755-8756.
21. Gaussian 09, Revision A.02, M. J. Frisch, G. W. Trucks, H. B. Schlegel, G. E. Scuseria, M. A. Robb, J. R. Cheeseman, G. Scalmani, V. Barone, G. A. Petersson, H. Nakatsuji, X. Li, M. Caricato, A. Marenich, J. Bloino, B. G. Janesko, R. Gomperts, B. Mennucci, H. P. Hratchian, J. V. Ortiz, A. F. Izmaylov, J. L. Sonnenberg, D. Williams-Young, F. Ding, F. Lipparini, F. Egidi, J. Goings, B. Peng, A. Petrone, T. Henderson, D. Ranasinghe, V. G. Zakrzewski, J. Gao, N. Rega, G. Zheng, W. Liang, M. Hada, M. Ehara, K. Toyota, R. Fukuda, J. Hasegawa, M. Ishida, T.

## CHAPTER 2.3

- Nakajima, Y. Honda, O. Kitao, H. Nakai, T. Vreven, K. Throssell, J. A. Montgomery, Jr., J. E. Peralta, F. Ogliaro, M. Bearpark, J. J. Heyd, E. Brothers, K. N. Kudin, V. N. Staroverov, T. Keith, R. Kobayashi, J. Normand, K. Raghavachari, A. Rendell, J. C. Burant, S. S. Iyengar, J. Tomasi, M. Cossi, J. M. Millam, M. Klene, C. Adamo, R. Cammi, J. W. Ochterski, R. L. Martin, K. Morokuma, O. Farkas, J. B. Foresman, and D. J. Fox, Gaussian, Inc., Wallingford CT, **2016**.
22. Chapman, S. and Bunker, D. L. *J. Chem. Phys.*, **1975**, 62, 2890-2899.
23. Thomas, J. B., Waas, J. R., Harmata, M. and Singleton, D. A. *J. Am. Chem. Soc.*, **2008**, 130, 14544.
24. Thorson, W.R. and Nakagawa, I. *J. Chem. Phys.*, **1960**, 33, 994-1004.
25. Quapp, W., Hirsch, M. and Heidrich, D. *Theor. Chem. Acc.*, **1998**, 100, 285-299.
26. Truhlar, D. G. and Garrett, B. C. *Annu. Rev. Phys. Chem.*, **1984**, 35, 159-189.

## 2.4 Relationships Between Product Ratios in Ambimodal Pericyclic Reactions, and Bond Lengths in the Transition Structure

(This work involves a collaboration with Xiaofei Dong, Yanmin Yu, Peiyuan Yu, Cooper Jamieson, and Yingzi Li. The paper is planned to submit to the *Journal of the American Chemical Society*)

### 2.4.1 Abstract

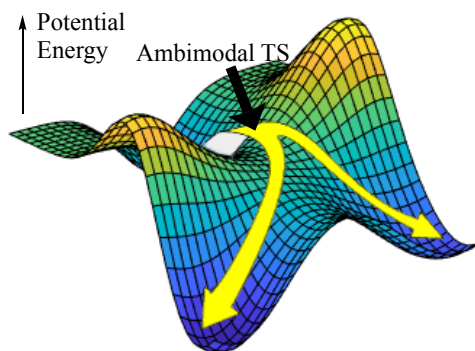
Ambimodal reactions involves a single transition state leading to multiple products. In such reactions, transition state theory gives no information about the ratio of products that are formed, and molecular dynamics must be performed to predict these things. Understanding the relationship between the transition structure and the product ratio is a long-standing problem in molecular dynamics. We have studied sixteen ambimodal pericyclic reactions and investigated the relationship between the TS bond lengths in the saddle point and the product ratio from trajectory simulations. A linear correlation,  $\ln(A:B) = -9.1(\text{bond2} - \text{bond3}) - 0.1$ , is found with  $R^2 = 0.92$ , where A and B refer to the products formed after bifurcation upon formation of bonds 2 and 3, respectively. The correlation shows that the ratio of products formed after the bifurcation is related to the partial bond lengths in the transition state.

### 2.4.2 Introduction

Post-transition state bifurcations (**Scheme 2.4.1**) are involved in reactions in which two or more products are generated from a single transition state.<sup>1,2</sup> The selectivity of these reactions is controlled by non-statistical dynamical effects, such as molecular motion and collisions, which

can be revealed from molecular dynamics trajectory simulations.<sup>3,4</sup> Chemical dynamics dates back to the birth of physical chemistry when Jacobus Henricus Van't Hoff, the founding father of the subject, published his seminal research in 1884, “*Études de Dynamique chimique*” (*Studies in Chemical Dynamics*).<sup>5</sup> The concept of “chemical dynamics” referred then to the study of kinetic properties, while nowadays, the concept has evolved to indicate the investigation of time-dependent processes of chemical transformations.

In 2002, Caramella proposed that the cyclopentadiene dimerization is a pericyclic reaction that involves a potential energy surface (PES) bifurcation.<sup>6</sup> The transition structure (TS) with C<sub>2</sub> symmetry was defined as a “bispericyclic” TS, where [4+2] and [2+4] TSs are merged into one single TS. We have proposed the more general term, “ambimodal transition structure”, to indicate a saddle point leading to two or more multiple products, pericyclic or otherwise.<sup>7</sup> Molecular dynamics simulations show that the ambimodal TS leads to formation of equal amounts of the two identical [4+2] and [2+4] products.<sup>8,9</sup> Unsymmetrical ambimodal reactions have been reported by Singleton,<sup>10,11,12</sup> Houk,<sup>13,14,15,16</sup> Tantillo,<sup>17,18,19</sup> Carpenter,<sup>20, 21,22</sup> etc,<sup>23,24,25</sup> where different products originate from one same TS. These reactions have been found in organic synthesis, biosynthesis, organocatalysis, and organometallic reactions, as previously reviewed by Houk<sup>1</sup> and Carpenter,<sup>26</sup> and recently by Tantillo.<sup>2</sup> The ambimodal reactions were even discovered in enzymatic reactions, as exemplified theoretically by Houk and coworkers, in the SpnF-catalyzed Diels–Alder reaction,<sup>27</sup> and experimentally and computationally by Tang and Houk, in the SAM-dependent LepI-catalyzed Diels–Alder and hetero-Diels–Alder reactions.<sup>28</sup>



**Scheme 2.4.1.** A potential energy surface with ambimodal transition state and a post-TS bifurcation surface.

Ambimodal reactions are receiving growing interest from organic and bioorganic communities, because of the new type of selectivity. Controlling the selectivity of ambimodal reaction is a key to harnessing ambimodal reactions for synthetic applications. Factors that influence the product ratio have been proposed, including momenta,<sup>29</sup> geometry<sup>12,13</sup> and the shape of PES.<sup>30</sup> Carpenter pioneered in the study of dynamic origins of organic reactions, and proposed momenta distribution in the TS as the determining factor for the stereoselectivity of the vinylcyclopropane-cyclopentene rearrangement; this is known as “dynamic matching”.<sup>29</sup> This effect was also observed by Singleton in the hetero-Diels-Alder reaction of acrolein with methylvinylketone,<sup>11</sup> in which a biased sampling of a vibrational mode with  $89\text{ cm}^{-1}$ , the wagging motion of the two dynamically competing bonds, alters the product ratio significantly. Singleton pointed out in his later paper that momenta control what product is generated in a particular trajectory, while the shape of PES can control the overall periselectivity. This was also emphasized by Hare and Tantillo for carbocation rearrangements.<sup>19</sup> Singleton also studied the diene-dienone cycloadditions, and found that the shorter forming bond in the TS always leads to

more product formation, indicating that TS geometry is another potential predictor for product ratio.<sup>12</sup>

While previous investigations reveal qualitative factors controlling ambimodal reaction product ratios, no quantitative model has been established. Here, we investigate how TS geometries influence ambimodal periselectivity. Sixteen ambimodal reactions were chosen from previous literature, primarily by Singleton et al. and our group, with TS geometries and product ratios of trajectory simulations obtained either from previous reports or calculated in the present study. These data enable us to explore the correlation between TS bond lengths and the dynamic product ratio.

### 2.4.3 Computational Methods

Density functional theory (DFT) computations were performed using Gaussian 09. Trajectory simulations were performed with ProgDyn/Gaussian interface developed by Singleton.<sup>10</sup> The geometries of ambimodal TSs and their corresponding bifurcating product ratios were mostly extracted from previous literature, but direct molecular dynamics (MD) simulations were performed here when not enough trajectories had been propagated (<50). Quasiclassical trajectories (QCTs) were initialized in the vicinity of the TS with normal mode sampling method, which involves adding zero-point energy and thermal energy for each real normal mode in the TS, and obtaining a Boltzmann distribution by randomly sampling a set of geometries and velocities. No additional velocities were added other than vibrations along modes perpendicular to the reaction coordinate. The trajectories were propagated forward and backward until either one of the

product is formed (bond 2 or bond 3 labeled in Table 1 smaller than 1.5 Å) or the reactant is generated. The classical equations of motion were integrated with a velocity-Verlet algorithm, with the energies and derivatives computed on the fly by the quantum mechanical method using Gaussian 09. The step length for integration is 1 fs.

## 2.4.4 Results and Discussion

### 2.4.4.1 Ambimodal reactions

Sixteen reactions were collected from previous literature, as shown in **Figure 2.4.1-3**. **Figure 2.4.1** shows ambimodal reactions leading to [4+2] and [2+4] adducts, the two adducts can be interconverted through [3,3]-sigmatropic rearrangements in each case. The first example, cyclopentadiene dimerization, was reported by Caramella as the first ambimodal pericyclic, or bis-pericyclic, reaction. The ambimodal TS was optimized previously with the B3LYP/6-31G(d) method. This TS has a C<sub>2</sub>-symmetric geometry with three forming **bonds 1, 2 and 3**, labeled on the Figure. During the reaction, **bond 1** always forms, and **bond 2** and **3** compete dynamically, but result in identical products. A similar situation is observed in the dimerization of butadiene<sup>31</sup> and of cyclopentadienone,<sup>32</sup> as thoroughly studied by Caramella. Cyclopentadiene dimerization was investigated originally by Woodward and Katz in their classic paper “*The mechanism of the Diels-Alder reaction*” in 1959,<sup>33</sup> where a two-stage mechanism was proposed. This reaction was studied using quasiclassical dynamic simulations by Singleton to investigate the Newtonian kinetic isotope effects,<sup>8</sup> and by our group to explore the involvement of two-stage versus concerted dynamic mechanisms in the reaction.<sup>34</sup>

The second example involves the hetero-Diels–Alder reaction of acrolein with methylvinylketone.<sup>11</sup> Hetero-Diels–Alder reactions have been used widely in synthesis, like the total synthesis of brevicomin.<sup>35</sup> Trajectory simulations by Singleton show that the reaction is ambimodal with the formation of **bond 3** occurring 2.7 times more frequently than that of **bond 2** with the MP2/6-311+G(d,p) method. The predicted product ratio is consistent with the experimental results. The third-seventh examples involve four diene-dienone cycloadditions, with four different dienes reacting with 3-methoxycarbonylcyclopentadienone.<sup>36</sup> These reactions were reported experimentally by Harmata,<sup>37</sup> and were investigated computationally by Singleton. The calculated kinetic isotope effects (KIE) for the TSs with MPW1K/6-31+G(d,p) method are consistent with the experimental values.<sup>36</sup> Trajectory simulations initiated from the TSs bifurcate to two types of cycloadducts as illustrated in **Figure 2.4.1**. Trajectory simulations of the four ambimodal TSs show that the shorter forming bond in the TS leads to the major product, which reveals the importance of ambimodal TS geometry in determining the ambimodal periselectivity.



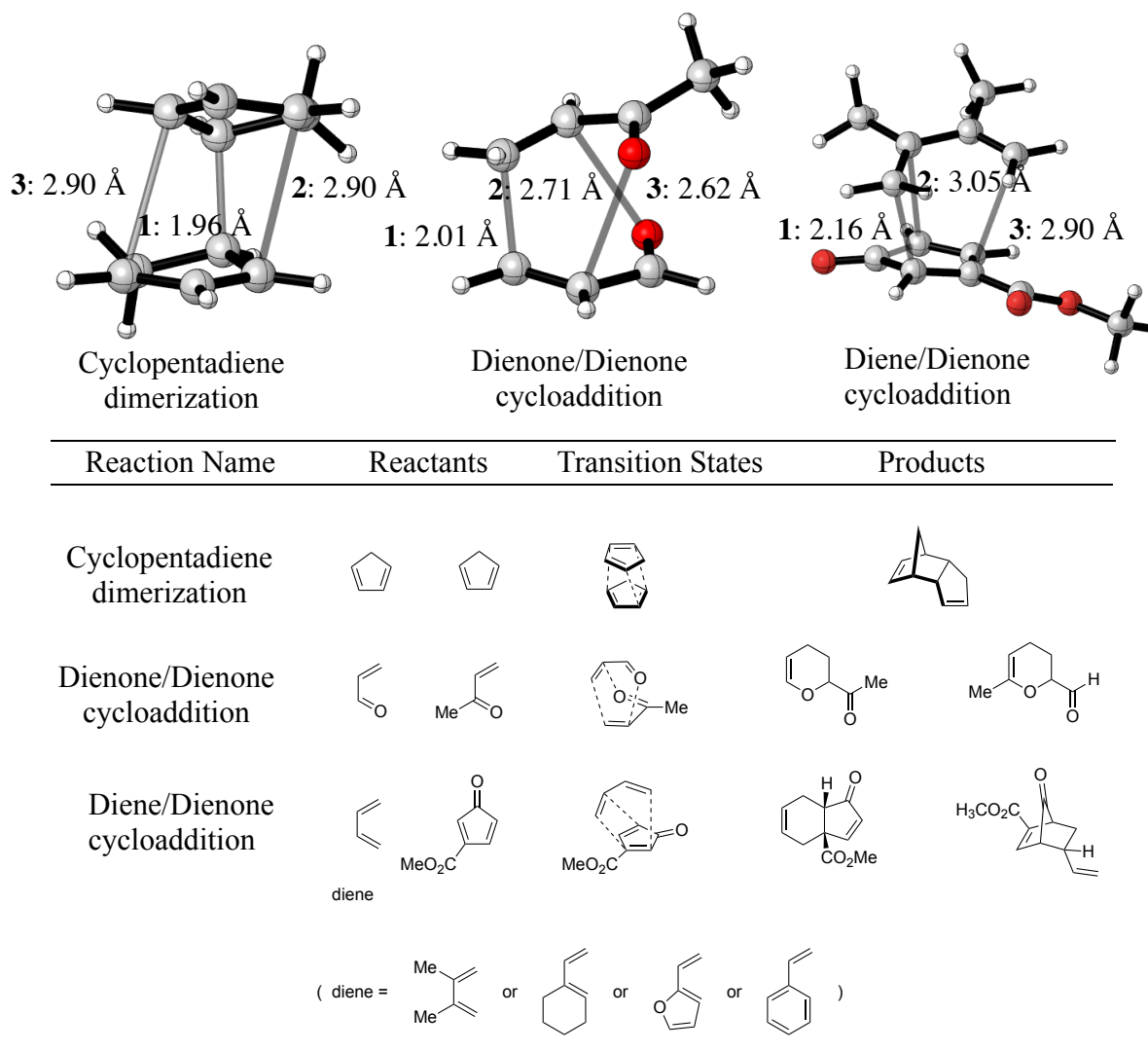


**Figure 2.4.1.** Ambimodal reactions for [4+2]/[2+4] bifurcation.

**Figure 2.4.2** lists ambimodal pericyclic reactions generating [4+2] and [6+4] adducts. The [6+4] cycloaddition was first predicted to be possible by Woodward and Hoffmann in 1965, and was the subject of the Ph. D. thesis of coauthor K. N. Houk in the Woodward group.<sup>38</sup> Cookson<sup>39</sup> and Ito<sup>40</sup> independently reported a [6+4] cycloaddition in 1966. The [6+4] reactions were later used in synthesis<sup>41,42</sup> and were discovered in organocatalysis reactions, as reviewed recently by Karl Jorgensen.<sup>43</sup> We first display the model [6+4] reaction of butadiene with hexatriene, and the

## CHAPTER 2.4

tethered transannular counterpart. The reactions were studied energetically by Yu and Houk as a comparison to the ambimodal cycloaddition in the biosynthesis of Heronamide A.<sup>44</sup> Product ratios for the two reactions were obtained with trajectory simulations performed in the current study using B3LYP/6-31G(d) method. The second reaction, SpnF-catalyzed Diels-Alder reaction was originally reported by Hung-wen Liu.<sup>45</sup> SpnF is the first stand-alone Diels-Alderase found in nature. Computational studies conducted by Houk and Singleton group reveal the formation of [4+2] and [6+4] adducts with a ratio of 2.5:1 in the gas phase using B3LYP-D2/6-31G(d) method.<sup>46</sup> Computations by M06-2X/6-31G(d) method gives a product ratio of 1.1:1 with a slightly different TS geometry. Both results are included in our model. Further studies with QM/MM method indicates that the enzyme-catalyzed reaction favors the formation of [4+2] adducts with the ratio of trajectories increasing to 11:1, in part by environmental alteration of the transition state.<sup>47</sup>

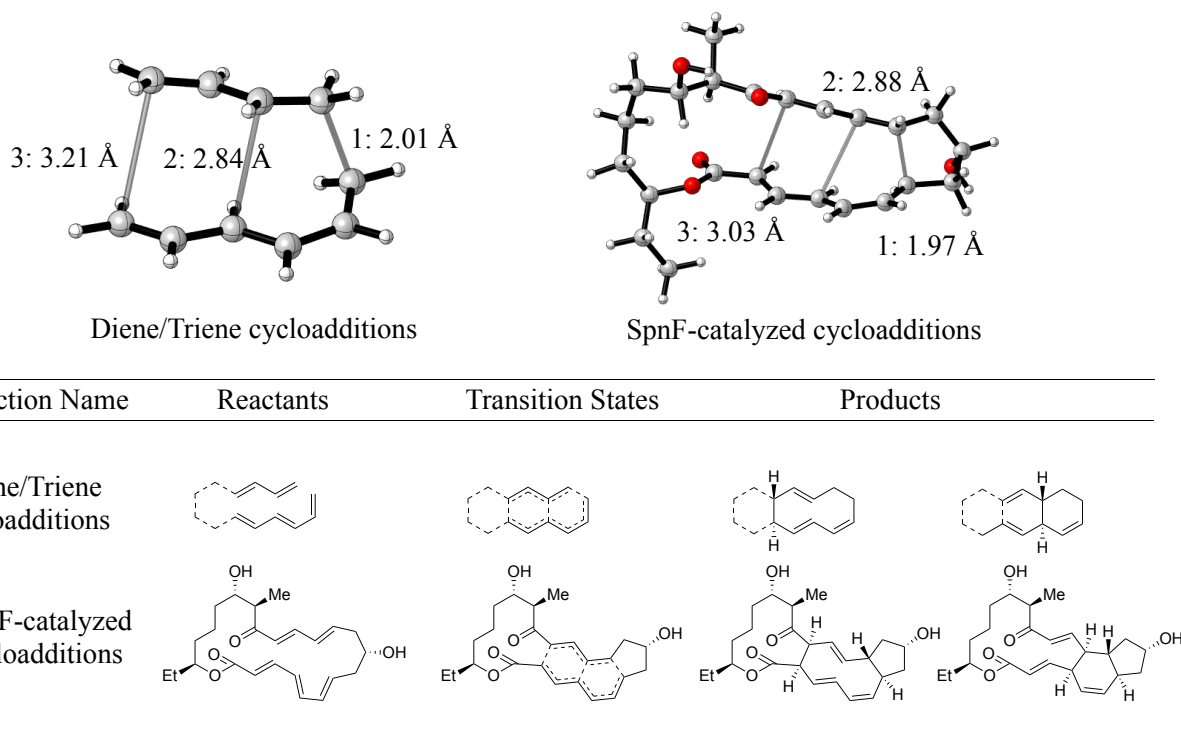


**Figure 2.4.2.** Ambimodal reactions for [4+2]/[6+4] bifurcation.

**Figure 2.4.3** displays some other types of ambimodal reactions. The first example involves [6+4]/[4+6] bifurcation in the cycloadditions of tropone to dimethylfulvene, which was studied experimentally by Houk as a Ph.D. subject and reported by the Houk group at Louisiana State University in 1970.<sup>38</sup> Computational studies were conducted recently by Yu and Houk, where ambimodal TSs were located using B3LYP-D3/6-31G(d) method, and both [6+4] and [4+6] adducts were observed from trajectory simulations. The second reaction is the [4+2] versus [2+2] cycloaddition of cyclopentadiene with diphenylketene.<sup>10</sup> The reaction surprised early researchers, because it affords cyclobutanones experimentally from a formal [2+2] cycloaddition rather than the expected [4+2] products. Machiguchi and Yamabe reported [4+2] cycloadducts as the initial adduct,<sup>48</sup> followed by a Claisen rearrangement that gives the ultimate cyclobutanones. This mechanism was challenged by a lower energy pathway proposed by Singleton, which

involves an ambimodal TS that bifurcates to both [4+2] and [2+2] adducts, as shown by the trajectory simulations. The ambimodal TSs located by mPW1K/6-31G(d) and mPW1K/6-31+G(d,p) methods were used here, because this method better rationalizes the experimental KIE, although recrossing is known to be important in the reaction. The third example involves the competition between a [3,3]-sigmatropic rearrangement and a  $S_N2$  cyclization that leads to fragmentation.<sup>49</sup> The ambimodal TS was located using the M06-2X/6-31G(d) method in a key step for the Fischer indole synthesis of a selective androgen receptor modulator, LY2452473. Equal amounts of rearrangement and fragmentation products were predicted from trajectory simulations. The last reaction involves the bifurcation to two different [3,3]-sigmatropic rearrangement products. The two forming bonds are quite late in comparison to the reactions we mentioned above, where two dynamically competing bonds are around 3 Å. The experimental work by the López group showed that perhalogenation of a C–C bond results in high selectivity for the corresponding rearrangement product.<sup>50</sup> Computational studies by the same group show the involvement of ambimodal transition structures in the reaction with M06-2X/Def2SVP method, where trajectory simulations give a ratio of 1:1 for the parent reaction, (symmetric) and 10:1 for the perfluorinated reaction, where the perfluorinated C-C bonds are favored. Both reactions were considered in our model.

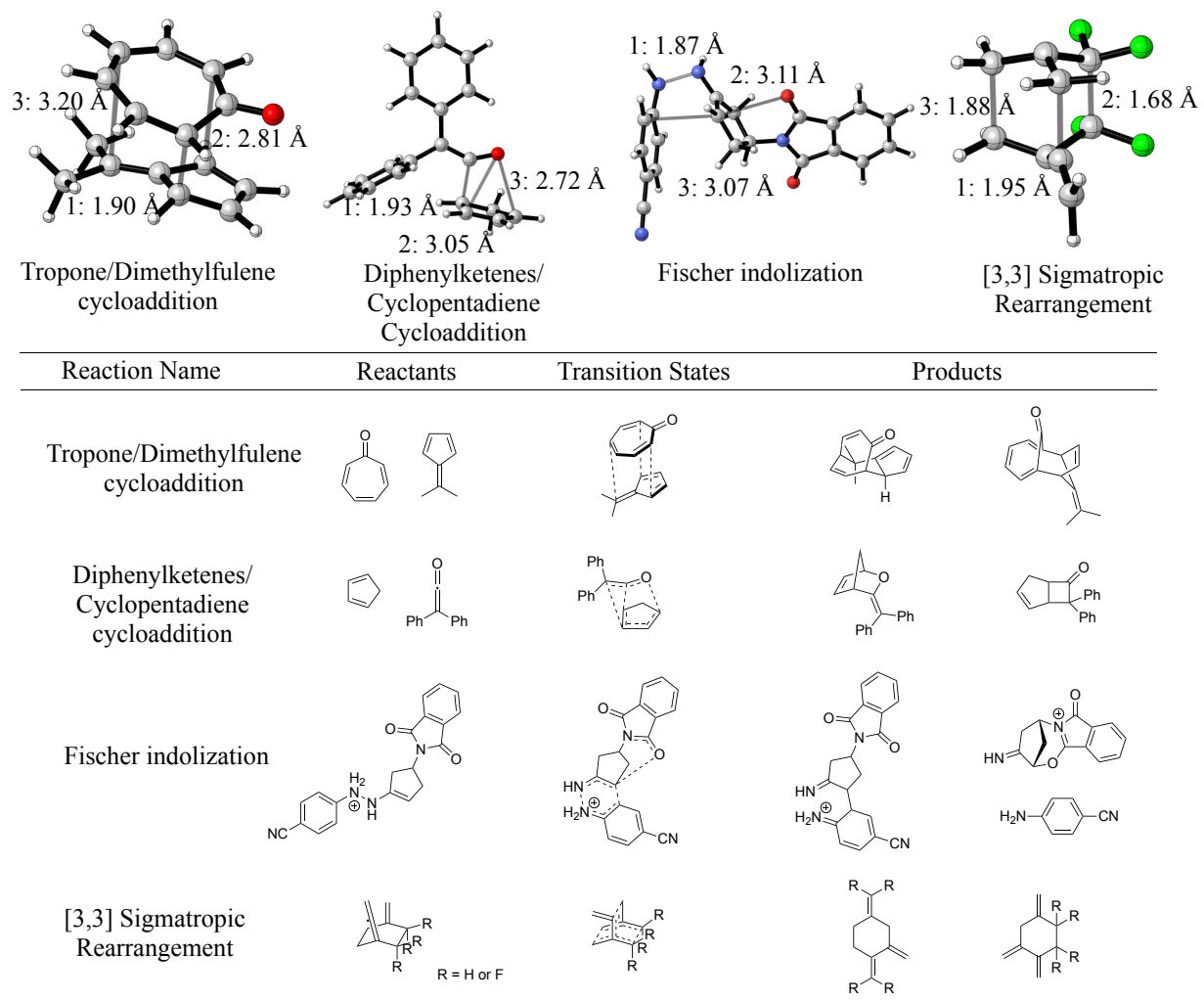


**Figure 2.4.3.** Other ambimodal reactions.

### 2.4.4.2 Correlation between ambimodal TS geometries and product ratio

**Table 2.4.1** summarizes the forming/breaking bond lengths of TSs for 16 ambimodal pericyclic reactions, along with the percentage of product with the formation of **bond 2**. In each reaction, **bond 1** always forms, and bifurcation occurs for the formation of **bond 2** or **3**, leading to products A or B, respectively. Ambimodal TSs and product ratios are extracted from previous literature, except for reactions 3-6<sup>12</sup> and 9-11<sup>14</sup>, where product ratios were determined/re-determined by trajectories simulations conducted in this study.

**Table 2.4.1.** Summary of forming bond lengths in the transition structures and product ratios for ambimodal reactions.

Label	Bifurcation	Reaction	Bond 1	Bond 2 (product A)	Bond 3 (product B)	A percentage (%)	ln(B:A)
1	[4+2]/[2+4]	Cp dimerization	1.96	2.90	2.90	50.0	0.0
2	[4+2]/[2+4]	Dienone+Dienone	2.01	2.71	2.62	27.0	1.0
3	[4+2]/[2+4]	Diene+Dienone a	2.04	2.83	3.18	99.1	-4.7
4	[4+2]/[2+4]	Diene+Dienone b	2.10	2.95	3.09	81.3	-1.5
5	[4+2]/[2+4]	Diene+Dienone c	2.15	2.99	2.95	23.2	1.2
6	[4+2]/[2+4]	Diene+Dienone d	2.16	3.05	2.90	13.0	1.9
7	[4+2]/[6+4]	SpnF a	1.97	2.88	3.03	71.1	-0.9
8	[4+2]/[6+4]	SpnF b	1.92	2.93	2.92	56.0	-0.2
9	[4+2]/[6+4]	Diene+Triene a	2.01	3.21	2.84	4.8	3.0
10	[4+2]/[6+4]	Diene+Triene b	2.08	2.82	2.87	58.9	-0.4
11	[6+4]/[4+6]	Tropone+Fulvene	1.90	2.81	3.20	94.0	-2.8
12	[4+2]/[2+2]	Cp+Ketene a	1.93	3.05	2.72	5.6	2.8
13	[4+2]/[2+2] [3,3]-sigma	Cp+Ketene b	1.94	3.05	2.75	11.1	2.1
14	shift/Fragmentation [3,3]-sigma	Fischer indolization	1.87	3.11	3.07	49.0	0.0
15	shift/[3,3]-sigma [3,3]-sigma	shift 3,3 sigmatropic a	1.95	1.68	1.88	90.8	-2.3
16	shift/[3,3]-sigma	shift 3,3 sigmatropic b	1.91	1.74	1.74	49.8	0.0

**Table 2.4.1** shows that the ambimodal TSs involve a large asynchronicity with bond 1 around 2 Å, and **bond 2** or **3** around 3 Å except for the two [3,3]-sigmatropic rearrangements, where the two competing bonds are more fully formed. This represents a general feature observed for ambimodal cycloadditions. The table also demonstrates that the percentage of one product (i.e. product A for the formation of **bond 2**) is closely related to relative bond length between **bond 2** and **3**. The percentage of A is around 50% when **bond 2** and **3** are almost equal, while less than 50% when **bond 2** is longer, and vice versa. This inspired us to inspect further the correlation between TS bond lengths and the product ratio.

**Figure 2.4.4** shows a plot of the percentage of A formed versus the difference between the lengths of **bonds 3** and **2**. Despite different density functionals used for the simulation, the

correlation still displays a reasonable linear correlation, with a  $R^2$  of 0.91. The plot shows quantitatively that the shorter forming bond in the TS leads to the major product. This suggests that the selectivity of ambimodal reactions is related to the extent of partial bonding in the transition structure. This trend was qualitatively proposed by Singleton as the “static factor” using reaction 3-6.<sup>12</sup> Singleton also stressed the influence of momenta distribution, the “dynamic factor”, using reaction 2.<sup>11</sup> Noticeably, these five reactions, along with others, fit well on one plot.

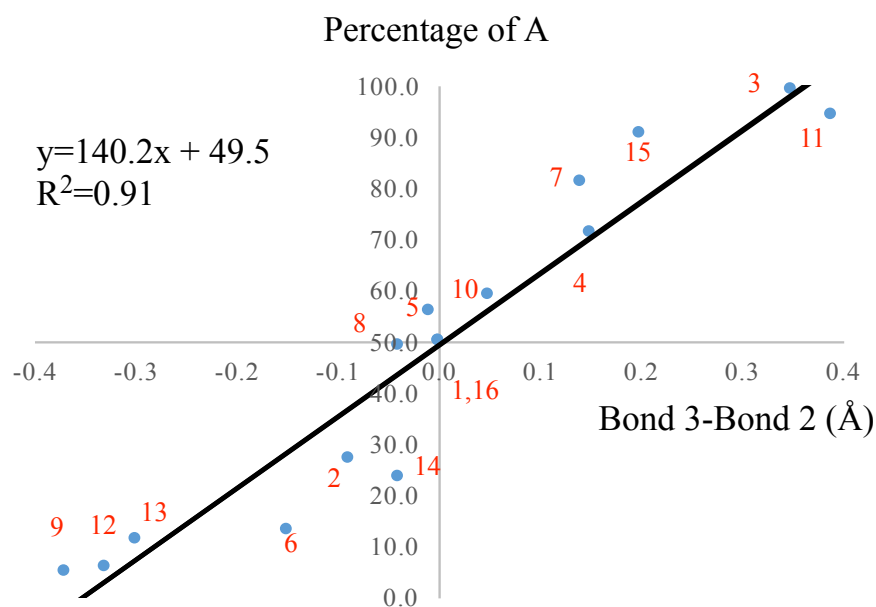


**Figure 2.4.4.** Plot of the yield of product A vs. the TS bond length difference.

The strength of a forming bond can be represented by bond order, which can be related to the bond length through Pauling bond order equation (1).<sup>51</sup> The labels  $n_0$  and  $r_0$  are the bond order and the bond length of a reference bond, and  $n_x$  and  $r_x$  are those of a forming bond. Here, a single C-C bond is used as reference so that  $n_0=1$  and  $r_0=1.54$  Å. The constant  $c$  determines how sharply the bond orders vary with bond distances.  $C=0.6$  is recommended for the bonds in

transition structures.<sup>52,53</sup> Derived from equation (1), the difference of two dynamically competing bond lengths, bond3-bond2, is related to the logarithm of the ratio of bond orders,  $\ln(n_{\text{bond3}}/n_{\text{bond2}})$ , as shown in equation (2).

$$n_x = n_0 \exp((r_0 - r_x)/c) \quad (1)$$

$$\ln(n_{\text{bond3}}/n_{\text{bond2}}) = -(bond3 - bond2)/c \quad (2)$$

$$B/A = (n_{\text{bond3}}/n_{\text{bond2}})^\lambda \quad (3)$$

$$\ln(B/A) = -\lambda (bond3 - bond2)/c \quad (4)$$

We postulate that the product ratio B/A is proportional to the  $\lambda$ th power of the ratio of bond order as shown in equation (3), in which  $\lambda$  represents an unknown coefficient. Combination of equation (2) and (3) generates equation (4), where the logarithm of product ratio  $\ln(B/A)$  equals the bond length difference, bond3-bond2, times a coefficient  $\lambda/c$ . **Figure 2.4.5** displays the correlation between the logarithm of the product ratio and the bond length difference. This plot supports equation (4) and indicate that the stronger partial bond results in the formation of the major product. The bonding strength also reflects the slope of the potential energy surface with respect to that coordinate. Presumably, the stronger bonding direction involves a sharper decrease of potential energy, and thus favors the corresponding product. When the difference between two bond length is 0.40 Å or greater, the percentage of the major product is >98%. This represents nearly exclusive formation of one single product. In such a case, only one product is formed, just as in a non-ambimodal transition state. Note that the use of bond order is important when the types of two forming bonds are different, such as a competition between C-O bond and C-H bond. ( $r_0=1.48$  or 1.08 Å, respectively)



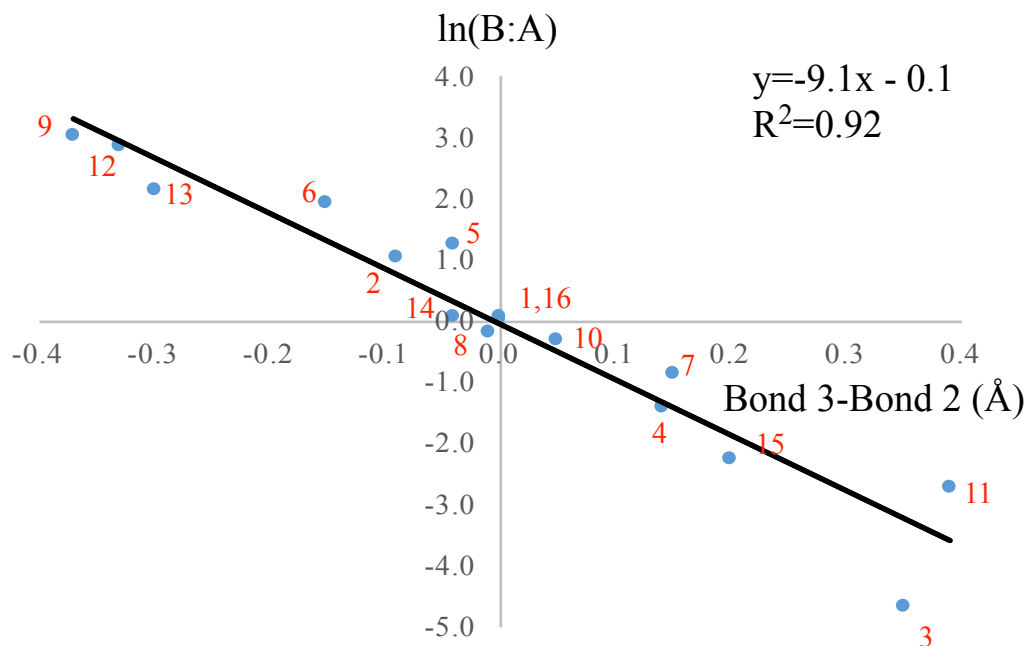


**Figure 2.4.5.** Correlation between logarithm of the product ratio  $\ln(B:A)$  and bond length difference bond3-bond2.

### 2.4.4.3 Application

The linear plot shown in **Figure 2.4.5** enables the estimation of initial product ratio without trajectory simulations. This was tested using the reaction between cyclopentadiene and  $\alpha$ -keto- $\beta$ ,  $\gamma$ -unsaturated phosphonates. The reaction was studied experimentally by Hanessian, Evans, and Denmark which showed that the Diels–Alder (DA) adduct is preferred intrinsically and the hetero-Diels–Alder (HDA) adduct is favored with the addition of Lewis acid catalyst  $\text{SnCl}_4$ . **Figure 2.4.6** shows the TSs reported previously by our group with the B3LYP/6-31G(d) method. The forming bond length of the DA adduct is 0.19 Å shorter than that of the HDA adduct, and is 0.37 Å longer with the coordination of  $\text{SnCl}_4$ . This shows the qualitative trend of the shift from the DA adduct to the HDA adduct with  $\text{SnCl}_4$ . No previous trajectory simulations

have been conducted.

The ratio of the HDA adduct versus the DA adduct is predicted to be 1.0:6.2 with the linear plot shown on **Figure 2.4.5**, and to be 1.0:5.6 with trajectory simulation. The two results are highly consistent, indicating the predictive power of the linear. The major product predicted is consistent with experiment. The model predicts the kinetic product ratio from the ambimodal TS, (ambimodal periselectivity) but the two resulting products may interconvert through another TS, giving a thermodynamic ratio instead. In this case, the DA and HDA products can be interchanged by a Claisen rearrangement TS.

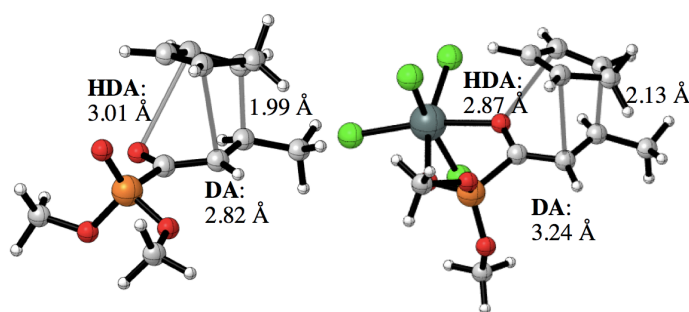


**Figure 2.4.6.** Transition structures of cyclopentadiene and  $\alpha$ -keto- $\beta,\gamma$ -unsaturated phosphonates with and without Lewis acid catalysts.

The linear correlation we found incorporates a limited number of ambimodal reactions in which the dynamic competition is between two forming bonds. New features might emerge when more types of ambimodal reactions are studied, such as the reactions involving the competition between a forming and a breaking bond (like Singleton's [1,2]-/[2,3]-sigmatropic rearrangement). The intrinsic linear trend we present is likely altered by the medium in which the reactions are performed, like solvent or enzyme. This would also be of interest to explore in the future study.

### 2.4.5 Conclusion

We have explained sixteen ambimodal pericyclic reactions and tested the correlation between the TS bond lengths and the product ratio. These reactions involve the bifurcation of [4+2]/[2+4], [4+2]/[6+4], [6+4]/[4+6], [4+2]/[2+2] adducts, and [3,3]-sigmatropic rearrangements. A linear correlation model is proposed between the logarithm of product ratio and the logarithm of bond order ratio, or the difference between two forming bonds. The model quantitatively shows that shorter forming bonds to more product formation, and allows the empirical estimation of product ratio without molecular dynamics simulations. The model also enables us to define a bond length difference of 0.40 Å, or logarithm of bond order ratio of 0.67 as the boundary between an ambimodal reaction and one leading to a more than 98% of one product.

### 2.4.6 Reference

1. Ess, D. H.; Wheeler, S. E.; Iafe, R. G.; Xu, L.; Çelebi-Ölçüm, N.; Houk, K. N. *Angew. Chem. Int. Ed.* **2008**, 47, 7592.
2. Hare, S. R.; Tantillo, D. J. *Pure Appl. Chem.* **2017**, 89, 679.
3. Pratihar, S.; Ma, X.; Homayoon, Z.; Barnes, G. L.; Hase, W. L. *J. Am. Chem. Soc.* **2017**, 139, 3570.
4. Carpenter, B. K. *Annu. Rev. Phys. Chem.* **2005**, 56, 57-89.
5. Van't Hoff, J. H. *Etudes de dynamique chimique 1884*, Vol. 1, Muller, Amsterdam.
6. Caramella, P.; Quadrelli, P.; Toma, L. *J. Am. Chem. Soc.* **2002**, 124, 1130.

7. Pham, H. V.; Houk, K. N. *J. Org. Chem.* **2014**, 79, 8968.
8. Kelly, K. K.; Hirschi, J. S.; Singleton, D. A. *J. Am. Chem. Soc.* **2009**, 131, 8382.
9. Yang, Z.; Zou, L.; Liu, F.; Yu, Y.; Dong, X.; Houk, K. N. (Submitted to *Chem. Phys.* in honor of Prof. Raphael Levine for his 80th birthday.)
10. Ussing, B. R.; Hang, C.; Singleton, D. A. *J. Am. Chem. Soc.* **2006**, 128, 7594.
11. Wang, Z.; Hirschi, J. S.; Singleton, D. A. *Angew. Chem. Int. Ed.* **2009**, 48, 9156.
12. Thomas, J. B.; Waas, J. R.; Harmata, M.; Singleton, D. A. *J. Am. Chem. Soc.* **2008**, 130, 14544.
13. Çelebi-Ölçüm, N.; Ess, D. H.; Aviyente, V.; Houk, K. N. *J. Am. Chem. Soc.* **2007**, 129, 4528.
14. Yu, P.; Patel, A.; Houk, K. N. *J. Am. Chem. Soc.* **2015**, 137, 13518.
15. Patel, A.; Chen, Z.; Yang, Z.; Gutiérrez, O.; Liu, H. W.; Houk, K. N.; Singleton, D. A. *J. Am. Chem. Soc.* **2016**, 138, 3631.
16. Yu, P.; Chen, T. Q.; Yang, Z.; He, C. Q.; Patel, A.; Lam, Y. H.; Liu, C. Y.; Houk, K. N. *J. Am. Chem. Soc.* **2017**, 139, 8251.
17. Hong, Y. J.; Tantillo, D. J. *Nat. Chem.* **2009**, 1, 384.
18. Hare, S. R.; Tantillo, D. J. *Chem. Sci.* **2017**, 8, 1442.
19. Hare, S. R.; Pemberton, R. P.; Tantillo, D. J. *J. Am. Chem. Soc.* **2017**, 139, 7485.
20. Carpenter, B. K.; Harvey, J. N.; Glowacki, D. R. *Phys. Chem. Chem. Phys.* **2015**, 17, 8372.
21. Kramer, Z. C.; Carpenter, B. K.; Ezra, G. S.; Wiggins, S. *J. Phys. Chem. A* **2015**, 119, 6611.
22. Carpenter, B. K. *Theo. Chem. Acc.* **2014**, 133, 1525.
23. Martin Birney, D. *Curr. Org. Chem.* **2010**, 14, 1658.

## CHAPTER 2.4

24. Yamataka, H.; Sato, M.; Hasegawa, H.; Ammal, S. C. *Faraday Discussions* **2010**, 145, 327.
25. Katori, T.; Itoh, S.; Sato, M.; Yamataka, H. *J. Am. Chem. Soc.* **2010**, 132, 3413.
26. Rehbein, J.; Carpenter, B. K.; *Phys. Chem. Chem. Phys.* **2011**, 13, 20906.
27. Yang, Z.; Yang, S.; Yu, P.; Li, Y.; Park, J.; Patel, A.; Doubleday, C.; Houk, K. N. Enzymatic Control of Reaction Dynamics (Submitted to *Proc. Natl. Acad. Sci. U. S. A.*)
28. Ohashi, M.; Liu, F.; Hai, Y.; Chen, M.; Tang, M. C.; Yang, Z.; Sato, M.; Watanabe, K.; Houk, K. N.; Tang, Y. *Nature*, **2017**, 549, 502.
29. Carpenter, B. K. *J. Am. Chem. Soc.* **1995**, 117, 6336.
30. Bogle, X. S.; Singleton, D. A. *Org. Lett.* **2012**, 14, 2528.
31. Quadrelli, P.; Romano, S.; Toma, L.; Caramella, P. *Tetrahedron Lett.* **2002**, 43, 8785-8789.
32. Quadrelli, P.; Romano, S.; Toma, L.; Caramella, P. *J. Org. Chem.* **2003**, 68, 6035-6038.
33. Woodward, R. B.; Katz, T. J. *Tetrahedron* **1959**, 5, 70.
34. Yang, Z.; Zou, L.; Liu, F.; Yu, Y.; Dong, X.; Houk, K. N. (Submitted to *Chem. Phys.* in honor of Prof. Raphael Levine for his 80th birthday.)
35. Mundy, B. P.; Otzenberger, R. D.; DeBernardis, A. R. *J. Org. Chem.* **1971**, 36, 2390.
36. Omas, J. B.; Waas, J. R.; Harmata, M.; Singleton, D. A. *J. Am. Chem. Soc.* **2008**, 130, 14544-14555.
37. Harmata, M.; Gomez, M. *Eur. J. Org. Chem.* **2006**, 2273.
38. Houk, K. N.; Luskus, L. J.; Bhacca, N. S. *J. Am. Chem. Soc.* **1970**, 92, 6392.
39. Cookson, R. C.; Drake, B. V.; Hudec, J.; Morrison, A. *Chem. Comm.* **1966**, 1, 15.
40. Itô, S.; Fujise, Y.; Okuda, T.; Inoue, Y.; *Bull. Chem. Soc. Jpn.* **1966**, 39, 1351.

41. Rigby, J. H. *Organic Reactions* **2004**, 49, 331.
42. Jørgensen, K.A. ed. *Cycloaddition reactions in organic synthesis*. 2002, John Wiley & Sons.
43. Palazzo, T. A.; Mose, R.; Jørgensen, K. A. *Angew. Chem. Int. Ed.* **2017**, 56, 10033.
44. Yu, P.; Patel, A.; Houk, K. N. *J. Am. Chem. Soc.* **2015**, 137, 13518-13523.
45. Kim, H. J.; Ruzsyczky, M. W.; Choi, S. H.; Liu, Y. N.; Liu, H. W. *Nature* **2011**, 473, 109-112.
46. Patel, A.; Chen, Z.; Yang, Z.; Gutiérrez, O.; Liu, H. W.; Houk, K. N.; Singleton, D. A. *J. Am. Chem. Soc.* **2016**, 138, 3631-3634.
47. Yang, Z.; Yang, S.; Yu, P.; Li, Y.; Park, J.; Patel, A.; Doubleday, C.; Houk, K. N. Submitted to Proc. Natl. Acad. Sci. U. S. A. In revision.
48. Machiguchi, T.; Hasegawa, T.; Ishiwata, A.; Terashima, S.; Yamabe, S.; Minato, T. *J. Am. Chem. Soc.* **1999**, 121, 4771.
49. Noey, E. L.; Yang, Z.; Li, Y.; Yu, H.; Richey, R. N.; Merritt, J. M.; Kjell, D. P.; Houk, K. N. *J. Org. Chem.* **2017**, 82, 5904.
50. Villar López, R.; Faza, O. N.; Silva López, C. *J. Org. Chem.* **2017**, 82, 4758.
51. Pauling, L. *J. Am. Chem. Soc.* **1947**, 69, 542-553.
52. Wilkie, J.; Williams, I. H. *J. Am. Chem. Soc.* **1992**, 114, 5423-5425.
53. Houk, K. N.; Gustavson, S. M.; Black, K. A. *J. Am. Chem. Soc.* **1992**, 114, 8565-8572.

## **Chapter 3. Energetics and Reaction Dynamics in Condensed Media: Methodology and Application**

### **3.1 Solvent-Perturbed Transition State Sampling and Application to Water-Accelerated Diels-Alder Reaction**

#### **3.1.1 Abstract**

We describe a solvent-perturbed transition state (SPTS) sampling scheme for simulating chemical reaction dynamics in condensed phase. The method, adapted from Truhlar and Gao's ensemble-averaged variational transition state theory, includes the effect of instantaneous solvent configuration on the potential energy surface of the reacting system (RS), and allows initial conditions for the RS to be sampled quasiclassically by TS normal mode sampling. We use a QM/MM model with direct dynamics, in which QM forces of the RS are computed at each trajectory point. The SPTS scheme is applied to the acceleration of the Diels-Alder reaction of cyclopentadiene (CP) + methyl vinyl ketone (MVK) in water. We explored the effect of number of SPTS and of solvent box size on the distribution of bond lengths in the TS. Statistical sampling of the sampling was achieved when distribution of forming bond lengths converged. We describe the region enclosing the partial bond lengths as the transition zone. Transition zones in the gas phase, SMD implicit solvent, QM/MM, and QM/MM+QM (3 water molecules treated by QM) vary according to the ability of the medium to stabilize zwitterionic structures. Mean time gaps between formation of C-C bonds vary from 11 fs for gas phase to 25 fs for QM/MM+QM. Mean H-bond lengths to O(carbonyl) in QM/MM+QM are 0.14 Å smaller at the

TS than in MVK reactant, and the mean O(carbonyl)-H(water)-O(water) angle of H-bonds at the TS is 10° larger than in MVK reactant.

### 3.1.2 Introduction

An increasing number of studies point to the importance of nonstatistical dynamics in organic reactions.<sup>1-25</sup> Experimental rate or product ratios in these reactions are poorly described by statistical theories (transition state theory or RRKM theory), but can be understood in terms of nonstatistical dynamical effects revealed by classical trajectory calculations. One area of concern is that most reactions are carried out in solution, but most trajectory calculations have either been applied to gas phase reactions, or have used a dynamical model without explicit solvent for reactions that occur in solution. In this paper, we describe and test a method that could be used to examine short-time nonstatistical dynamics in solution with explicit solvent. The emphasis on short simulation times, typically < 500 fs, is useful for minimizing the nonphysical flow of zero-point energy (ZPE) within the reacting system. In addition, nonstatistical effects tend to be largest at short times.

In recent years, trajectory calculations (or molecular dynamics, MD) for reactions involving covalent bonding changes in condensed phase have been reported with explicit solvation.<sup>26</sup> These pioneering calculations are a significant advance over gas phase models. For our purposes, there are specific features that would be useful. The method should: (1) sample initial conditions in a way that includes the effect of instantaneous solvent configuration on the potential energy surface of the reacting system, and (2) allow initial conditions for the reacting system to be



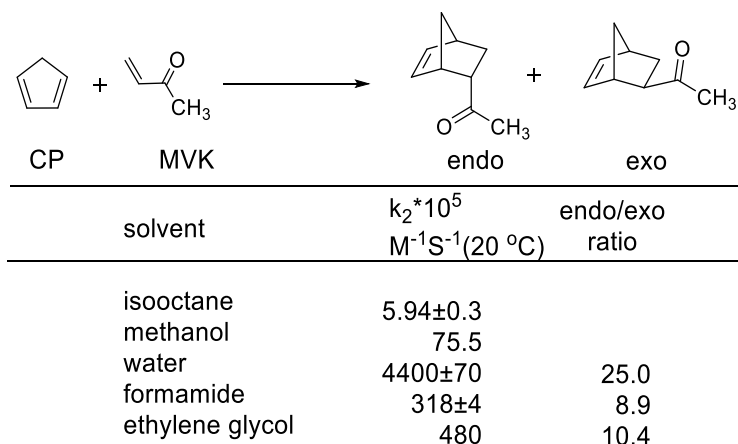
sampled quasiclassically, the method typically used to study nonstatistical dynamics. In quasiclassical thermal sampling, each vibrational normal mode is given at least the ZPE, and any additional energy is quantized to mimic a quantum Boltzmann distribution of vibrational levels. The proposed method satisfies these requirements.

We use a QM/MM model (quantum mechanics for the reacting system, molecular mechanics for solvent) with direct-dynamics trajectories, in which QM forces are computed at each MD point. The calculation is run within AMBER,<sup>27</sup> which has an interface to Gaussian 09<sup>28</sup> that supports electronic embedding (i.e., allows the electron density of QM solute to be polarized by the MM solvent). AMBER handles the MD part of the calculation (creation of solvent box, equilibration, and propagation of trajectories). The method for sampling initial coordinates and momenta for the QM reacting system is adapted from Truhlar and Gao's ensemble-averaged variational transition state theory, EA-VTST,<sup>29</sup> coupled with transition state (TS) normal mode sampling,<sup>30</sup> a method for quasiclassical sampling of the TS dividing surface used in gas-phase simulations. EA-VTST, which has been extensively applied to enzyme reactions,<sup>29,31</sup> was developed to include vibrational contributions of the reacting system to free energies of activation in condensed phase, and to compute quantum mechanical tunneling. It employs a separation of time scales of fast solute vibrations vs slower solvent motions, such that the reacting system maintains a Boltzmann distribution of vibrational levels for any arbitrary configuration of solvent molecules. Our protocol inherits this characteristic.

After describing our model, we apply it to the acceleration of Diels-Alder reactions in water. This reaction is accurately described by statistical theory; it has been well characterized

experimentally<sup>32</sup> and computationally,<sup>33</sup> and is used here to test statistical convergence in the sampling and to compare the dynamics in several solvent models. The acceleration of Diels–Alder reactions in water was first reported by Breslow,<sup>32</sup> who found that both reactivities and endo/exo selectivities are enhanced by water. **Scheme 3.1.1** shows Breslow's results for cyclopentadiene (CP) + methyl vinyl ketone (MVK) in several solvents.<sup>32b</sup> The rates span nearly 3 orders of magnitude from isooctane to water. Jorgensen and coworkers<sup>33</sup> have given strong evidence that the largest contribution to the water-acceleration of Diels-Alder reactions comes from enhanced hydrogen bonding in the TS vs reactants. In ab initio calculations, they found that larger polarization in the TS than in MVK leads to an increase in H-bond strength at the TS by 1.5 to 2.0 kcal/mol.<sup>33a</sup> In QM/MM calculations,<sup>33b,c</sup> H-bonding provides a larger free energy contribution in the TS than in reactants or products.

**Scheme 3.1.1.** Second-order rate constants and endo/exo product ratios for the CP + MVK Diels-Alder reaction in several solvents.<sup>32b</sup>



### 3.1.3 Computational Methods

M06-2X/6-31G(d) is the QM method used for optimizations and trajectories, and water is represented by the TIP3P<sup>34</sup> MM model. The SMD solvation model of Cramer and Truhlar and coworkers<sup>35</sup> is used in calculations involving implicit solvent.

The full QM/MM system with  $N$  atoms consists of a small reacting zone ( $N_1$  reacting atoms treated by QM) and a large solvent zone ( $N_2 = N - N_1$  solvent atoms treated by MM). The QM/MM protocol consists of six steps. Further details are in the SI.

1. The M06-2X/6-31G(d) endo transition structure  $TS_w$  is computed with continuum water solvation using SMD.

2.  $TS_w$  is surrounded with a cubic solvent box (periodic boundary conditions, electrostatic cutoff is 8 Å), whose size is determined in an iterative method leading to statistical convergence, described below. For a given box size and with  $TS_w$  fixed, the solvent is equilibrated for 200 ps in an NPT ensemble (fixed number of atoms  $N$ , pressure  $P$ , and temperature  $T$ )<sup>36,37</sup>

3. As solvent equilibration continues with fixed  $TS_w$ , a set of instantaneous frozen solvent coordinates and momenta are extracted and stored at 5 ps intervals. This is continued until a specified number (usually  $\leq 25$ ) of frozen solvent configurations has been picked.

4. For each frozen solvent configuration, the transition structure for the  $N_1$  reacting atoms is optimized using ONIOM,<sup>38</sup> keeping the  $N_2$  solvent atoms fixed. Since each of these solvent-perturbed transition states (SPTSs) is optimized in the field of a different frozen solvent configuration, their geometries and vibrational frequencies differ. The number of SPTS saddle points,  $N_{SPTS}$ , is equal to the number of frozen solvent configurations in step 3.

5. At each SPTS saddle point, several sets (currently 10) of initial coordinates and momenta for the reacting system are selected quasiclassically by TS normal mode sampling at 300 K. In previous work we have used Venus<sup>39</sup> or Progdyn<sup>9b</sup> for TS normal mode sampling; here we use Progdyn. The bound modes were the  $3N_1 - 1$  real frequencies of the reacting system, and the transition vector was the reaction coordinate.<sup>40</sup> This gives initial conditions for  $10 \times N_{\text{SPTS}}$  trajectories.

6. All constraints on the frozen solvent zone are released, and  $10 \times N_{\text{SPTS}}$  trajectories for the full system are propagated forward and backward from the initial point until either reactants or products are formed, using velocity Verlet with a 1 fs step size. In the current application, trajectories were stopped after 150 fs in each direction.<sup>41</sup>

To include a QM description of hydrogen bonding during the trajectories, the general procedure above was modified to include 2-3 water molecules in the QM zone. In step 3, up to 3 water molecules were identified in each of the  $N_{\text{SPTS}}$  frozen MM solvent configurations by searching for O-O distances  $< 3 \text{ \AA}$  between oxygen atoms of water and MVK. Most of these involved H-bonding to the carbonyl oxygen to varying degrees. If only 2 water molecules were found, a search was made for a third water whose O-O distance to one of the first two waters was  $< 3 \text{ \AA}$ . In step 4, the chosen water molecules, while frozen, were included in the QM reacting zone during the SPTS optimizations; MM was maintained for the remaining frozen solvent. This allowed the SPTS geometry to be optimized in the presence of frozen QM H-bonds. As a result, the initial coordinates and momenta for CP + MVK determined in step 5 include a QM description of H-bonding to 2-3 frozen waters. Although the QM waters were represented by

MM in the equilibration step, the main features of their dynamics should be simulated by this procedure. We refer to this method as QM/MM+QM.

To reach statistical convergence in the sampling, steps 2-5 are repeated with different cubic box sizes in step 2 and different values for  $N_{\text{SPTS}}$ , the number of frozen solvent configurations in step 3, which is equal to the number of SPTSs in step 4. For each combination of box size and  $N_{\text{SPTS}}$ , we compute the distribution of forming CC bond lengths in the  $10 \times N_{\text{SPTS}}$  sampled TS structures. Statistical convergence is achieved at the smallest values of box size and  $N_{\text{SPTS}}$  at which the distribution stops changing, as illustrated below.

Trajectory calculations were also carried out in the gas phase and with SMD implicit water, for comparison to QM/MM. They were initialized at the saddle point with TS normal mode sampling at 300 K, and propagated 150 fs in forward and reverse directions from the initial point using velocity Verlet with 1 fs step size.

### 3.1.4 Results and discussion

**Figure 3.1.1** shows the H-bonds identified in four solvent configurations after the equilibration with fixed  $\text{TS}_w$  in step 3. Two of these configurations have two H-bonds to the carbonyl oxygen, one configuration has one H-bond, and one configuration has three H-bonds. **Figure 3.1.2a** shows the distribution of forming bonds in  $N_{\text{SPTS}} = 20$  saddle points produced in step 4. The distribution in **Figure 3.1.2a** illustrates the substantial effect that solvent can exert on the potential energy surface of the reacting system.<sup>29,31</sup> In step 5, each SPTS is sampled to give 10 sets of coordinates and momenta, 200 in all. **Figure 3.1.2b** shows the transition zones,

defined as the most probable 98% of the distribution in the forming bond lengths produced by TS normal mode sampling. The 200 sampled TS coordinates are superimposed in the inset.

**Figure 3.1.3** shows the test for statistical convergence, in which steps 2-5 are carried out with cubic box sizes of 10, 12 and 13 Å (617, 944 and 1137 water molecules, respectively) and  $N_{\text{SPTS}} = 15, 20, 25$ . This generates nine combinations whose transition zones are shown. As box size and  $N_{\text{SPTS}}$  are increased, the mean and variance of the transition zones stop changing and convergence is achieved with a 12 Å box and  $N_{\text{SPTS}} = 20$ .

**Figure 3.1.4** shows the transition zones for gas phase, SMD implicit solvent, and QM/MM explicit solvent with a 12 Å box and  $N_{\text{SPTS}} = 20$ . The three QM/MM transition zones include zero, two and three H-bonded water molecules as described above. The asynchronicity, defined here as the difference between mean bond lengths in the transition zone, is 0.35 Å in the gas phase and 0.52 Å in SMD. Asynchronicities for QM/MM are close to the SMD value: 0.48, 0.54, 0.54 for 0, 2 and 3 H-bonded waters respectively. The difference from the gas phase is consistent with zwitterionic stabilization of asynchronous bond formation in water. In Acevedo and Jorgensen's QM/MM study of CP + MVK using PDDG/PM3 as QM in OPLS water, the asynchronicities were 0.1 Å for gas phase and 0.33 in water.<sup>33c</sup>

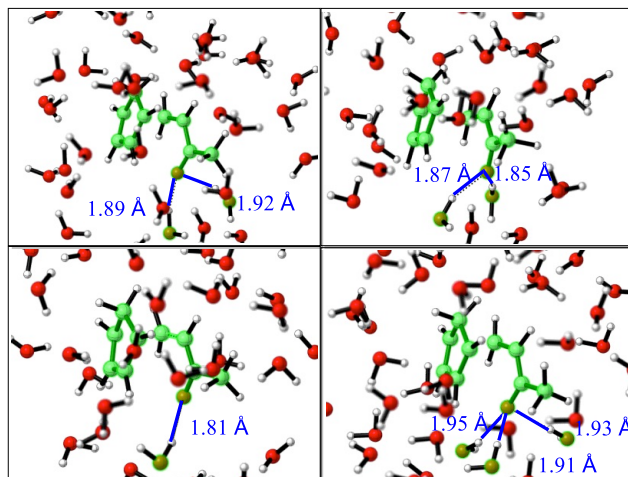


**Figure 3.1.1.** Four solvent configurations after the equilibration with fixed  $TS_w$  in step 3. Hydrogen bond lengths are shown (Black solid lines).

**Figure 3.1.5** shows the same set of TS points as in **Figure 3.1.4**, projected onto the plane of  $C_1C_2$  and  $C_3C_4$  distances. From visual inspection it is clear that the QM/MM methods have broader distributions than those for gas phase and SMD. Quantitatively, the standard deviations along the direction of the reaction coordinate (perpendicular to the long axes of the TS distributions) are in the ratio 1 : 1.2 : 1.9 : 2.7 for gas phase, SMD, QM/MM (no QM H-bonds), and QM/MM+QM (3 QM H-bonds), respectively. Inclusion of explicit solvent, and particularly QM H-bonding, is seen to have a substantial effect on the TS distribution.

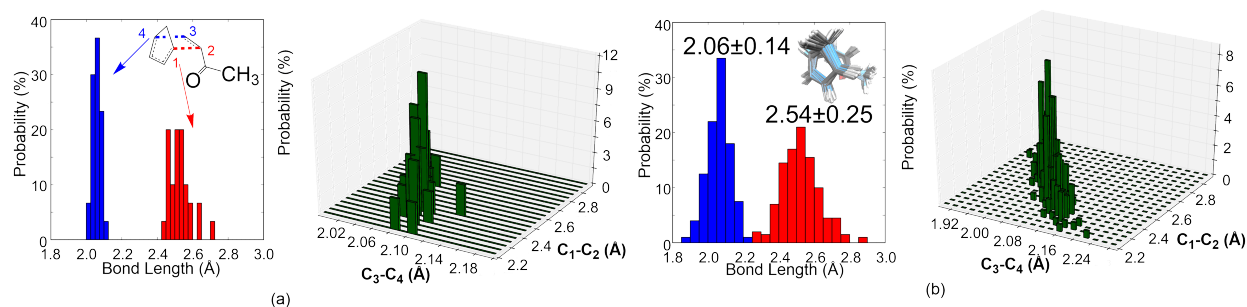


**Figure 3.1.2.** (a) Distribution of forming bond lengths of 20 SPTSs of the endo Diels-Alder reaction between CP and MVK according to step 4. Forming bonds are shown as blue and red

## CHAPTER 3.1

dotted lines on the Figure. (b) Transition zones for the forming bonds, i.e., the most probable 98% of the distribution of forming bond lengths of 200 sampled transition states according to step 5.

Inset: 200 superimposed sampled structures.

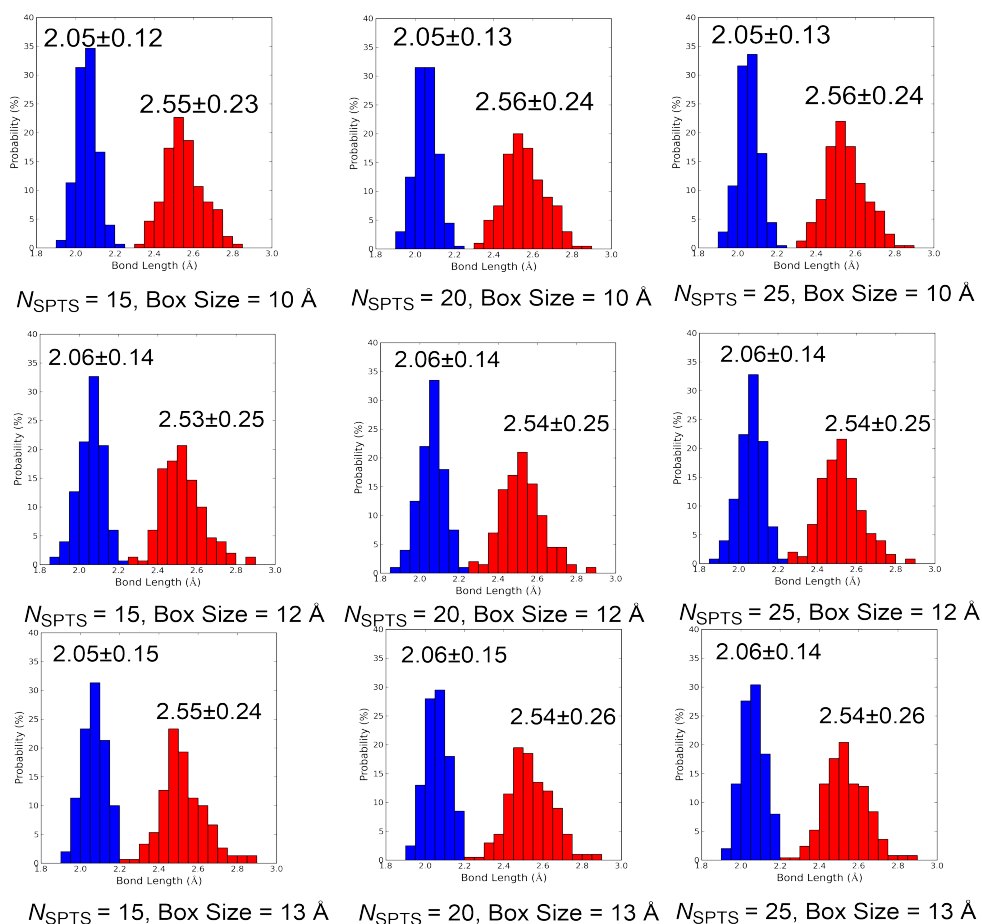


**Figure 3.1.3.** Test for statistical convergence. Protocol steps 2-5 are carried out with box sizes of 10, 12 and 13 Å and  $N_{\text{SPTS}} = 15, 20, 25$ ; transition zones are plotted for each combination.

Statistical convergence occurs with a 12 Å box and  $N_{\text{SPTS}} = 20$ .



## CHAPTER 3.1

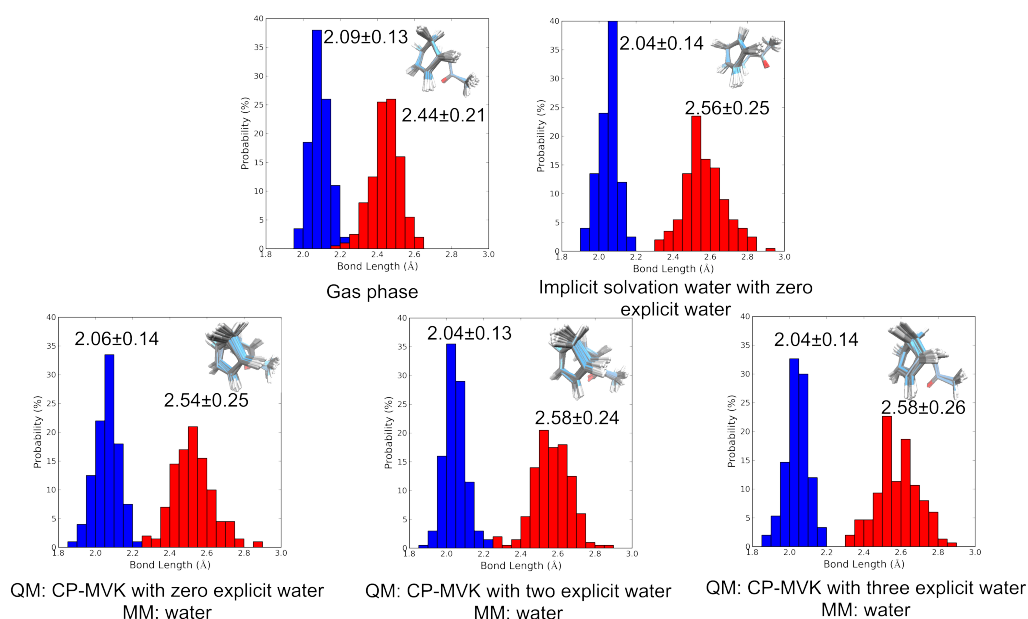


**Figure 3.1.4.** Transition zones of endo-CP-MVK reaction at 300 K in the gas phase, with SMD implicit water solvation and with explicit water (12 Å box,  $N_{\text{SPTS}} = 20$ ). Insets at upper right show 200 superimposed sampled structures.

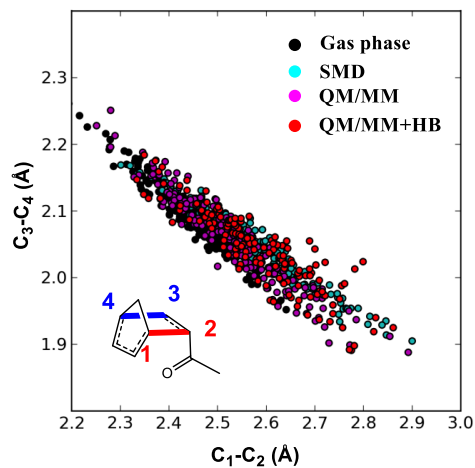


**Figure 3.1.5.** C-C bond lengths for sampled TS points in gas phase, SMD, QM/MM and QM/MM+QM. 150 points are plotted for each.

**Table 3.1.1.** Time gaps (fs) for bond formation, and the percent of time gaps > 35 fs.<sup>a</sup>

	gas phase	SMD	QM/MM	
			0 QM <sup>b</sup>	3 QM <sup>b</sup>
Mean gap $\pm\sigma^c$	11 $\pm$ 6	17 $\pm$ 11	20 $\pm$ 11	25 $\pm$ 14
Maximum gap	27	86	82	88
Percent > 35 fs	0	5	9	19

<sup>a</sup>Vibrational period of a C-C single bond is 30-40 fs. <sup>b</sup>Number of QM water molecules as described in text. <sup>c</sup>Std. Dev.

The time gap distributions are broad with tails extending above 80 fs for the aqueous models including SMD. The percent of time gaps above 35 fs gives an indication of the fraction of trajectories that persist for one or more C-C vibrational periods after forming the first bond. A related measure is the fraction of trajectories in which the reactants, having passed through the TS, reverse direction and start moving apart, before reversing again and forming the product. Only 14 - 15% of gas phase and SMD trajectories do this, but nearly half (43 - 46%) of QM/MM and QM/MM+QM trajectories encounter C-C turning points on the product side near the TS (C-C > 1.9 Å). Of these trajectories, the ratio of C<sub>1</sub>C<sub>2</sub> to C<sub>3</sub>C<sub>4</sub> turning points (**Figure 3.1.5** numbering) is 90:10 for the QM/MM methods but 60:40 for gas phase and SMD. Both the large fraction of QM/MM turning points, and the strong preference of the QM/MM methods for the zwitterionic stabilization<sup>42</sup> afforded by large amplitude C<sub>1</sub>C<sub>2</sub> motion, indicate a substantive change in the computed dynamics in explicit solvent compared to implicit solvent. In this reaction, which has a steep drop in energy from TS to drop in energy from TS to product, complex motion on the product side of the TS lengthens the time gap but does not affect the

exo/endo product ratio. The time gaps of more than 90% trajectories are within the lifetime of transition state (60 fs),<sup>43</sup> indicating that the reaction proceeds in a dynamically concerted fashion. Since Jorgensen's results imply that preferential H-bonding in the TS accounts for the lower barrier in water,<sup>33</sup> we analyzed the H-bond lengths and angles in the QM/MM+QM results. Figure 3.1.6a gives the distribution of H-bond lengths in the reactant region (-150 fs), the TS (0 fs), and product region (+150 fs). The mean H-bond length at the TSs is 1.88 Å, which is substantially shorter than reactants (2.02 Å) and products (2.03 Å). The value of 1.88 Å at the TS is close to the 1.9 Å H-bond length reported by Jorgensen, obtained from the O(carbonyl)-H(water) pair distribution function at the TS.<sup>33c</sup> The distribution of H-bond lengths at the TS is narrower than that at the reactant and at the product. **Figure 3.1.6b** shows the distribution of H-bond angle(O(carbonyl)-H(water)-O(water)) in the reactant, the TS, and the product.<sup>44</sup> The mean value of 158° at the TS is about 10° higher than that at the reactant and at the product. The distribution of H-bond angle at the TS is narrower than that at the reactant and at the product. These results indicate the enhancement of H-bonding during the reaction.

In 14% of trajectories, the O(carbonyl)-H(water)-O(water) angle rotates by more than 30 degree from the reactant to the TS. Inspection of these trajectories revealed that the formation of H-bonds in the TS occurs by reorientation of a neighboring water molecule during the reaction. **Figure 3.1.7** shows an example. In the upper left frame, at -150 fs, MVK has one strong H-bond (1.93 Å) to water A. The neighboring water molecule B is situated such that an H atom is 3.12 Å away from the carbonyl oxygen of MVK. B then reorients itself towards the oxygen of MVK as the reaction progresses. At -75 fs, the H-O distance is 2.80 Å, and at 0 fs it becomes 1.99 Å,

indicating the formation of a second strong hydrogen bond. In the product region at 150 fs, the lengths of the A and B H-bonds are 1.97 and 2.20 Å, respectively. The reorientation of water over a 75 fs time scale illustrates a potent mechanism for preferential stabilization of the TS.

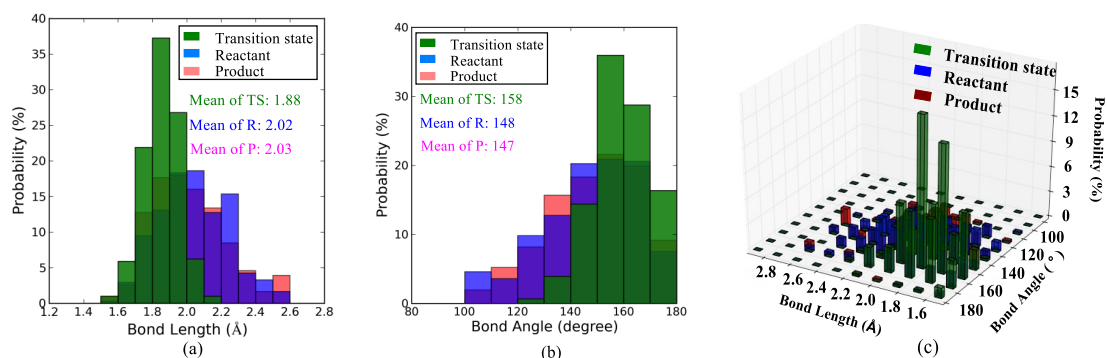


**Figure 3.1.6.** Distribution of (a) hydrogen bonding length (O(carbonyl)-H(water) distance), and (b) hydrogen bonding angle (O(carbonyl)-H(water)-O(water) angle) in transition states (in green, at 0 fs), reactants (in blue, at -150 fs), and products (in pink, at 150 fs). 150 reactive trajectories are used for the analysis. (c) 3D representation of distribution of hydrogen bonding length and angle in the transition states, reactants and products.

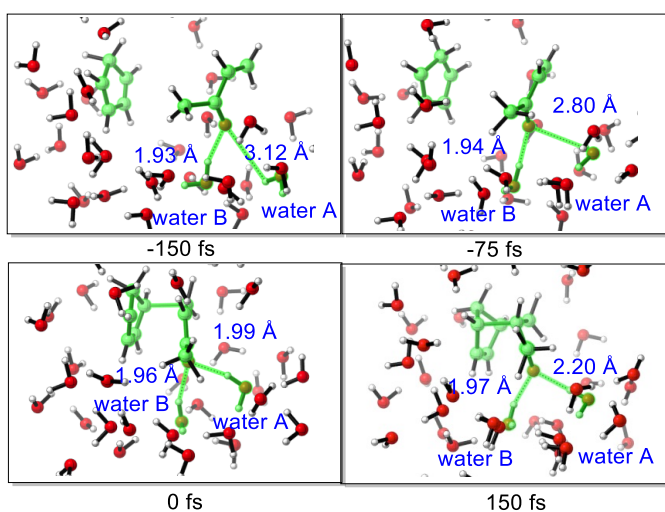


**Figure 3.1.7.** Snapshots taken at -150fs, -75 fs, 0 fs and 150 fs of a typical trajectory with three water molecules added into the QM region.

### 3.1.5 Conclusion

We propose a solvent-perturbed transition state (SPTS) sampling scheme as a new QM/MM protocol for solution-phase direct dynamics simulation of chemical reactions. This protocol includes the effect of solvent configuration on the potential energy surface of the reacting system, and allows initial conditions for the reacting system to be sampled quasiclassically by TS normal mode sampling. As a proof of concept, we applied the SPTS scheme to the dynamics of water-accelerated Diels–Alder reaction of cyclopentadiene (CP) and methyl vinyl ketone (MVK). Statistical convergence of the sampling is conveniently monitored by computing the transition zone as a function of the number SPTSs and solvent box size. Mean time gaps between formation of C-C bonds vary from 11 fs for gas phase to 25 fs for QM/MM+QM, with tails of the distributions up to > 80 fs. Nearly half of QM/MM and QM/MM+QM trajectories encounter C-C turning points on the product side of the TS. This complex motion lengthens the time gap but does not affect the exo/endo product ratio. The time gaps of more than 90% trajectories are within the lifetime of transition state (60 fs), indicating that the reaction proceeds in a dynamically concerted fashion. In QM/MM+QM trajectories, the mean O(carbonyl)-H(water) distance of H-bonds at the TS is 0.14 Å shorter than in MVK reactant, and the mean O(carbonyl)-H(water)-O(water) angle of H-bonds at the TS is 10° larger than in MVK reactant. In 14% of these trajectories, the formation of H-bonds in the TS occurs by reorientation of a

water molecule during the reaction. These results support the conclusion of Jorgensen and coworkers<sup>33</sup> that preferential H-bond stabilization in the TS makes the largest contribution to water acceleration of Diels-Alder reactions.

### 3.1.6 Reference

- (1) (a) Newman-Evans, R. H.; Carpenter, B. K. *J. Am. Chem. Soc.* **1984**, 106, 7995-7996. (b) Carpenter, B. K. *J. Am. Chem. Soc.* **1985**, 107, 5130-5132. (c) Newman-Evans, R. H.; Simon, R. J.; Carpenter, B. K. *J. Org. Chem.* **1990**, 55, 695-711. (d) Carpenter, B. K. *Acc. Chem. Res.* **1992**, 25, 520-528.
- (2) (a) Lourderaj, U.; Hase, W. L. *J. Phys. Chem. A* **2009**, 113, 2236-2253. (b) Lourderaj, U.; Park, K.; Hase, W. L. *Int. Rev. Phys. Chem.* **2008**, 27, 361-403.
- (3) (a) Carpenter, B. K. *Chemical Reviews* **2013**, 113, 7265-7286. (b) Carpenter, B. K. *Annu. Rev. Phys. Chem.* **2005**, 56, 57-89. (c) Carpenter, B. K. In *Reactive Intermediate Chemistry*, Moss, R. A.; Platz, M. A.; Jones, M., Jr., Ed., Wiley: Hoboken, **2004**, pp 925-960. (d) Carpenter, B. K. *J. Phys. Org. Chem.* **2003**, 16, 858-868.
- (4) Rehbein, J.; Carpenter, B. K. *Phys. Chem. Chem. Phys.* **2011**, 13, 20906-20922.
- (5) Yamataka, H. *Adv. Phys. Org. Chem.* **2010**, 44, 173-222.
- (6) Sun, L. P.; Song, K. Y.; Hase, W. L. *Science* **2002**, 296, 875-878.
- (7) Sun, R.; Park, K.; de Jong, W. A.; Lischka, H.; Windus, T. L.; Hase, W. L. *J. Chem. Phys.* **2012**, 137, 044305.

## CHAPTER 3.1

- (8) (a) Ammal, S. C.; Yamataka, H.; Aida, M.; Dupuis, M. *Science* **2003**, 299, 1555-1556. (b) Yamataka, H.; Aida, M.; Dupuis, M. *J. Phys. Org. Chem.* **2003**, 16, 475. (c) Yamataka, H.; Aida, M.; Dupuis, M. *Chem. Phys. Lett.* **2002**, 353, 310. (d) Yamataka, H.; Aida, M.; Dupuis, M. *Chem. Phys. Lett.* **1999**, 300, 583-587.
- (9) (a) Bekele, T.; Christian, C. F.; Lipton, M. A.; Singleton, D. A. *J. Am. Chem. Soc.* **2005**, 127 (25), 9216-9223. (b) Ussing, B. R.; Hang, C.; Singleton, D. A. *J. Am. Chem. Soc.* **2006**, 128, 7594-7607.
- (10) Bach, A.; Hostettler, J. M.; Chen, P. *J. Chem. Phys.* **2006**, 125, 024304.
- (11) Litovitz, A. E.; Keresztes, I.; Carpenter, B. K. *J. Am. Chem. Soc.* **2008**, 130, 12085-12094.
- (12) Glowacki, D. R.; Marsden, S. P.; Pilling, M. J. *J. Am. Chem. Soc.* **2009**, 131, 13896-13897.
- (13) Zheng, J.; Papajak, E.; Truhlar, D. G. *J. Am. Chem. Soc.* **2009**, 131, 15754-15760.
- (14) Glowacki, D. R.; Liang, C. H.; Marsden, S. P.; Harvey, J. N.; Pilling, M. J. *J. Am. Chem. Soc.* **2010**, 132, 13621-13623.
- (15) Zhang, X. H.; Zummack, W.; Schroder, D.; Weinhold, F. A.; Schwarz, H. *Chem.-Eur. J.* **2009**, 15, 11815-11819.
- (16) McKee, M. L.; Reisenauer, H. P.; Schreiner, P. R. *J. Phys. Chem. A* **2014**, 118, 2801-2809.
- (17) (a) Ezra, G. S.; Waalkens, H.; Wiggins, S. *J. Chem. Phys.* **2009**, 130, 164118. (b) Collins, P.; Carpenter, B. K.; Ezra, G. S.; Wiggins, S. *J. Chem. Phys.* **2013**, 139, 154108. (c) Collins, P.; Kramer, Z. C.; Carpenter, B. K.; Ezra, G. S.; Wiggins, S. *J. Chem. Phys.* **2014**, 141, 034111.
- (18) (a) Merrer, D. C.; Rablen, P. R. *J. Org. Chem.* **2005**, 70, 1630-1635. (b) Rablen, P. R.; Paiz, A. A.; Thuronyi, B. W.; Jones, M. *J. Org. Chem.* **2009**, 74, 4252-4261.

## CHAPTER 3.1

- (19) Zhou, J.; Schlegel, H. B. *J. Phys. Chem. A* **2009**, 113, 1453-1458.
- (20) (a) Schmittel, M.; Vavilala, C.; Jaquet, R. *Angew. Chem., Int. Ed.* **2007**, 46, 6911-6914. (b) Samata, D.; Rana, A.; Schmittel, M. *J. Org. Chem.* **2014**, 79, 2368-2376. (c) Samata, D.; Rana, A.; Schmittel, M. *J. Org. Chem.* **2014**, 79, 8435-8439.
- (21) Biswas, B.; Collins, S. C.; Singleton, D. A. *J. Am. Chem. Soc.* **2014**, 136, 3740-3743.
- (22) (a) Siebert, M. R.; Zhang, J. X.; Addepalli, S. V.; Tantillo, D. J.; Hase, W. L. *J. Am. Chem. Soc.* **2011**, 133, 8335-8343. (b) Siebert, M. R.; Manikandan, P.; Sun, R.; Tantillo, D. J.; Hase, W. L. *J. Chem. Theory Comput.* **2012**, 8, 1212-1222.
- (23) (a) Pemberton, R. P.; Hong, Y. J.; Tantillo, D. J. *Pure and Applied Chemistry* **2013**, 85, 1949-1957. (b) Hong, Y. J.; Tantillo, D. J. *Nature Chemistry* **2014**, 6, 104-111. (c) Pemberton, R. P.; Tantillo, D. J. *Chemical Science* **2014**, 5, 3301-3308.
- (24) (a) Carpenter, B. K. *J. Am. Chem. Soc.* **1995**, 117, 6336-6344. (b) Hrovat, D. A.; Fang, S.; Borden, W. T.; Carpenter, B. K. *J. Am. Chem. Soc.* **1997**, 119, 5253-5254. (c) Nummela, J. A.; Carpenter, B. K. *J. Am. Chem. Soc.* **2002**, 124, 8512-8513.
- (25) (a) Doubleday, C.; Bolton, K.; Hase, W. L. *J. Am. Chem. Soc.* **1997**, 119, 5251-5252. (b) Doubleday, C. *J. Phys. Chem. A* **2001**, 105, 6333-6341. (c) Doubleday, C.; Suhrada, C. P.; Houk, K. N. *J. Am. Chem. Soc.* **2006**, 128, 90-94.
- (26) (a) Chen, Z.; Nieves-Quinones, Y.; Waas, J. R.; Singleton, D. A. *J. Am. Chem. Soc.* **2014**, 136, 13122-13125. (b) Glowacki, D. R.; Orr-Ewing, A. J.; Harvey, J. N. *J. Chem. Phys.* **2011**, 134, 214508. (c) Sato, M.; Yamataka, H.; Komeiji, Y.; Mochizuki, Y.; Ishikawa, T.; Nakano, T. *J. Am. Chem. Soc.* **2008**, 130, 2396-2397. (d) Ruiz-Pernía, J. J.; Tuñón, I.; Moliner, V.; Hynes, J. T.;



## CHAPTER 3.1

- Roca, M. *J. Am. Chem. Soc.* **2008**, 130, 7477-7488. (e) Mann, D. J.; Halls, M. D. *Phys. Chem. Chem. Phys.* **2002**, 4, 5066-5071. (f) Bolton, K.; Hase, W. L.; Doubleday, C. *J. Phys. Chem. B* **1999**, 103, 3691-3698.
- (27) Case, D. A. et al., AMBER 14, University of California, San Francisco, **2014**.
- (28) Frisch, M. J. et al., Gaussian 09, Revision D.01, Gaussian Inc., Wallingford, CT, **2013**.
- (29) (a) Alhambra, C.; Gao, J. L.; Corchado, J. C.; Villa, J.; Truhlar, D. G. *J. Am. Chem. Soc.* **1999**, 121, 2253-2258. (b) Alhambra, C.; Corchado, J. C.; Sanchez, M. L.; Gao, J. L.; Truhlar, D. G. *J. Am. Chem. Soc.* **2000**, 122, 8197-8203. (c) Alhambra, C.; Corchado, J.; Sanchez, M. L.; Garcia-Viloca, M.; Gao, J.; Truhlar, D. G. *J. Phys. Chem. B* **2001**, 105, 11326-11340. (d) Truhlar, D. G.; Gao, J. L.; Garcia-Viloca, M.; Alhambra, C.; Corchado, J.; Sanchez, M. L.; Poulsen, T. D. *Int. J. Quantum Chem.* **2004**, 100, 1136-1152.
- (30) Peslherbe, G. H.; Wang, H. B.; Hase, W. L., *Adv. Chem. Phys.* **1999**, 105, 171-201.
- (31) (a) Garcia-Viloca, M.; Alhambra, C.; Truhlar, D. G.; Gao, J. L. *J. Comput. Chem.* **2003**, 24, 177-190. (b) Poulsen, T. D.; Garcia-Viloca, M.; Gao, J. L.; Truhlar, D. G. *J. Phys. Chem B* **2003**, 107, 9567-9578. (c) Tejero, I.; Garcia-Viloca, M.; Gonzalez-Lafont, A.; Lluch, J. M.; York, D. M. *J. Phys. Chem B* **2006**, 110, 24708-24719. (d) Kanaan, N.; Ferrer, S.; Marti, S.; Garcia-Viloca, M.; Kohen, A.; Moliner, V. *J. Am. Chem. Soc.* **2011**, 133, 6692-6702.
- (32) (a) Rideout, D. C.; Breslow, R. *J. Am. Chem. Soc.* **1980**, 102, 7816. (b) Breslow, R.; Guo, T. *J. Am. Chem. Soc.* **1988**, 110, 5613. (c) Breslow, R. *Acc. Chem. Res.* **1991**, 24, 159-164.

- (33) (a) Blake, J. F.; Lim, D.; Jorgensen, W. L. *J. Org. Chem.* **1994**, 59, 803-805. (b) Chandrasekhar, J.; Shariffskul, S.; Jorgensen, W. J. *J. Phys. Chem. B* **2002**, 106, 8078-8085. (c) Acevedo, O.; Jorgensen, W. L. *J. Chem. Theory Comput.* **2007**, 3, 1412-1419.
- (34) Jorgensen, W. L.; Chandrasekhar, J.; Madura, J. D.; Impey, R. W.; Klein, M. L. *J. Chem. Phys.* 1983, 79, 926-935.
- (35) Marenich, A. V.; Cramer, C. J.; Truhlar, D. G. *J. Phys. Chem. B* **2009**, 113, 6378-6396.
- (36) In the general case, step 2 would be preceded by a search for the TS region, which typically involves umbrella sampling to compute the potential of mean force along a reaction coordinate to find the region of highest free energy. We currently assume that the TS region is close to the saddle point determined in step 1.
- (37) Use of the gas phase saddle point in place of  $TS_w$  in steps 2-6 made a negligible difference in the final results for this test case. In general, however, a transition structure computed with implicit solvation is expected to be the better zero-order choice and we use  $TS_w$  in the subsequent description.
- (38) (a) Dapprich, S.; Komáromi, I.; Byun, K. S.; Morokuma, K.; Frisch, M. J. *J. Mol. Struct. (Theochem)* **1999**, 462, 1-21. (b) T. Vreven, T.; Byun, K. S.; Komáromi, I.; Dapprich, S.; Montgomery, J. A., Jr.; Morokuma, K.; Frisch, M. J. *J. Chem. Theory and Comput.* **2006**, 2, 815-26.
- (39) Hase, W. L.; Duchovic, R. J.; Hu, X.; Lim, K.; Lu, D.-h.; Peslherbe, G. H.; Swamy, K. N.; VandeLinde, S. R.; Wang, H.; Wolfe, R. J. "VENUS 96, a General Chemical Dynamics Computer Program", *QCPE671*.

## CHAPTER 3.1

(40) SPTS saddle points have  $3N_1 - 1$  vibrational frequencies instead of  $3N_1 - 7$  as in the gas phase. Translational and rotational motions of the solute are transformed into vibrational motions by interaction with surrounding solvent molecules.

(41) After 150 fs propagation in the product direction, the forming C-C bond lengths are  $< 1.59$  Å in all reactive trajectories. In the reactant direction, both C-C bonds are  $> 3.5$  Å after 150 fs.

(42) Mulliken charge distribution of reactant, TS and endo-product are calculated to support the zwitterionic character of the TS.

(43) (a) Eyring, H. *Trans. Faraday Soc.* **1938**, 34, 41-48. (b) Black, K.; Liu, P.; Xu, L.; Doubleday, C.; Houk, K. N. *Proc. Natl. Acad. Sci.* **2012**, 109, 12860-12865.

(44) The water molecules that form H-bond with the MVK is located by the criteria: 1. O(carbonyl)-O(water) distance is within 3.0 Å. 2. O(carbonyl)-H(water) is within 2.6 Å. 3. O(carbonyl)-H(water)- O(water) is higher than 180 degree

## 3.2 QM/QM' Direct Molecular Dynamics of Water-Accelerated Diels-Alder Reaction

### 3.2.1 Abstract

A QM/QM' direct molecular dynamics study of a water-accelerated Diels-Alder reaction in aqueous solution is reported. Cyclopentadiene and methyl vinyl ketone are known to react faster in water than in non-polar solvents. We have explored how polarization of water molecules afforded by PM3 influences the nature of the transition state, and the reaction dynamics. We compare the results with previous studies on QM/MM and QM/MM+3QM water simulations from our laboratory. Transition state sampling in vacuum PM3 water boxes indicates that the asynchronicity is 0.54 Å in QM/QM', as compared to 0.48 Å in QM/MM, and 0.54 Å in QM/MM+3QM water. The mean time gap between formation of two C-C bonds is 19 fs for QM/QM', compared to 20 fs for QM/MM, and 25 fs for QM/MM+3QM water. The samplings and time gaps are qualitatively consistent, indicating that water polarization is not significant in sampling and dynamics of bonding changes. The dynamics of hydrogen bonding between reacting molecules and water molecules was also analyzed. From reactants to transition states, H-bond shortening is 0.4 Å by QM/QM', while only 0.15 Å for QM/MM and QM/MM+3QM water. From reactants to transition states, the mean value of the H-bond angle increases by 19° in QM/QM', but only 4° in QM/MM, and 10° in QM/MM+3QM water. These suggest that water polarization is essential for the correct representation of dynamical formation of hydrogen bonding in the transition state by water reorientation. QM/QM' overestimates the hydrogen

bonding enhancement because of its underestimation of neutral hydrogen bonding within the reactants, a general deficiency of PM3.

### 3.2.2 Introduction

Solvent effects on chemical reactions are one of major developments in computational organic chemistry. Continuum polarization models (e.g. PCM, CPCM, SMD, etc.)<sup>1-4</sup> are generally used to compute solvent effects in solution-phase reaction calculations.<sup>5-10</sup> In recent years, trajectory calculations (or molecular dynamics, MD) for chemical processes with explicit solvation have been conducted.<sup>11-20</sup> These studies provide time-resolved information about how solvent molecules are involved in barrier climbing, and how nascent hot intermediates may lead to products without first achieving vibrational relaxation.

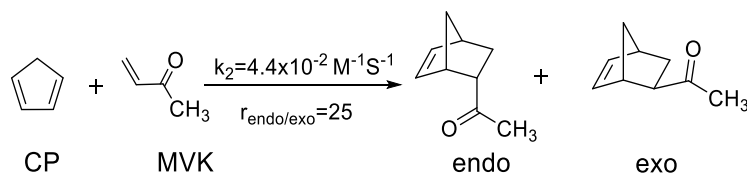
We have proposed a QM/MM method, called the solvent-perturbed transition state sampling (SPTSS) method, for quasiclassical direct-dynamics trajectory calculations in solution with explicit solvent.<sup>17</sup> The method samples initial conditions by including the effect of various instantaneous solvent configurations on the potential energy surface of the reaction. The method samples initial conditions quasiclassically. Zero-point energy is added to each real normal mode, plus a Boltzmann sampling of thermal energy with a random phase.<sup>21-23</sup> To test statistical convergence in the sampling, the method was previously applied to a classic water-accelerated Diels-Alder reaction, cyclopentadiene (CP) + methyl vinyl ketone (MVK), which is shown in **Scheme 3.2.1**.<sup>24</sup> The reaction was first reported by Breslow in 1980.<sup>25</sup> Jorgensen and Acevedo performed QM/MM Monte Carlo simulations, and gave strong evidence that the largest

contribution to the water-acceleration of Diels-Alder reactions comes from enhanced hydrogen bonding in the TS.<sup>26-29</sup> Our QM/MM MD simulations involved CP+MVK(+3 water) molecules in the QM region (M06-2X/6-31G(d) method), and the remaining water molecules in the MM region (TIP3P model). Enhancement of hydrogen bonding to the transition state was observed in our QM/MM MD simulations, with 14% trajectories showing reorientation of water molecules towards the carbonyl oxygen of MVK.<sup>17</sup>

In our previous study, the TIP3P water model, proposed by Jorgensen, was used to describe the bulk water. This model shows a good agreement with many experimental properties of liquid water, including density, heat of vaporization, isothermal compressibility, etc, and has been widely applied in many organic and biological systems.<sup>30,31</sup> Reaction dynamics in solution, however, in this case involves a transition state with charge separation, which could polarize its surrounding water molecules. TIP3P model is a fixed charge model and does not allow water polarization. We have explained the role of water polarization in MD simulations. We report a QM/QM' direct molecular dynamics of the water-accelerated Diels-Alder reaction, and compare this with our previous QM/MM and QM/MM+3QM water simulations, to see how polarization of water molecules influences the reaction dynamics. The PM3 method<sup>32</sup> was applied for the QM' region to describe water molecules. As reported by Stewart,<sup>33</sup> PM3 qualitatively reproduces molecular dipole moments for 125 compounds with an average 0.38 Deybe difference from experimental values. This suggests that PM3 gives a relatively accurate description of the charge distribution of molecules, as well as polarization, despite its approximation. Most importantly, it has been widely reported that the geometries of the PM3 hydrogen bonded complexes agree with

the high-resolution spectroscopic observations and high level *ab initio* calculations, although hydrogen bond lengths were underestimated by 0.1-0.2 Å.<sup>34-36</sup>

**Scheme 3.2.1.** Second-order rate constants and endo/exo product ratio for the CP + MVK Diels-Alder reaction in water at room temperature.



### 3.2.3 Computational Methods

Solvent-perturbed transition state sampling (SPTSS) was applied in the QM/QM' studies with AMBER,<sup>37</sup> Gaussian,<sup>38</sup> and Progdyn.<sup>11</sup> The full QM/QM' system is represented as a solvent sphere, with  $N$  atoms consisting of a small reacting zone ( $N_1$  reacting atoms treated by QM) and a large solvent zone ( $N_2=N-N_1$  solvent atoms treated by QM'). In current study, M06-2X/6-31G(d) and PM3 were used as QM and QM' methods, respectively. The protocol consists of six steps.

1. The M06-2X/6-31G(d) endo transition structure  $\text{TS}_w$  is computed in implicit water with SMD solvation model.<sup>4</sup>
2.  $\text{TS}_w$  is surrounded with a cubic solvent box (periodic boundary conditions, electrostatic cutoff is 10 Å), whose size is 12 Å from the mass center of the  $\text{TS}_w$  to one face of the solvent box. The size of the box was determined in an iterative method reported in our previous paper.<sup>17</sup> With  $\text{TS}_w$  fixed, the solvent is equilibrated for 200 ps with TIP3P water model in an NPT ensemble (fixed number of atoms, pressure, and temperature). RESP charges was applied on the  $\text{TS}_w$  during the equilibration.<sup>39</sup>

3. As solvent equilibration continues with fixed  $TS_w$ , 20 instantaneous frozen solvent coordinates and momenta are extracted and stored at 5 ps intervals. In each of the cubic solvent boxes, a solvent sphere was generated by removing the water molecules whose distance to the mass center of  $TS_w$  is larger than 12 Å.
4. For each frozen solvent configuration, the transition structure for the  $N_1$  reacting atoms is optimized using QM/QM' ONIOM scheme, keeping the  $N_2$  solvent atoms fixed. The number of SPTS saddle points,  $N_{SPTS}$ , equal to the number of frozen solvent configurations in step 3 ( $N_{SPTS}=20$ ).
5. At each SPTS saddle point, 10 sets of initial coordinates and momenta for the reacting system are selected quasiclassically by TS normal mode sampling at 300 K. The bound modes were the  $3N_1 - 1$  real frequencies of the reacting system, and the transition vector was the reaction coordinate. This gives initial conditions for  $10 \times N_{SPTS}$  trajectories ( $10 \times N_{SPTS}=200$ ).
6. All constraints on the frozen solvent zone are released, and 200 trajectories for the full system are propagated forward and backward from the sampled transition state, using velocity Verlet with a 1 fs step size in an NVE ensemble (fixed number of atoms, volume, and energy). Trajectories were stopped after 150 fs in each direction.

### 3.2.4 Results and Discussion

**Figure 3.2.1** shows the distribution of forming bond lengths of 200 sampled solvent-perturbed transition states (SPTSs) produced by TS normal mode sampling. The transition zone, defined as the 98% confidence interval of a forming bond distribution, was used



here to quantify the width of the distribution. **Figures 3.2.1a** to 1c show the forming bond length distributions and transition zones of the endo Diels-Alder reaction between CP and MVK, sampled using QM/MM, QM/MM+3QM water, and QM/QM' simulations, respectively. The asynchronicity, defined here as the difference between mean bond lengths in the transition zone, is 0.48 Å in QM/MM, 0.54 Å in QM/MM+3QM water, and 0.54 Å in QM/QM'. The transition state sampled in QM/QM' is on average 0.02 Å earlier than that in QM/MM+3QM water. The larger number of early transition states sampled in QM/QM' suggests that PM3 water model increase the amount of charge transfer between CP and MVK.

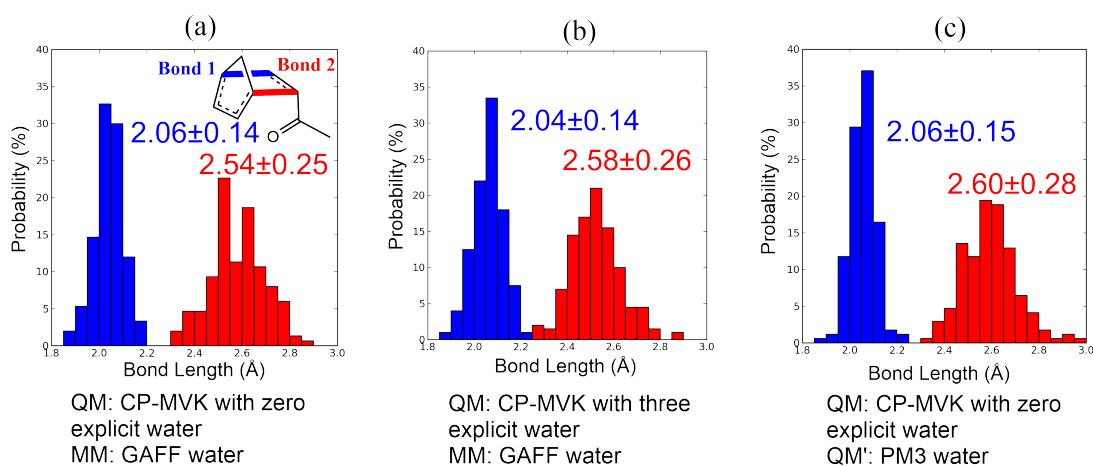


**Figure 3.2.1.** Distribution of forming bond lengths of 200 SPTSs of the endo Diels-Alder reaction between CP and MVK, sampled using (a) QM/MM, (b) QM/MM+3QM water, and (c) QM/QM' method. Forming bonds are shown as blue and red dotted lines on the Figure.

**Table 3.1.1** shows the time gaps for bond formation,<sup>40-43</sup> defined as the difference between the times at which the forming bond lengths first drop below 1.59 Å. Subsequent vibrations above 1.59 Å are ignored. TS distributions in **Figure 3.2.1** evolve into distributions of time gaps that reflect the bonding asynchronicities in a time-resolved fashion. The mean time gap is 20 fs

for QM/MM, 25 fs for QM/MM+3QM water, and 19 fs for QM/QM'. The differences of mean time gap among the three methods (1-6 fs) are smaller than the standard deviations (11-15 fs), which indicates that three methods give quantitatively consistent results. The time gap distributions are broad with tails extending to 82 fs in QM/MM, 88 fs in QM/MM+3QM water, and 107 fs in QM/QM'. We have proposed that QM/MM methods have a strong preference for zwitterionic stabilization.<sup>17</sup> Here, the QM/QM' method displays a similar trend. The time gaps of more than 90% trajectories are within the lifetime of transition state (60 fs), indicating that the reaction proceeds in a dynamically concerted fashion. It is interesting that these moderately polar reactions do involve some dynamically stepwise trajectories.

**Table 3.2.1.** Time gaps (fs) for bond formation, and maximum gap.<sup>a</sup>

	QM/MM	QM/MM+3QM Water	QM/QM'
Mean gap $\pm\sigma^b$	20 $\pm$ 11	25 $\pm$ 14	19 $\pm$ 15
Maximum gap	82	88	107

<sup>a</sup>Vibrational period of a C-C single bond is 30-40 fs. <sup>b</sup>Std. Dev.

The dynamics of preferential H-bonding is found to be significant in the TS for the CP + MVK Diels-Alder reaction in water. Figure 3.2.2 shows the distribution of H-bond lengths and angles in QM/MM, QM/MM+3 QM water, and QM/QM' results. From reactants to transition states, the mean H-bond length decreases from 1.93 Å to 1.78 Å in QM/MM, from 2.02 Å to 1.88 Å in QM/MM+3QM water, and from 2.21 Å to 1.82 Å in QM/QM'. All three methods show a substantial hydrogen bonding enhancement. The H-bond shortening for QM/MM and

QM/MM+3QM water method is about 0.15 Å, while that for QM/QM' is nearly 0.4 Å. This shows a much stronger H-bonding enhancement using QM/QM' method. In addition, the distribution of H-bond lengths in reactants obtained by QM/QM' is much broader than those by the other two methods (shown in Figures 3.2.2a-c). These results likely originate from the underestimation of neutral hydrogen bond by the QM' method (PM3 model), which has been discussed in many studies.<sup>34-36</sup> The mean H-bond lengths in the transition states are 1.78 Å in QM/MM, 1.88 Å in QM/MM+3QM water, and 1.82 Å in QM/QM'. A fixed charge model, TIP3P, was used in MM. While the model gives an excellent description of neutral H-bonding, it may overestimate the strength of H-bonding in the TS with zwitterionic character. The QM/MM+3QM water tends to provide a good model of H-bonding interaction in the TS because high level QM methods were involved for the TS-water complex. The PM3 model gives a result better than TIP3P because PM3 involves polarization in water molecules.

**Figures 3.2.2d-f** show the distribution of the H-bond angles (O(carbonyl)-H(water)-O(water)) in the reactant, the TS, and the product. From reactants to transition states, the mean value of the H-bond angle increases by 4° in QM/MM, 10° in QM/MM+3QM water, and 19° in QM/QM'. The increase in angles towards 180° indicates a reorientation of water molecules for H-bonding enhancement. The reorientation involves a process in which water molecules break old hydrogen bonds to other waters and form new hydrogen bonds to the TS. This is consistent with “water jump” model described by Hynes, which was observed in liquid water using femtosecond spectroscopy.<sup>44,45</sup> The water reorientation was not significant with QM/MM, because the TIP3P water forms strong hydrogen bonds with

reactants. Hydrogen bonding sites of the carbonyl oxygen of MVK are already occupied, and thus the reorientation seldom occurs. In contrast, the QM or QM' treatment of water molecules lead to observation of water reorientation, because hydrogen bonds between water and reactants are relatively loose, and get much stronger in the transition state because of polarization. However, the large magnitude of water reorientation observed for PM3 water model is likely resulted from a poor description of neutral hydrogen bonds in the reactants.

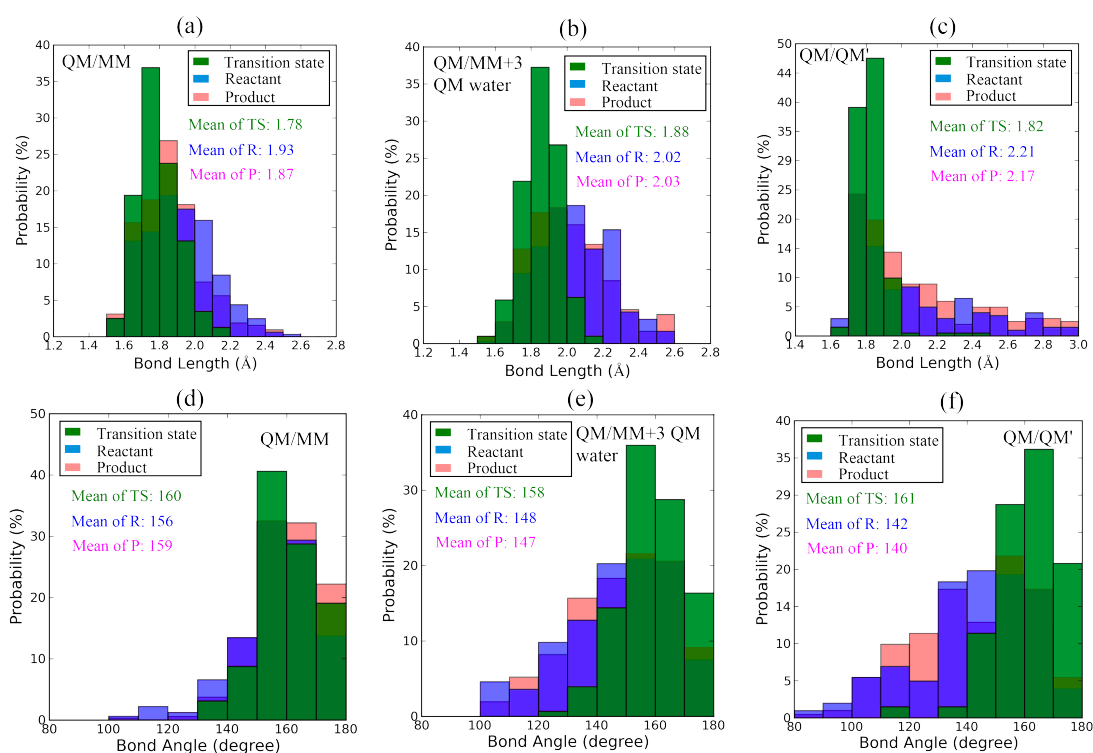


**Figure 3.2.2.** Distribution of hydrogen bonding lengths (O(carbonyl)-H(water) distance) and hydrogen bonding angles (O(carbonyl)-H(water)-O(water) angle) in transition states (in green, at 0 fs), reactants (in blue, at -150 fs), and products (in pink, at 150 fs). (a), (b), and (c) are distributions of H-bond lengths in QM/MM, QM/MM+3QM water, and QM/QM' methods. (d), (e), and (f) are distributions of H-bonding angles in QM/MM, QM/MM+3QM water, and

QM/QM' methods. 200 reactive trajectories from QM/MM and QM/QM', and 150 reactive trajectories from QM/MM+3 QM waters are used for the analysis.

### 3.2.5 Conclusion

We have studied the water-accelerated Diels-Alder reaction of CP+MVK in aqueous solution using QM/QM' direct dynamics simulations. Solvent-perturbed transition state sampling and reaction dynamics of cycloaddition have been performed to explore how polarization of water molecules influences trajectories. We have compared the results with our previous studies on QM/MM and QM/MM+3QM water simulations. The asynchronicity, defined here as the difference between mean bond lengths in the transition zone, is 0.48 Å in QM/MM, and 0.54 Å with QM/MM+3QM water, or QM/QM'. The mean time gap is 20 fs for QM/MM, 25 fs for QM/MM+3QM water, and 19 fs for QM/QM'. Water polarization is not significant in transition state sampling or for dynamics of bonding changes. Dynamics of hydrogen bonding shows that H-bond shortens from reactant to TS by 0.15 Å with QM/MM and QM/MM+3QM water, and 0.4 Å for QM/QM'. The mean value of the H-bond angle increases along the reaction. Computational models that include polarization for water molecules is important for studying the detail of hydrogen bonding dynamics. QM/QM' overestimate the hydrogen bonding enhancement because of its poor description of neutral hydrogen bonding in reactant. Our results suggest that water polarization is not significant in transition state sampling and dynamics of reactant bonding changes, but is essential for the observation of H-bond reorientation of water molecules adjacent to the reacting molecules in reactive trajectories

**3.2.6 Reference**

- (1) Miertuš, S.; Scrocco, E.; Tomasi, J. *Chem. Phys.* **1981**, 55, 117-129.
- (2) Tomasi, J.; Mennucci, B.; Cancès, E. *J. Mol. Struct: THEOCHEM* **1999**, 464, 211-226.
- (3) Barone, V.; Cossi, M. *J. Phys. Chem. A* **1998**, 102, 1995-2001.
- (4) Marenich, A. V.; Cramer, C. J.; Truhlar, D. G. *J. Phys. Chem. B* **2009**, 113, 6378-6396.
- (5) Onsager, L. *J. Am. Chem. Soc.* **1936**, 58, 1486-1493.
- (6) Kirkwood, J. G. *J. Chem. Phys.* **1934**, 2, 351-361.
- (7) Foresman, J. B.; Keith, T. A.; Wiberg, K. B.; Snoonian, J.; Frisch, M. J. *J. Phys. Chem.* **1996**, 100, 16098-16104.
- (8) Cramer, C. J.; Truhlar, D. G. *Acc. Chem. Res.* **2008**, 41, 760-768.
- (9) Roux, B. t.; Simonson, T. *Biophys. Chem.* **1999**, 78, 1-20.
- (10) Cramer, C. J.; Truhlar, D. G. *Chem. Rev.* **1999**, 99, 2161-2200.
- (11) Oyola, Y.; Singleton, D. A. *J. Am. Chem. Soc.* **2009**, 131, 3130-.
- (12) Glowacki, D. R.; Liang, C. H.; Marsden, S. P.; Harvey, J. N.; Pilling, M. J. *J. Am. Chem. Soc.* **2010**, 132, 13621-13623.
- (13) Biswas, B.; Collins, S. C.; Singleton, D. A. *J. Am. Chem. Soc.* **2014**, 136, 3740-3743.
- (14) Chen, Z.; Nieves-Quinones, Y.; Waas, J. R.; Singleton, D. A. *J. Am. Chem. Soc.* **2014**, 136, 13122-13125.
- (15) Carpenter, B. K.; Harvey, J. N.; Orr-Ewing, A. J. *J. Am. Chem. Soc.* **2016**, 38, 4695-4705
- (16) Biswas, B.; Singleton, D. A. *J. Am. Chem. Soc.* **2015**, 137, 14244-14247.
- (17) Yang, Z.; Doubleday, C.; Houk, K. N. *J. Chem. Theory Comput.* **2015**, 11, 5606-5612.

## CHAPTER 3.2

- (18) Glowacki, D. R.; Rose, R. A.; Greaves, S. J.; Orr-Ewing, A. J.; Harvey, J. N. *Nature Chem.* **2011**, 3, 850-855.
- (19) Glowacki, D. R.; Orr-Ewing, A. J.; Harvey, J. N. *J. Chem. Phys.* **2011**, 134, 214508.
- (20) Orr-Ewing, A. J.; Glowacki, D. R.; Greaves, S. J.; Rose, R. A. *J. Phys. Chem. Lett.* **2011**, 2, 1139-1144.
- (21) Doubleday, C.; Bolton, K.; Hase, W. L. *J. Phys. Chem. A* **1998**, 102, 3648-3658.
- (22) Black, K.; Liu, P.; Xu, L.; Doubleday, C.; Houk, K. N. *Proc. Natl. Acad. Sci.* **2012**, 109, 12860-12865.
- (23) Bunker, D. L.; Hase, W. L. *J. Chem. Phys.* **1973**, 59, 4621-4632.
- (24) Breslow, R.; Guo, T. *J. Am. Chem. Soc.* **1988**, 110, 5613-5617.
- (25) Rideout, D. C.; Breslow, R. *J. Am. Chem. Soc.* **1980**, 102, 7816-7817.
- (26) Acevedo, O.; Jorgensen, W. L. *J. Chem. Theory Comput.* **2007**, 3, 1412-1419.
- (27) Blake, J. F.; Lim, D.; Jorgensen, W. L. *J. Org. Chem.* **1994**, 59, 803-805.
- (28) Blake, J. F.; Jorgensen, W. L. *J. Am. Chem. Soc.* **1991**, 113, 7430-7432.
- (29) Jorgensen, W. L.; Blake, J. F.; Lim, D.; Severance, D. L. *J. Chem. Soc., Faraday Trans.* **1994**, 90, 1727-1732.
- (30) Jorgensen, W. L.; Chandrasekhar, J.; Madura, J. D.; Impey, R. W.; Klein, M. L. *J. Chem. Phys.* **1983**, 79, 926-935.
- (31) Mark, P.; Nilsson, L. *J. Phys. Chem. A* **2001**, 105, 9954-9960.
- (32) Stewart, J. J. P. *J. Comput. Chem.* **1989**, 10, 209-220.
- (33) Stewart, J. J. P. *J. Comput. Chem.* **1989**, 10, 221-264.

- (34) Jurema, M. W.; Shields, G. C. *J. Comput. Chem.* **1993**, 14, 89-104.
- (35) Geerke, D. P.; Thiel, S.; Thiel, W.; van Gunsteren, W. F. *Phys. Chem. Chem. Phys.* **2008**, 10, 297-302.
- (36) Monard, G.; Bernal-Uruchurtu, M. I.; van der Vaart, A.; Merz, K. M.; Ruiz-López, M. F. *J. Phys. Chem. A* **2005**, 109, 3425-3432.
- (37) Pearlman, D. A.; Case, D. A.; Caldwell, J. W.; Ross, W. S.; Cheatham, T. E.; DeBolt, S.; Ferguson, D.; Seibel, G.; Kollman, P. *Comput. Phys. Commun.* **1995**, 91, 1-41.
- (38) Frisch, M. J.; Trucks, G. W.; Schlegel, H. B.; Scuseria, G. E.; Robb, M. A.; Cheeseman, J. R.; Scalmani, G.; Barone, V.; Mennucci, B.; Petersson, G. A.; et al. *Gaussian 09*, Gaussian, Inc.: Wallingford, CT, USA, 2009.
- (39) Bayly, C. I.; Cieplak, P.; Cornell, W.; Kollman, P. A., *J. Phys. Chem.* **1993**, 97, 10269-10280.
- (40) Hong, X.; Bercovici, D. A.; Yang, Z.; Al-Bataineh, N.; Srinivasan, R.; Dhakal, R. C.; Houk, K. N.; Brewer, M. *J. Am. Chem. Soc.* **2015**, 137, 9100-9107.
- (41) Patel, A.; Chen, Z.; Yang, Z.; Gutiérrez, O.; Liu, H.-w.; Houk, K. N.; Singleton, D. A. *J. Am. Chem. Soc.* **2016**, 138, 3631-3634.
- (42) Yang, Z.; Yu, P.; Houk, K. N. *J. Am. Chem. Soc.* **2016**, 138, 4237-4242.
- (43) Xu, L.; Doubleday, C. E.; Houk, K. N. *J. Am. Chem. Soc.* **2011**, 133, 17848-17854.
- (44) Laage, D.; Hynes, J. T. *J. Phys. Chem. B* **2008**, 112, 14230-14242.
- (45) Jimenez, R.; Fleming, G. R.; Kumar, P. V.; Maroncelli, M. *Nature* **1994**, 369, 471-473.



### 3.3 Chronology of C-H $\cdots$ O Hydrogen Bonding of the Phosphoric Acid-Catalyzed Allylboration of Benzaldehyde

#### 3.3.1 Abstract

CH $\cdots$ O hydrogen bonds involving formyl groups have been invoked as a crucial factor controlling many asymmetric transformations. We have conducted quasi-classical direct molecular dynamics simulations on the phosphoric acid-catalyzed allylboration of benzaldehyde to understand the synergy between the phosphoric acid OH $\cdots$ O hydrogen bond and the secondary CH $\cdots$ O formyl hydrogen bond as the reaction occurs, which can not be accessible by IRC. In the gas phase, both the CH $\cdots$ O and OH $\cdots$ O hydrogen bonds are enhanced from reactants to transition states. In toluene, the trend of H-bond enhancement is observed with a smaller magnitude because of solvent caging. The strength of the formyl hydrogen bond in the TS, a second CH $\cdots$ O interaction between the P=O oxygen and *ortho*-hydrogen of the phenyl ring and the OH $\cdots$ O hydrogen bond were determined using quantum mechanical calculations (4.6, 1.0 and 14.5 kcal mol<sup>-1</sup> respectively).

#### 3.3.2 Introduction

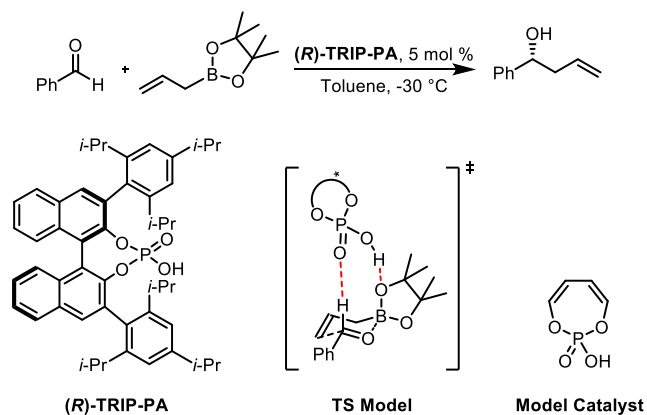
In a series of communications in 1997 and after, E. J. Corey proposed the importance of formyl CH $\cdots$ O hydrogen bonds for transition state stabilization in enantioselective asymmetric reactions.<sup>1-5</sup> This interaction was proposed based on X-ray crystal structures of aldehyde-Lewis acid complexes that contained formyl H to oxygen distances well within the sum of the van der Waals radii.<sup>1</sup> Since these pioneering studies, computational work has revealed that the formyl

hydrogen bond plays a crucial role in many asymmetric transformations<sup>6</sup> including aldol,<sup>7-9</sup> allylboration,<sup>10-11</sup> aza-ene-type,<sup>12</sup> cycloaddition,<sup>13</sup> hydrohydroxyalkylation<sup>14</sup> and propargylation<sup>15</sup> reactions. X-ray crystallographic evidence has been debated, but seems in favor of the importance of CH $\cdots$ X interactions.<sup>16</sup>

Goodman and co-workers<sup>10</sup> found that Antilla's BINOL-derived phosphoric acid-catalyzed asymmetric allylboration of aldehydes<sup>17</sup> (**Scheme 3.2.1**) proceeds via a six-membered transition structure (TS) in which the Brønsted acidic site of the catalyst interacts with the pseudoaxial oxygen of the cyclic boronate and the P=O oxygen interacts with the formyl proton (TS Model, **Scheme 3.3.1**).

We have now conducted direct molecular dynamics (MD) simulations on this reaction to understand more about the timing and nature of this formyl hydrogen bond to O=P. Quantum mechanical calculations were also performed to provide an estimate of the strength of this interaction in the TS. The reaction of interest involves TRIP-PA catalysis of the allylboration of benzaldehyde shown in **Scheme 3.3.1**. For the computational studies, buta-1,3-diene-1,4-diol-phosphoric acid was used as a model for the full catalyst system (Model Catalyst, **Scheme 3.3.1**). Previous computational studies have shown that this truncated catalyst is a reliable model for BINOL-derived phosphoric acids.<sup>10,15,18-22</sup>

**Scheme 3.3.1.** Asymmetric Allylboration of Benzaldehyde.



### 3.3.3 Computational Methods

Direct molecular dynamics (MD) simulations were performed for the allylboration of benzaldehyde using our model catalyst (**Scheme 3.3.1**) in the gas phase and in toluene. We initialized 150 quasiclassical trajectories (QCTs) in the gas phase within the region of the potential energy surface near the transition structure. Zero-point energy was added to each sampled TS for each real normal mode, along with a Boltzmann sampling of thermal energy available at 300 K with a random phase.<sup>23,24</sup> The trajectories were propagated forward and backward, for 150 fs in each direction. The classical equations of motion were integrated with a velocity-Verlet algorithm using Singleton's program ProgDyn,<sup>25</sup> with the energies and derivatives computed on the fly by the B3LYP/6-31G(d) method using Gaussian 09. The step length for integration was 1 fs. When 150 QCTs were propagated in the gas phase, 142 of them were productive, and 8 recrossed.

For dynamics in toluene, solvent-perturbed transition state sampling protocol was applied.<sup>26,27</sup> Twenty-five solvent configurations were sampled with frozen TSs using classical MD. In each snapshot, the transition structure was optimized using the QM/MM method in

Gaussian, with B3LYP/6-31G(d) applied for QM and GAFF for MM. Frequencies for each transition structure were calculated, and TS normal mode sampling was performed to obtain a Boltzmann distribution of TS geometries for dynamics. This is defined as a solvent-perturbed transition state (SPTS), which is used to initialize trajectories in a solvent box.<sup>26</sup> Twenty-five QCTs were propagated in toluene with the B3LYP/6-31G(d)/GAFF method forward and backward for 150 fs in each direction. Twenty-two were productive, and three recrossed.

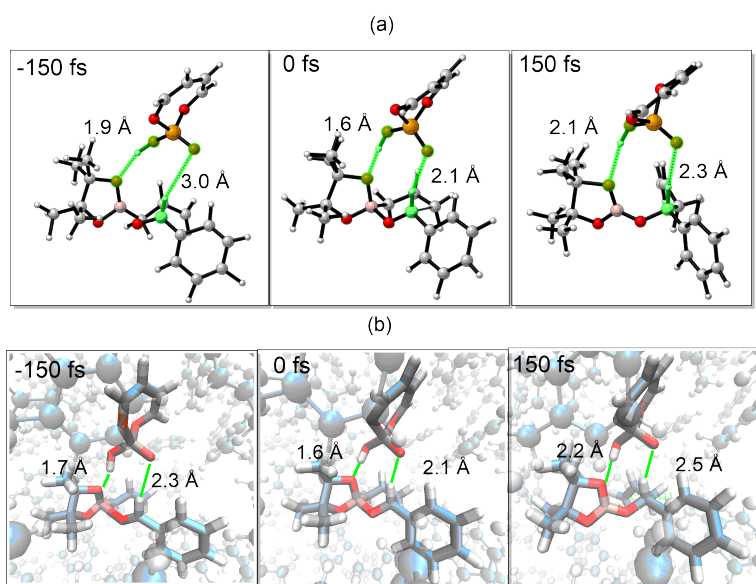
The strength of the formyl hydrogen bond (H-bond) was determined using quantum mechanical calculations performed with Gaussian 09 (Revision D.01).<sup>28</sup> All geometries were optimized using the B3LYP density functional,<sup>29,30</sup> and the 6-31G(d) basis set. Single point energies were calculated using M06-2X<sup>31</sup> and the polarized, triple- $\zeta$  valence quality def2-TZVPP basis set.<sup>32</sup> Computed structures were illustrated with CYLView.<sup>33</sup> To ensure that the B3LYP TS geometries were reliable, the allylboration of benzaldehyde TS was reoptimized using M06-2X. Superposition of the six reacting ring atoms and the catalyst phosphorous atom in these TSs allowed calculation of an RMSD value of 0.09 Å, suggesting minimal geometric change between the 2 TSs.

### 3.3.4 Results and Discussion

Direct dynamics simulations were conducted to study the timing of changes in H-bonding, that we call the chronology of the benzaldehyde formyl H-bond to O=P (CH $\cdots$ O) and the phosphoric acid hydrogen bond to the boronate O (OH $\cdots$ O) in the gas phase and in toluene.

**Figure 3.3.1a** shows the snapshots of a typical productive trajectory in the gas phase. The

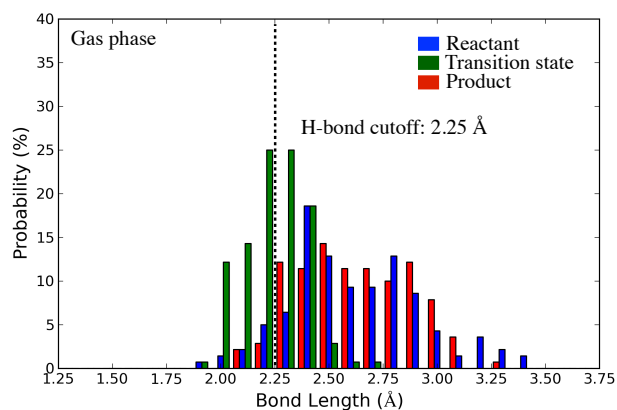
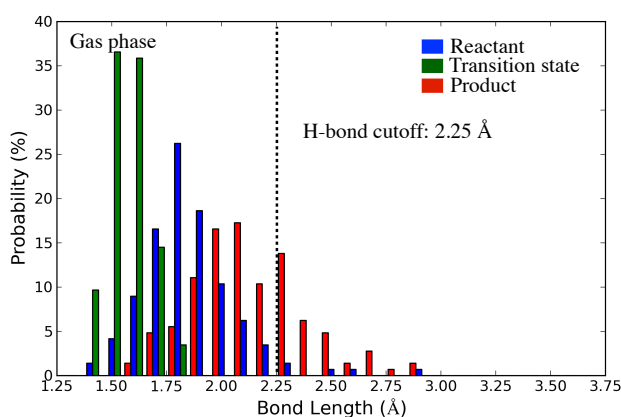
phosphoric acid catalyst stabilizes the transition state by H-bonding to the boronate O. The boronate ester becomes partially negative in the TS as the aldehyde O forms a bond to B. The boronate O becomes a good H-bond acceptor. At the same time, the formyl group becomes more positive and becomes a CH H-bond donor. For this trajectory, the length of the CH $\cdots$ O distance is 3.0 Å at -150 fs (hardly an H-bond at all), 2.1 Å at 0 fs, and 2.3 Å at 150 fs. In comparison, the length of the OH $\cdots$ O H-bond is 1.9 Å at -150 fs, 1.6 Å at 0 fs, and 2.3 Å at 150 fs. From -150 fs to 0 fs, the CH $\cdots$ O H-bond decreases by 0.9 Å, and the OH $\cdots$ O H-bond decreases by 0.3 Å. This indicates that both hydrogen bonds are enhanced in the transition state. **Figure 3.3.1b** displays the snapshots for a typical productive trajectory in toluene. The length of the CH $\cdots$ O H-bond is 2.3 Å at -150 fs, 2.1 Å at 0 fs and 2.5 Å at 150 fs, while that of the OH $\cdots$ O H-bond is 1.7 Å at -150 fs, 1.6 Å at 0 fs, and 2.2 Å at 150 fs. A smaller magnitude of enhancement is observed relative to the gas phase, which is likely caused by the solvent caging effect of toluene molecules.



**Figure 3.3.1.** Snapshots for typical reactive trajectories in the catalyzed allylboration of benzaldehyde (a) in the gas phase, and (b) in toluene.

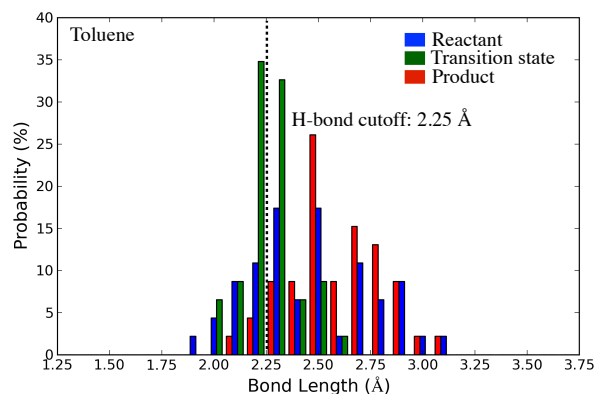
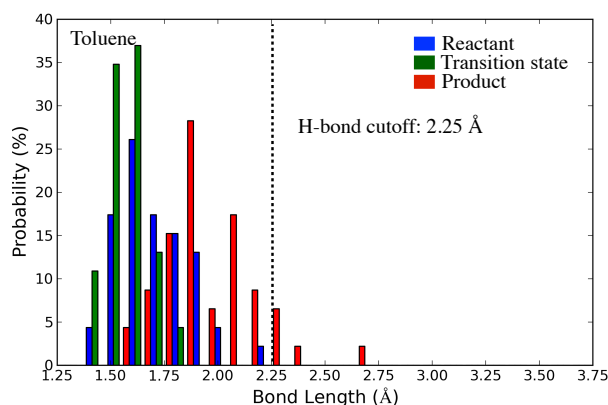
The statistics of the CH $\cdots$ O and OH $\cdots$ O distances in the gas phase are shown in Figure 3.3.2a and 2b, respectively. In each trajectory, the geometries at -150 fs, 0 fs, and 150 fs are defined as reactant, transition state and product, respectively. **Figure 3.3.2a** shows that in the gas phase, the distribution of the CH $\cdots$ O distances in the transition states range from 1.8 Å to 2.8 Å, which is about half as narrow as that in the reactant or products (from 1.8 Å to 3.5 Å). Here we define the H-bond cutoff as 2.25 Å.<sup>34</sup> The percentage of trajectories possessing a CH $\cdots$ O H-bond is 8% in reactants, 53% in transition states, and 5% in products. This shows a significant increase in the percentage of CH $\cdots$ O H-bonds from reactant to transition state. **Figure 3.3.2b** shows that the OH $\cdots$ O H-bond lengths of the transition state range from 1.3 Å to 2.0 Å, which is also about half as narrow as that in reactants or products (from 1.3 Å to 3.0 Å). The percentage of trajectories involving H-bond is 95% in reactants, 100% in transition states, and 70% in products. This indicates that the OH $\cdots$ O H-bond is formed in most trajectories from reactant to the TS. The average distance of the OH $\cdots$ O H-bond is 1.9 Å for reactants, 1.6 Å for transition states, and 2.2 Å for products. This indicates an enhancement of the OH $\cdots$ O H-bond from reactant to the TS.

(a) CH $\cdots$ O Hydrogen Bond

(b) OH $\cdots$ O Hydrogen Bond

**Figure 3.3.2.** Distribution of (a) benzaldehyde formyl hydrogen bond (CH $\cdots$ O) distances and (b) phosphoric acid hydrogen bond (OH $\cdots$ O) distances in the gas phase at reactants, transition states, and products. In each trajectory, the transition state is at 0 fs, and the reactants and products are defined as structures at -150 fs, and 150 fs, respectively. H-bond cutoff is set as 2.25 Å.

As shown in **Figure 3.3.3**, in toluene, the percentage of trajectories possessing a CH $\cdots$ O H-bond is 28% in reactants, 50% in the TS, and 8% in products, while the average distance of the OH $\cdots$ O H-bond lengths is 1.7 Å for reactants, 1.5 Å for transition states, and 1.9 Å for products. The enhancements of both CH $\cdots$ O and OH $\cdots$ O hydrogen bonds are also observed in toluene, even though with a smaller magnitude for the CH $\cdots$ O H-bond.

(a) CH $\cdots$ O Hydrogen Bond(b) OH $\cdots$ O Hydrogen Bond

**Figure 3.3.3.** Distribution of (a) benzaldehyde formyl hydrogen bond (CH $\cdots$ O) distances and (b) phosphoric acid hydrogen bond (OH $\cdots$ O) distances in toluene at reactants, transition states, and products. In each trajectory, the transition state is at 0 fs, and the reactants and products are defined as structures at -150 fs, and 150 fs, respectively. H-bond cutoff is set as 2.25 Å.

**Figure 3.3.4** shows the average of CH $\cdots$ O and OH $\cdots$ O distances versus time. Both bond lengths decrease from reactant to transition state, and then increase until the formation of products. This indicates the enhancement of both hydrogen bonds during the allylboration of benzaldehyde. This synergy results from a partial charge separation as the B-O bond forms between the allylboronate and benzaldehyde in the transition state. The charge separation



increase the acidity of the benzaldehyde hydrogen and the basicity of the allylboronate oxygen. This reinforces the formation of both  $\text{CH}\cdots\text{O}$  and  $\text{OH}\cdots\text{O}$  hydrogen bonds. The charge separation decreases, however, as the product forms, which is accompanied by a change of the hybridization state of the carbonyl carbon from  $\text{sp}^2$  to  $\text{sp}^3$ . This causes the decline in both hydrogen bond lengths from TS to product. Other possibilities, such as statistical fluctuation and entropic effects, were excluded as reasons for the observed bond length decrease.

We also investigated the difference between the averaged dynamics motion and the IRC. Singleton recently pointed out that the difference between hydrogen and heavy atoms results in their different time scales of motion.<sup>35</sup> This makes the dynamical behaviors of trajectories sometimes deviate from what IRC would expect. Our results show that the IRC does not reveal the enhancement of hydrogen bonds during the reaction course, but trajectories do. This highlights the importance of time-resolved studies in the elucidation of reaction mechanisms.

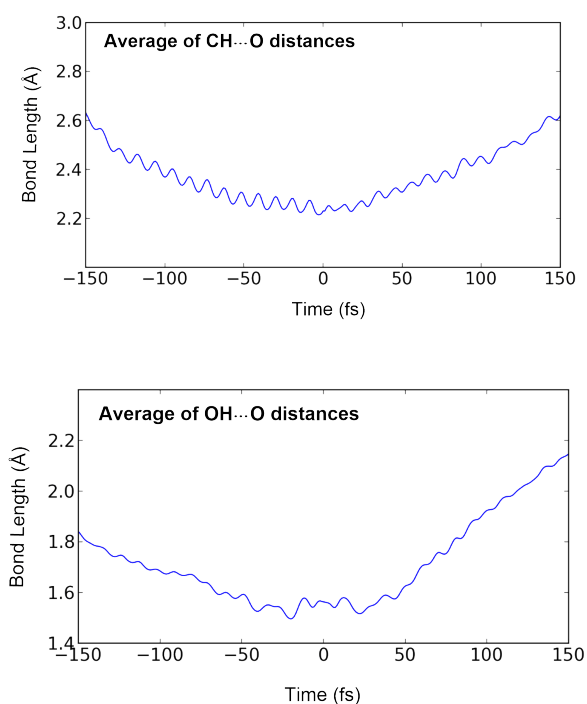


**Figure 3.3.4.** Dynamics of averaged CH $\cdots$ O and OH $\cdots$ O distances in the gas phase. One hundred and forty two product trajectories were averaged.

CH $\cdots$ O H-bond is a weak interaction that might be dynamically affected by neighboring solvent molecules. Consequently, we investigated the evolution of CH $\cdots$ O H-bond from reactant to the transition state for trajectories in the gas phase and in toluene. As shown in **Figure 3.3.5**, in the gas phase, the percentage of trajectories possessing CH $\cdots$ O H-bond is low (8%), and keeps increasing until it reaches the maximum (about 60%) around the transition state. In contrast, for trajectories in toluene, the percentage fluctuates between 20% and 40% from reactant to transition state. This suggests that toluene molecules favor the formation of CH $\cdots$ O H-bond in reactant by keeping two reacting molecules in one solvent cage, but detracts from H-bonding in the TS. Our results only provide a qualitative understanding because of the limited number of trajectories in toluene.

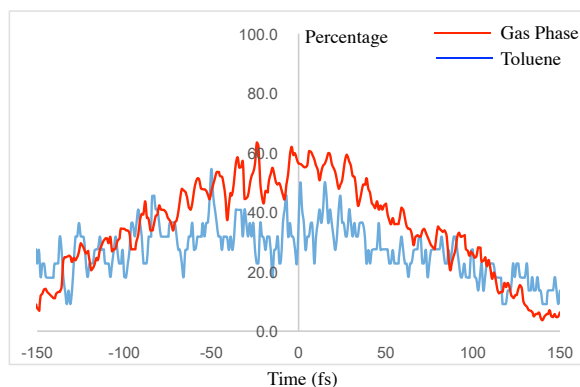


**Figure 3.3.5.** Evolution of percentage of trajectories possessing CH $\cdots$ O hydrogen bonds in the gas phase and in toluene. The H-bond criteria is defined as 2.25 Å.

To provide an estimate of the strength of the formyl hydrogen bond in the TS, quantum mechanical calculations were also performed (**Figure 3.3.6**). Allylboronic acid pinacol ester was removed from the gas phase TS, TS-1, and without further optimization, the energy of the catalyst-aldehyde complex was evaluated. This energy value was compared to the sum of the energy of the individual unoptimized fragments to determine the interaction energy between them (5.6 kcal mol $^{-1}$ , **Figure 3.3.6**). However, the P=O of the catalyst also interacts with the *ortho*-hydrogen of the phenyl ring. TS-2 (aldehyde = ethanal) was located in which the *ortho*-hydrogen interaction was absent and, using the same process as outlined above, the interaction energy was calculated to be 4.6 kcal mol $^{-1}$  (**Figure 3.3.6**). Therefore, the strength of the formyl hydrogen bond and the second CH $\cdots$ O interaction are approximately 4.6 and 1.0 kcal mol $^{-1}$  respectively. The OH $\cdots$ O hydrogen bond strength was estimated to be 14.5 kcal mol $^{-1}$  by measuring the interaction energy between the allylboronic acid pinacol ester and model phosphoric acid catalyst in TS-1.

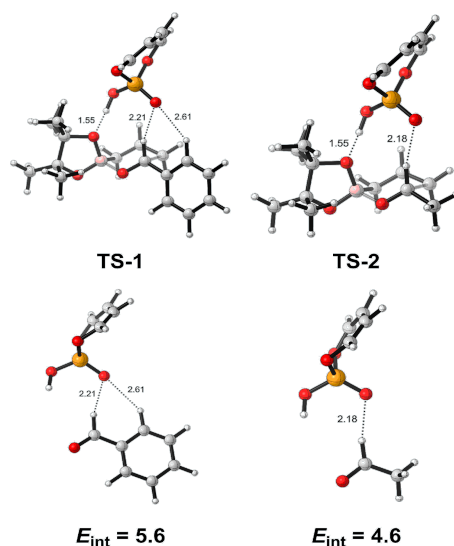


**Figure 3.3.6.** Catalyst-aldehyde interaction energies for TS-1 (aldehyde = benzaldehyde) and TS-2 (aldehyde = ethanal). M06-2X/def2-TZVPP//B3LYP/6-31G(d). All energies in kcal mol<sup>-1</sup>.

### 3.3.5 Conclusion

Molecular dynamics simulations on the phosphoric acid-catalyzed allylboration of benzaldehyde have shown that in the gas phase and toluene, a synergy between the enhancement of both the formyl hydrogen bond (CH $\cdots$ O) and the phosphoric acid hydrogen bond (OH $\cdots$ O) occurs in the TS relative to the reactants. Toluene molecules favor the formation of the CH $\cdots$ O H-bond in the reactant by keeping two reacting molecules in one solvent cage, but diminish the further enhancement of CH $\cdots$ O H-bonds in the TS. The strengths of the formyl hydrogen bond in the TS, and of the CH $\cdots$ O interaction between the P=O oxygen and *ortho*-hydrogen of the phenyl ring and the OH $\cdots$ O hydrogen bond were determined using quantum mechanical calculations and were found to be 4.6, 1.0, and 14.5 kcal mol<sup>-1</sup>, respectively.

**3.3.6 Reference**

- (1) Corey, E. J.; Rohde, J. J.; Fischer, A.; Azimioara, M. D. *Tetrahedron Lett.* **1997**, 38, 33–36.
- (2) Corey, E. J.; Rohde, J. J. *Tetrahedron Lett.* **1997**, 38, 37–40.
- (3) Corey, E. J.; Barnes-Seeman, D.; Lee, T. W. *Tetrahedron Lett.* **1997**, 38, 1699–1702.
- (4) Corey, E. J.; Barnes-Seeman, D.; Lee, T. W. *Tetrahedron Lett.* **1997**, 38, 4351–4354.
- (5) Corey, E. J.; Lee, T. W. *Chem. Commun.* **2001**, 1321–1329.
- (6) Johnston, R. C.; Cheong, P. H.-Y. *Org. Biomol. Chem.* **2013**, 11, 5057–5064.
- (7) Paton, R. S.; Goodman, J. M. *Org. Lett.* **2006**, 8, 4299–4302.
- (8) Paton, R. S.; Goodman, J. M. *J. Org. Chem.* **2008**, 73, 1253–1263.
- (9) Yang, H.; Mahapatra, S.; Cheong, P. H. Y.; Carter, R. G. *J. Org. Chem.* **2010**, 75, 7279–7290.
- (10) Grayson, M. N.; Pellegrinet, S. C.; Goodman, J. M. *J. Am. Chem. Soc.* **2012**, 134, 2716–2722.
- (11) Rodríguez, E.; Grayson, M. N.; Asensio, A.; Barrio, P.; Houk, K. N.; Fustero, S. *ACS Catal.* **2016**, 6, 2506–2514.
- (12) Terada, M.; Soga, K.; Momiyama, N. *Angew. Chem. Int. Ed.* **2008**, 47, 4122–4125.
- (13) Paddon-Row, M. N.; Anderson, C. D.; Houk, K. N. *J. Org. Chem.* **2009**, 74, 861–868.
- (14) Grayson, M. N.; Krische, M. J.; Houk, K. N. *J. Am. Chem. Soc.* **2015**, 137, 8838–8850.
- (15) Grayson, M. N.; Goodman, J. M. *J. Am. Chem. Soc.* **2013**, 135, 6142–6148.
- (16) Taylor, R.; Kennard, O. *J. Am. Chem. Soc.* **1982**, 104, 5063–5070.
- (17) Jain, P.; Antilla, J. C. *J. Am. Chem. Soc.* **2010**, 132, 11884–11886.
- (18) Simón, L.; Goodman, J. M. *J. Am. Chem. Soc.* **2008**, 130, 8741–8747.

### CHAPTER 3.3

- (19) Simón, L.; Goodman, J. M. *J. Am. Chem. Soc.* **2009**, 131, 4070–4077.
- (20) Simón, L.; Goodman, J. M. *J. Org. Chem.* **2010**, 75, 589–597.
- (21) Simón, L.; Goodman, J. M. *J. Org. Chem.* **2011**, 76, 1775–1788.
- (22) Overvoorde, L. M.; Grayson, M. N.; Luo, Y.; Goodman, J. M. *J. Org. Chem.* **2015**, 80, 2634–2640.
- (23) Chapman, S.; Bunker, D. L. *J. Chem. Phys.* **1975**, 62, 2890–2899.
- (24) Doubleday, C. E.; Bolton, K.; Hase, W. L. *J. Phys. Chem. A* **1998**, 102, 3648–3658.
- (25) Wang, Z.; Hirschi, J. S.; Singleton, D. A. *Angew. Chem. Int. Ed.* **2009**, 48, 9156–9159.
- (26) Yang, Z.; Doubleday, C.; Houk, K. N. *J. Chem. Theory Comput.* **2015**, 11, 5606–5612.
- (27) Liu, F.; Yang, Z.; Mei, Y.; Houk, K. N. *J. Phys. Chem. B* **2016**, 120, 6250–6254.
- (28) Frisch, M. J., et al. Gaussian 09; Gaussian, Inc., Wallingford, CT, **2013**.
- (29) Becke, A. D. *Phys. Rev. A* **1988**, 38, 3098–3100.
- (30) Lee, C.; Yang, W.; Parr, R. G. *Phys. Rev. B* **1988**, 37, 785–789.
- (31) Zhao, Y.; Truhlar, D. *Theor. Chem. Acc.* **2008**, 120, 215–241.
- (32) Weigend, F.; Ahlrichs, R. *Phys. Chem. Chem. Phys.* **2005**, 7, 3297–3305.
- (33) Legault, C. Y. CYLView, 1.0b; Université de Sherbrooke: Sherbrooke, Quebec, Canada, **2009**; <http://www.cylview.org>.
- (34) Desiraju, G. R. *Acc. Chem. Res.* **1996**, 29, 441–449.
- (35) Azi, D. A.; Singleton, D. A. *J. Am. Chem. Soc.* **2017**, 139, 5965–5972.

## **3.4 Environment-Perturbed Transition State Sampling and Application to SpnF-catalyzed Diels-Alder**

### **3.4.1 Abstract**

SpnF is the first monofunctional Diels–Alder/[6+4]-ase that catalyzes a reaction leading to both Diels–Alder and [6+4] adducts through a single transition state. The Environment-Perturbed Transition State Sampling method has been developed to calculate free energies, kinetic isotope effects and quasi-classical reaction trajectories of enzyme-catalyzed reactions and the uncatalyzed reaction in water. Energetics calculated in this way reproduce the experiment and show that the normal Diels–Alder transition state is stabilized by H-bonds with water molecules, while the ambimodal transition state is favored in the enzyme SpnF by both intramolecular hydrogen bonding and hydrophobic binding. Molecular dynamics simulations show that trajectories passing through the ambimodal transition state bifurcate to the [6+4] adduct and the Diels–Alder adduct with a ratio of 1:1 in the gas phase, 1:1.6 in water and 1:11 in the enzyme. This is the first example that shows how enzymes alter product formation in a reaction where two different products can be formed from the same transition state.

### **3.4.2 Introduction**

The wide applications of the Diels–Alder reaction<sup>6,7</sup> inspire the identification of natural enzymes that catalyze Diels–Alder reactions (Diels–Alderases or DAases).<sup>8</sup> While extensive surveys of secondary metabolites indicate that hundreds of natural products are potentially biosynthesized by DAases,<sup>9</sup> only a handful of purified enzymes have been demonstrated to

catalyze DA reactions. These enzymes often catalyze other reactions, such as oxidations or degradations, thus leaving uncertain their specific influence on the DA reactions.<sup>10</sup> In 2011, Liu et al. discovered the first monofunctional DAase, SpnF, which solely catalyzes a Diels–Alder reaction in the biosynthetic pathway of spinosyn A. Although the crystal structure of SpnF was reported in 2015,<sup>11</sup> the mechanism by which the enzyme catalyzes the DA reaction is still largely unknown.

Computational simulations have been employed to rationalize the reaction mechanism,<sup>12,13</sup> but accurate mechanistic studies in solvent and in enzyme remain challenging, because this requires both accurate description of interatomic interactions and extensive sampling of molecular conformations.<sup>14</sup> For instance, the recent study of AbyU-catalyzed Diels–Alder reaction by Race et al. has shown that the proposed DA reaction likely proceeds via a concerted, yet highly asynchronous transition state in the active site of the enzyme AbyU.<sup>15</sup> However, the calculated potential of mean force (PMF) barrier using an hybrid quantum mechanics-classical molecular mechanics (QM(SCC-DFTB)/MM(FF14SB)) method severely underestimates the experimental barrier.

Additionally, as single-molecule experimental techniques to study reaction advance,<sup>16</sup> mechanistic study is no longer limited to the description of ensemble-average properties, such as thermodynamics and kinetics. The exploration of chemical reactions now extends to the atomic level and fs-ps time scale, which informs how atomic motions, conformational fluctuations, and solvent effects alter the reaction pathways of single molecules.<sup>17</sup> This accordingly calls for the



development of computational tools that investigate the energetics and dynamics of single molecules in condensed media.

We have developed an Environment-Perturbed Transition State Sampling (EPTSS) method for individual trajectories, but also for free energy calculations, and kinetic isotope effect simulations in solvents and enzymes. This enables the unraveling of the role of solvents and enzymes on control of single-molecule reaction pathways involving ambimodal transition states and PES bifurcations.<sup>5,18</sup> Quasiclassical trajectories have been employed previously in the gas phase to understand and predict selectivities of reactions with post-TS bifurcations on the PES,<sup>5,19,20,21</sup> such as for the cationic rearrangements occurring in terpene biosynthesis.<sup>22,23,24</sup> We report for the first time how solvent and enzyme influence the dynamical behavior of a bifurcating reaction path in SpnF-catalyzed Diels–Alder reaction.

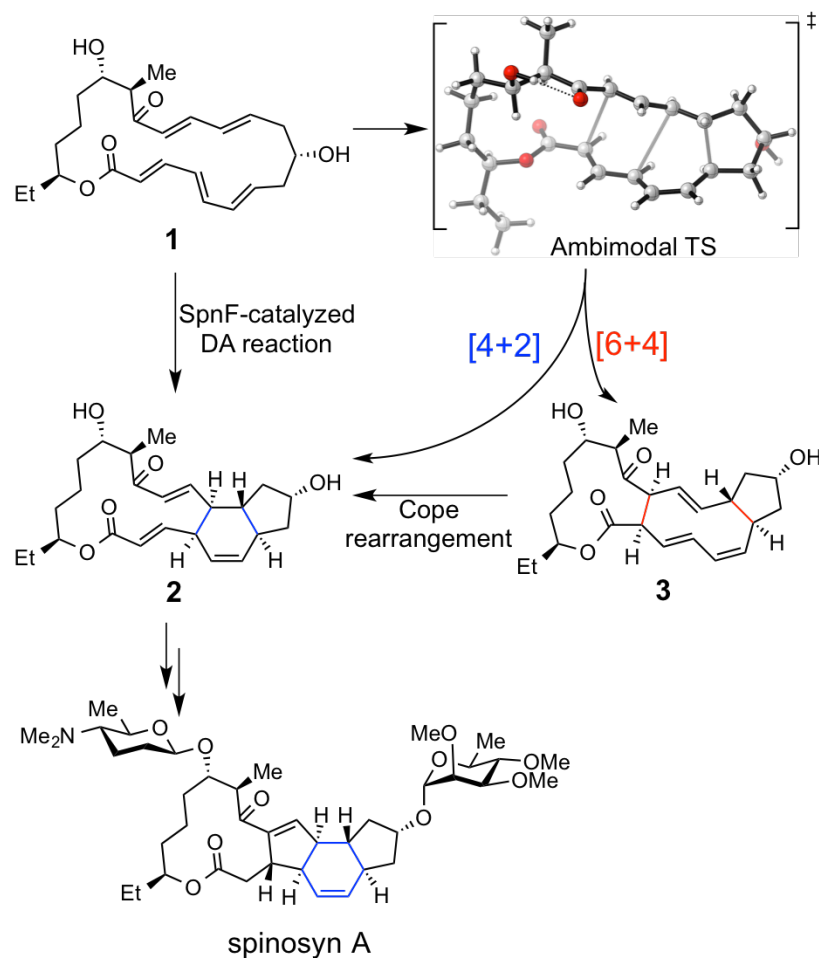


**Figure 3.4.1.** SpnF-catalyzed transannular Diels–Alder reaction of **1** to form **2**. This is a step in the biosynthesis of spinosyn A.

### 3.4.3 Computational Methods

The Enzyme-perturbed Transition State Sampling (EPTSS) method consists of four major steps. (1) *Construction of the reaction/medium models*. Initial structures of reactants and transition states were optimized in the gas phase at the M06-2X/6-31G(d) level of theory,<sup>37</sup> using Gaussian 09.<sup>38</sup> The optimized structures were then solvated in a water box using AmberTools 14<sup>39</sup> for the aqueous system. For the reaction in enzyme, the substrate or TS were docked into the

enzyme active site using AutoDock Vina. (2) *Configuration Sampling*. Separate ensembles of R-A and R-B reactants were constructed by carrying out classical MD equilibrations in water and SpnF using MM for reactant and environment. Classical molecular dynamics (MD) was performed using Amber 14 on the substrate and the transition state for 10 ns in water and for 500 ns in SpnF. The FF99SBildn force field was used for protein residues. General Amber Force Field (GAFF) was used for reactant and transition structures. During the classical MD on the transition state, restraining potentials of  $500 \text{ kcal/mol/\AA}^2$  were applied to the reaction coordinates in the transition state. Snapshots (typically 100) of reactant and TS were sampled from production MD runs at 5 ps intervals in water and 1 ns intervals in SpnF. (3) *Free energy calculations*. To compute the QM/MM free energy differences, we used a modified form of the ensemble-averaged variational transition state theory (EA-VTST) of Truhlar and Gao and coworkers,<sup>27,40</sup> which incorporates vibrational contributions to the PMF in condensed phase. For each snapshot, the coordinates of the environment (water or SpnF) were frozen, the geometry of 1 was optimized with QM/MM with M06-2X/6-31G(d) as QM, and the free energy was computed from harmonic vibrational partition functions at the stationary point. Free energies of TS-A and TS-B were computed similarly, using conventional TST instead of locating the TS variationally (VTST). This form of the theory is called EA-TST. In our previous study, the reaction path-VTST calculation is performed along the IRC initiated from the ambimodal TS-A in the gas phase. The rate-determining VTS highly resembles the TS, which justifies the EA-TST we used here. In the TS equilibrations, reacting bond lengths were restrained as described in the Methods section. Free energy barriers were computed as  $\langle E(\text{TS-A}) \rangle - \langle E(\text{R}) \rangle$  and  $\langle E(\text{TS-B}) \rangle -$

$\langle E(R) \rangle$ , where angle brackets indicate an ensemble average over 100 snapshots. Our free energy scheme assumes that enzyme is well pre-organized. The assumption has been justified in other studies.<sup>22</sup> On the other hand, for reactions without large charge separation, the preorganization energy is relatively trivial. (4) *Reaction dynamics*. Reactive trajectory simulations were initiated from the random normal mode sampled transition states in water or in enzyme. Normal mode sampling was conducted at 300K for each sampled TS structure to obtain coordinates and momenta in a quasiclassical manner. These trajectories were propagated forward and backward for 150 fs each.

Online Content Methods, along with any additional Extended Data display items and Source Data, are available in the online version of the paper; references unique to these sections appear only in the online paper.

### 3.4.4 Results and Discussion

Using quantum mechanics/molecular mechanics (QM/MM) methods,<sup>25</sup> we have examined the effect of water and SpnF on the dynamics and initial product ratio of the transannular cycloadditions of **1**. We enhanced our previously described solvent-perturbed TS sampling method<sup>26</sup> to carry out quasiclassical normal mode sampling of the ensemble of transition states in enzyme. The method is called the Environment-Perturbed Transition State (EPTS) sampling.

#### 3.4.4.1 Conformational ensembles for reactant, ambimodal TS-A and Diels–Alder TS-B

The substrate **1** is a conformationally flexible 22-membered polyene lactone. The conformation complexity was thoroughly analyzed by Medvedev et al.<sup>27</sup> We find that the

conformers of 1 consist mainly of two collections represented in **Figure 3.4.2** by the gas phase conformers R-A and R-B. They differ mainly in the presence or absence of an intramolecular hydrogen bond. This is reflected in the highlighted dihedral angle  $\Phi$ . R-A has an intramolecular hydrogen bond (H-bond) and R-B does not. (**Figure 3.4.3**) TS-A is more stable than TS-B by 3.3 kcal/mol in the gas phase, and by 0.9 kcal/mol in implicit water.

Classical MD equilibrations in water and SpnF predict an 80:20 equilibrium mixture of R-B: R-A in both water and SpnF. This contrasts with the gas phase where R-A is 5.2 kcal/mol below R-B, largely due to the intramolecular H-bond. In water and in SpnF, hydrogen bonds to the carbonyl of R-B (Q148, I40 in SpnF) stabilize R-B.

MD simulations with restrained TS<sup>28</sup> geometries were conducted separately on both TS conformers in water and enzyme SpnF. Ensembles for ambimodal TS-A and for Diels–Alder TS-B were constructed separately by taking 100 snapshots of the solvent box with a 100 ps interval in water and a 1 ns interval in the enzyme. For each ensemble, subsequent QM/MM calculations were conducted to optimize the reactant, ambimodal TS-A or Diels–Alder TS-B in the perturbing environment. The free energies were computed by averaging over the entire ensemble.

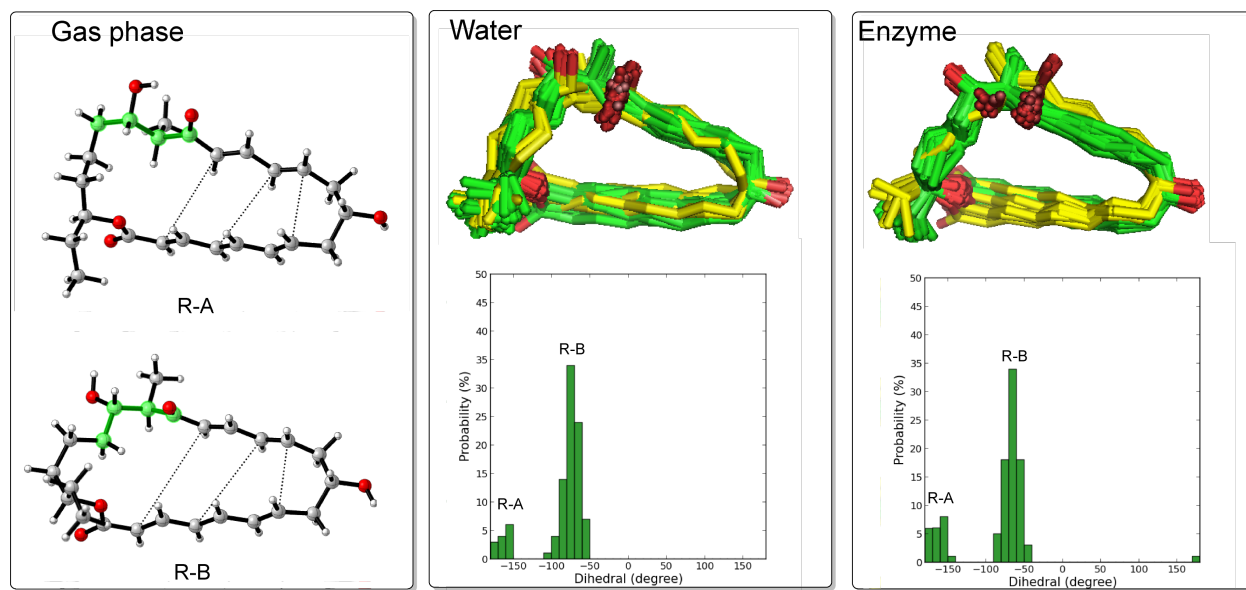


**Figure 3.4.2.** Ensembles of reactants from classical MD in water and in the enzyme. Water molecules and enzyme residues are not displayed. R-A and R-B are two representative conformations optimized in the gas phase. The dihedral angle used for discriminating between the two conformations is highlighted.

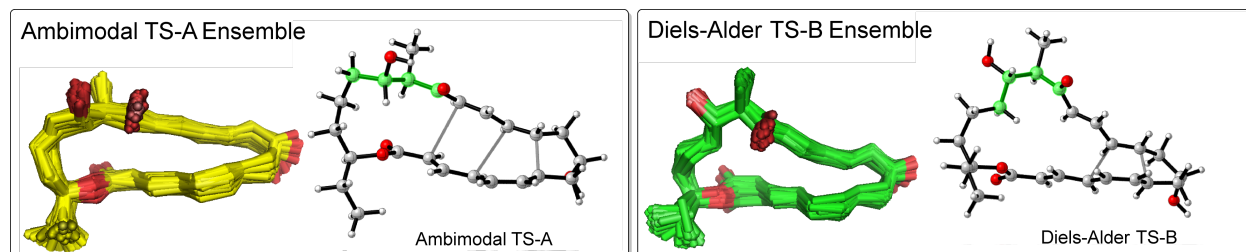


**Figure 3.4.3.** Ensembles of ambimodal TS-A and Diels-Alder TS-B in enzyme. Ambimodal TS-A and Diels-Alder TS-B are representative conformations for their corresponding ensembles. The dihedral angle used for discriminating two conformations is highlighted. The intramolecular H-bond is the first case stabilizes a conformation suitable for the ambimodal TS-A.

### 3.4.4.2 Computed free energies of activation

**Table 3.4.1** shows the averaged free energy barriers for ambimodal TS-A and Diels–Alder TS-B in water and in the enzyme SpnF. The averages based on a small number of snapshots have large standard errors. The standard errors decrease, and the energetics converge after including a large number of snapshots. Sufficient conformational sampling is essential for the free energy calculations of reactions in condensed media.<sup>29,30</sup>

The Diels–Alder TS-B is preferred in water, while the ambimodal TS-A is favored in the enzyme. This is a dramatic difference between the reaction in water and SpnF. The computed barriers are consistent with the experimental values of  $22.0 \pm 0.01$  kcal/mol in water and  $18.3 \pm 0.1$  kcal/mol in SpnF, calculated from rates measured at 25 °C.<sup>1</sup> We have also computed the secondary kinetic isotopic effect (KIE) for the reaction in water and in enzyme, and compared with the experimental results.<sup>31</sup> Given experimental errors and statistical errors due to our limited computational sampling, the results are in reasonable agreement. The EPTS KIEs are averaged over the entire TS ensemble. Both experiment and theory establish a significant inverse  $k_H/k_D$  at C7-C11, in the rate-determining TSs in both water and enzyme, indicating bond formation. Nearly negligible KIE are found experimentally and computationally at C4, C12, C2 and C14. The only exception is for C4 where both experiment and theory predict no KIE in water, but small inverse in the enzyme. These results support that TS-B is favored in water, while TS-A is preferred in the enzyme.

The elucidation of hydrogen bonding patterns gives insight into the origins of catalysis. In water, TS-B is better stabilized than TS-A, by forming more intermolecular H-bonds with water

molecules. TS-A already has an intramolecular H-bond and forms less H-bonds with water. Additionally, TS-B is more polarized than TS-A.

The hydrogen bonds measured in the reactant and two conformers of the TS in the enzyme are shown in **Table 3.4.2**. H-Bonds between substrate and H42, E152 (to the TS), A252 (to the reactant) stabilize the binding configuration of the TS and the reactant. Two typical snapshots are also shown for ambimodal TS-A and Diels–Alder TS-B with H-bonding to their surrounding residues. H-Bonds between the residues and the highlighted C=O decrease the energy barriers of the cycloadditions.<sup>32</sup>

In one hundred snapshots in the enzyme, H-bonds to W256 are present in 61% of the reactant snapshots, and in 86% and 87% of the ambimodal TS and Diels–Alder TS, respectively. From reactant to TS, the ambimodal TS-A experiences an enhancement of H-bond c (intramolecular H-bond) from 9% to 99%, while Diels–Alder TS-B shows only a small increase in H-bond b (to T195) percentage from 0% to 21%. This explains in part why the ambimodal TS is more favorable in the enzyme. The protein pocket is highly hydrophobic, and no water molecules are detected within 4 Å of the TS during the MD. The Diels–Alder TS-B in the enzyme is not stabilized by intermolecular H-bonds provided by water or protein residues.

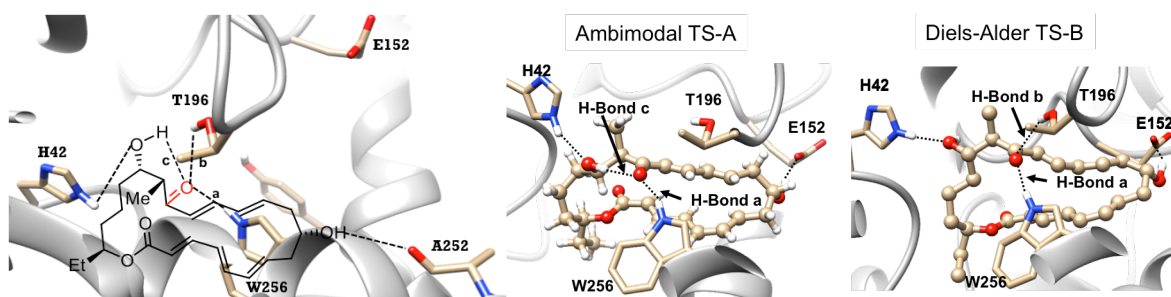
**Table 3.4.1.** Free energy barriers for cycloadditions of **1** in water and SpnF enzyme.



	Ambimodal TS-A (kcal/mol)	Diels-alder TS-B (kcal/mol)	Experiment (kcal/mol) <sup>b</sup>	Experiment (min <sup>-1</sup> )
Water	27.8±1.9 <sup>a</sup>	22.9±2.1 <sup>a</sup>	22.0	0.288±0.0004
Enzyme	18.8±1.0 <sup>a</sup>	23.4±1.1 <sup>a</sup>	18.3	14±1.6

<sup>a</sup> standard error after averaging over 100 snapshots. <sup>b</sup> Barrier obtained from experimental rate via the Eyring equation.

**Table 3.4.2.** Percentage of structures that have H-bond interactions with enzyme residues in ensembles of Reactant, TS-A, and TS-B after QM/MM optimizations. An H-bond is defined as having an H–O bond length shorter than 2.25 Å and an O–H–O bond angle greater than 150°.



	H-bond a	H-bond b	H-bond c
Ambimodal TS-A	86%	0%	99%
Diels-Alder TS-B	87%	21%	0%
Reactant	61%	0%	9%

### 3.4.4.3 Reaction dynamics simulations

Enzymes can bind reactants and transition states by both electrostatic and hydrophobic interactions. These interactions may favor certain transition state geometries, and influence reaction dynamics as well.

The role of dynamics on catalysis by enzymes has been a significant topic of discussion ever since Wright and Benkovic reported correlations between dynamical motions of remote residues and changes in rate by mutation of these residues.<sup>33</sup> After considerable debate, the current consensus is that relatively slow (ms- $\mu$ s) motions of loops and remote residues do indeed alter the structure of the active site,<sup>34</sup> but fast (ps-fs) couplings of vibrational motions to motions along the reaction coordinate have little or no influence on the rate of reactions. We note that residues in contact with the reactant as they vibrate through the transition zone can influence energetics, and the fs motions of these residues can be coupled to the reaction event, while ns loop motion is too slow to influence reaction dynamics.

**Figure 3.4.4** shows the distribution of sampled geometries for Diels–Alder TS-B in water (4a), and ambimodal TS-A in the gas phase (4b), in water (4c) and in enzyme (4d). Bonds 2 and 3 are formed in the [4+2], and the [6+4] adducts, respectively. For Diels–Alder TS-B in water, the distribution of bond 2 is  $2.62 \pm 0.42$  Å, and that of bond 3 is  $3.65 \pm 0.51$  Å. The two bonds on average differ by  $\sim 1$  Å. The formation of the [4+2] adduct is almost always observed in dynamics from this TS (*vide infra*). In contrast, the ambimodal TS-A in enzyme shows that bonds 2 and 3 are much closer in length with  $2.96 \pm 0.25$  Å for bond 2, and  $3.12 \pm 0.26$  Å for bond 3. In the gas phase, the difference between bonds 2 and 3 is further narrowed, making the

formation of [6+4] adduct more likely. These results indicate that the nature of the TS varies in the gas, water, and enzyme environment. This is a result of the average dynamical environment and alters the transition state geometries. Reaction dynamics simulations are essential to elucidate how these environment-perturbations change the pathways that trajectories have to take to achieve product formation.

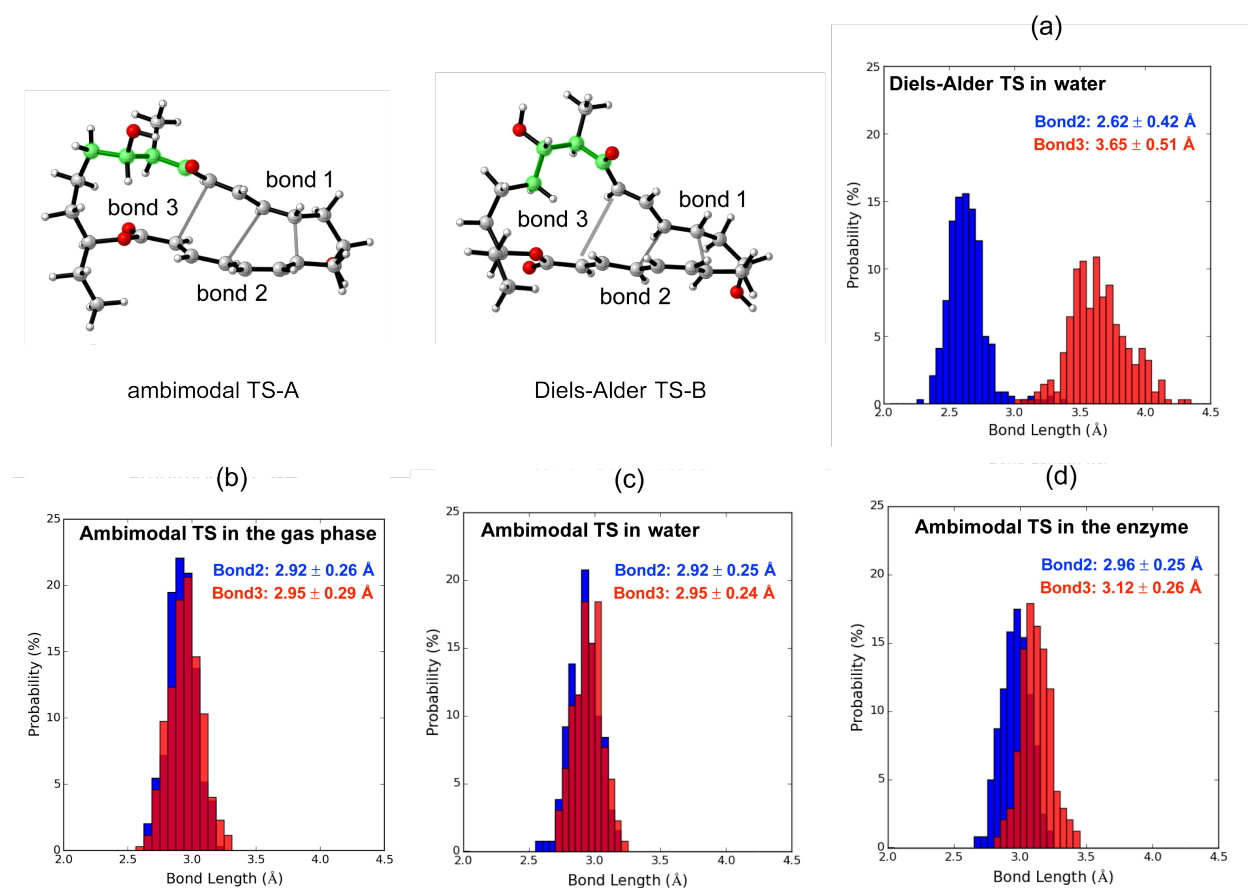


**Figure 3.4.4.** Distribution of bonds 2 and 3 in 240 transition state geometries for (a) Diels-Alder TS-B in water, (b) ambimodal-A TS in the gas phase, (c) ambimodal TS-A in water, and (d) ambimodal TS-A in the enzyme. Bond 2 in blue leads to the [4+2] adduct, while bond 3 in red leads to the [6+4] adduct. For (a), (c), and (d), transition state geometries were sampled by using

normal mode sampling on 60 transition structures optimized in various snapshots of enzyme or of water.

Reaction dynamics trajectories were initiated from transition state geometries after normal mode sampling to explore the dynamics of product formation. Each reactive trajectory was propagated for 300 fs using the QM/MM method (see the Method section).

**Figure 3.4.5** displays typical trajectories propagated in water and in the enzyme. The third and fourth panels in each row indicate the time at which bond 1 and either bonds 2 or 3 are formed, defined as achieving a distance of  $1.6 \text{ \AA}$ .<sup>35</sup> (Bonds 1, 2, and 3 are labeled in **Figure 3.4.4**.) Bond 1 forms in both adducts. Bond 2 forms in the [4+2] adduct, while bond 3 forms in the [6+4] adduct. **Figures 3.4.5a** and **5b** show the production of [4+2] adduct and [6+4] adduct, respectively. In **Figure 3.4.5a**, bond 1 forms at 30 fs, then bond 2 forms at 90 fs. In **Figure 3.4.5b**, bond 1 forms at 18 fs, then bond 3 forms at 42 fs. Likewise, **Figure 3.4.5c** and **5d** represents the formation of [4+2] adduct and [6+4] adduct, respectively, in the enzyme, with two bonds forming at 36 fs and 86 fs for the formation of the [4+2] adduct, and at 67 fs and 138 fs for the formation of the [6+4] adduct.

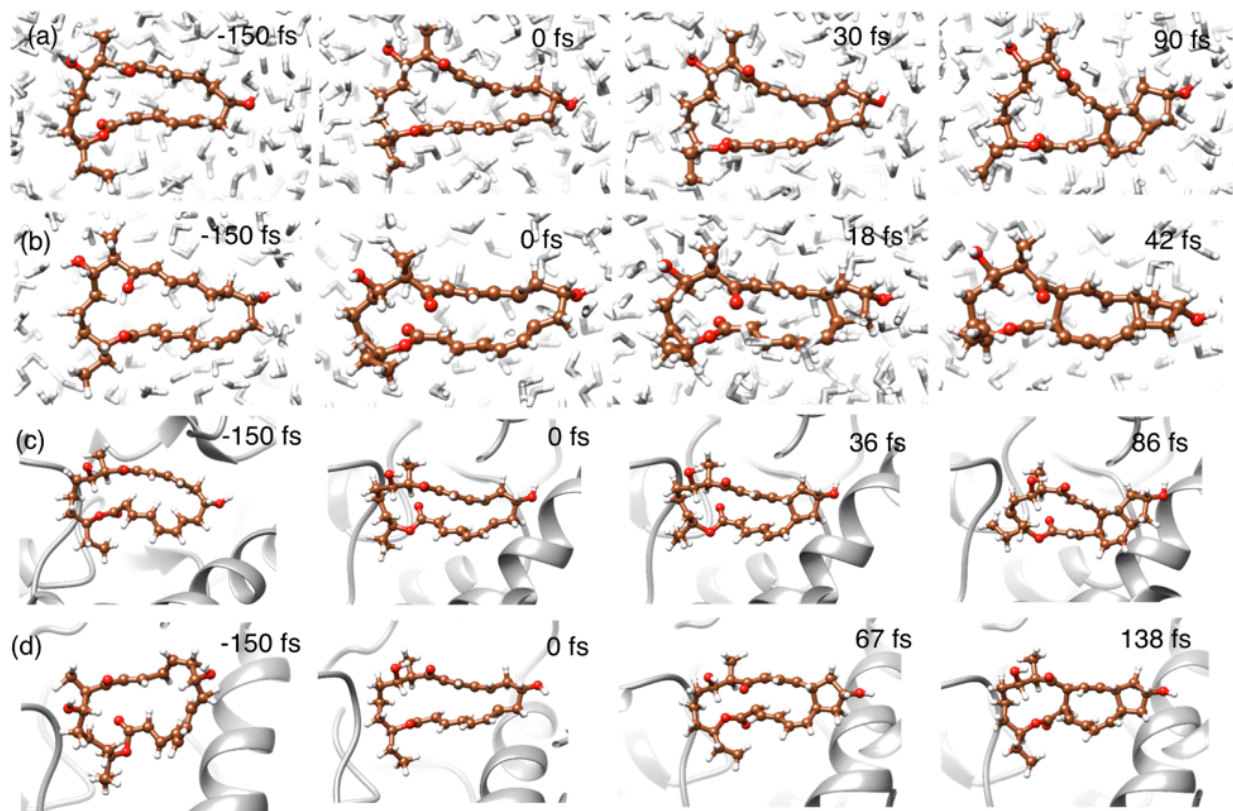


**Figure 3.4.5.** Typical trajectories for the formation of (a) [4+2] adduct in water, (b) [6+4] adduct in water, (c) [4+2] adduct in enzyme, (b) [6+4] adduct in enzyme. We define 1.6 Å as the criterion for C-C bond formation.

**Figure 3.4.6** shows overlays of 100 trajectories plotted according to lengths of forming bonds 1, 2, and 3. The ratios of [4+2]:[6+4] products are also presented. In water, the Diels–Alder TS leads almost exclusively to Diels–Alder adduct, with only one out of 100 trajectories leading to a [6+4] adduct. For trajectories passing through the ambimodal TS, bifurcation is observed with a [4+2]:[6+4] ratio of 11:1 in enzyme, 1.6:1 in water, and 1:1.1 in the gas phase. The selectivity for [4+2] and [6+4] adduct results from the competition between the formation of bond 2 and bond 3. From gas phase to water, a trend towards [4+2] adduct was observed, even though the distributions of the transition state geometries for ambimodal TS-A are very similar in

both media. The dipole moment of the [4+2] adduct is 4.74 Debye, while that of the [6+4] adduct is 3.46 Debye, and the [4+2] adduct is better stabilized by polar solvent. In addition, trajectories were propagated in implicit solvents (SMD model<sup>36</sup>) to explore how the polarity of the medium influences the product distribution. The [4+2]:[6+4] ratio is 1:1 in implicit hexane, and 1.5:1 in implicit water. This further supports that increase in solvent polarity promotes the formation of the [4+2] adduct over the [6+4] adduct.

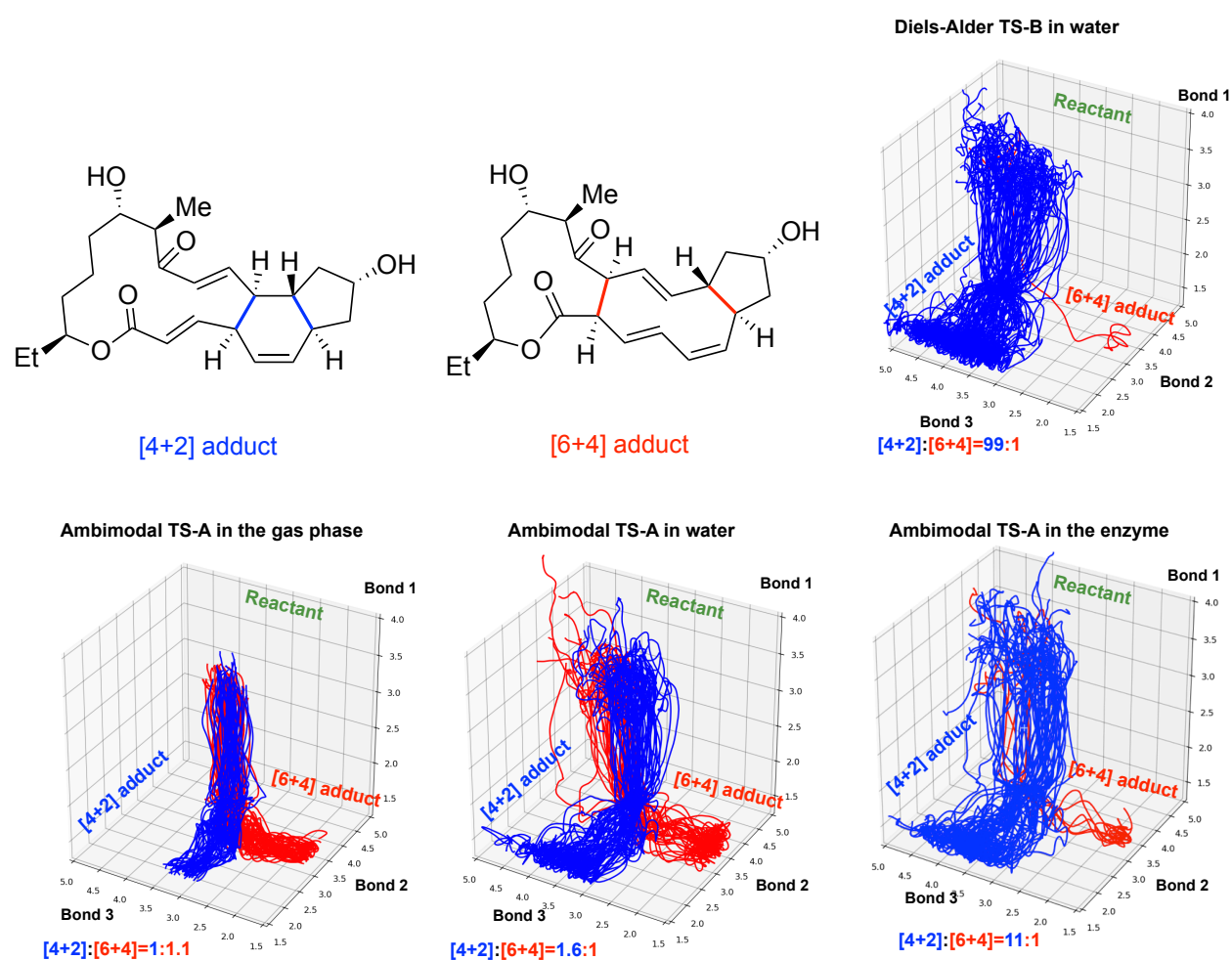


**Figure 3.4.6.** Distributions of reactive trajectories initiated from Diels-Alder TS in water, ambimodal TS in the gas phase, in water, and in enzyme. One hundred randomly chosen

trajectories were plotted in each case. Trajectories leading to [4+2] adduct are shown in blue, and those leading to [6+4] adduct are shown in red.

**Figure 3.4.7a** shows how hydrophobic residue valine V26 influences the formation of the two adducts through interactions with bond 2 (C4-C12) and bond 3 (C2-C14). The distribution of hydrophobic contacts shows a stronger compression on bond 2 than bond 3, as framed on the graph. This leads to relatively larger difference of lengths of partial bond 2 and 3 in the ambimodal TS in the enzyme compared to the gas phase and in water, which favors the formation of the [4+2] adduct. Leucine L198, the other residue nearby the TS, involves similar hydrophobic interactions with the two bonds.

We analyzed the evolution of averaged potential energy (PE), kinetic energy (KE) and total energy (KE+PE) for 159 reactive trajectories leading to the [4+2] adduct. (**Figure 3.4.7b**) From -100 fs to -30 fs, KE increases by about 10 kcal/mol while PE remains relatively unchanged. This is a phase of thermal activation of the substrate to achieve reactive conformations. Subsequently, 15 kcal/mol KE is transferred into PE to form the TS at 0 fs. After passing the TS, the product is gradually formed with KE increasing and PE decreasing. The formation of the bond 2 takes relatively longer time than bond 1, and PE and KE change smoothly. **Figure 3.4.7c** displays the decreases of the kinetic energies for the three hydrophobic residues (V26, L30, and L198) surrounding the reacting molecule from -100 fs to 0 fs. Their kinetic energy in total decreases by ~3 kcal/mol. We found that the KEs for polar residues that form H-bonds to the substrate are always within 0.5 kcal/mol. These results indicate a kinetic energy transfer from the hydrophobic residues to the reacting substrate by vibrational collisions on a fs time scale.

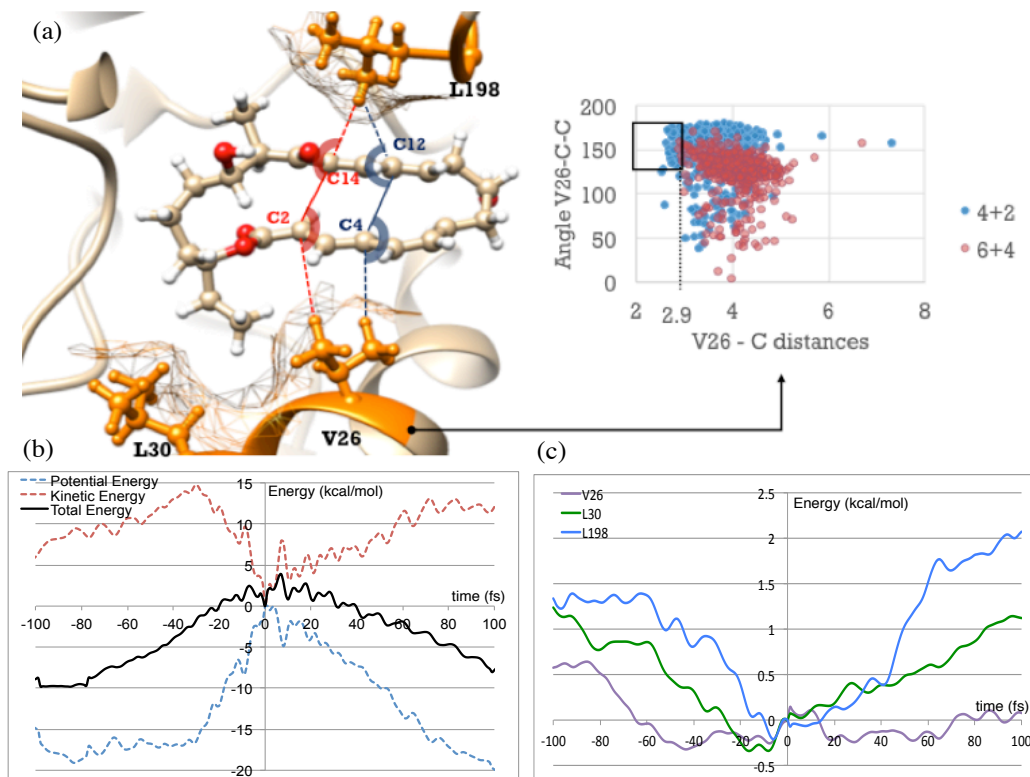


**Figure 3.4.7.** (a) Hydrophobic interactions in SpnF-TS complex. The distance is measured from the closest H on V26 or L30 (depending which residue is closer in the snapshot) to C4 or C2, and the angle is the closest H-C4-C14 or H-C2-C14. Framed are the strong hydrophobic contacts, defined as the angle larger than  $150^\circ$  and the distance shorter than  $2.9 \text{ \AA}$ . (b) Average of potential energy, kinetic energy and total energy of the substrate versus time. (c) Average of kinetic energy for residues V26, L30 and L198 versus time. Energies are averaged from 159 trajectories leading to the [4+2] adduct. The energy at 0 fs are set as zero.

### 3.4.5 Conclusion

The Environment-Perturbed Transition State Sampling (EPTSS) method<sup>22</sup> has been developed and applied to compute free energy barriers and quasiclassical dynamics in aqueous solution and in the enzyme SpnF. Using this method, we investigated medium effects and



femtosecond dynamics of SpnF-catalyzed transannular Diels–Alder reactions. Two distinct transition states were found for the reaction in water and in the enzyme. The computed reaction barriers are in good agreement with the experimentally measured rates of reaction. Important residues that contribute to the overall catalytic process and product distributions were identified. Our study shows how water and enzyme residues influence the rates of reaction and the distributions of products in a dynamically controlled ambimodal reaction mechanism.

### 3.4.6 References

1. Kim, H. J., Ruszczycky, M. W., Choi, S.-H., Liu, Y.-N., Liu, H.-w. *Nature* **2011**, 473, 109–112.
2. Patel, A., Chen, Z., Yang, Z., Gutiérrez, O., Liu, H.-w., Houk, K. N., Singleton, D. A. *J. Am. Chem. Soc.* **2016**, 138, 3631–3634.
3. Yu, P., Patel, A., Houk, K. N. *J. Am. Chem. Soc.* 2015, 137, 13518–13523.
4. Carpenter, B. K. *J. Am. Chem. Soc.* **1995**, 117, 6336–6344.
5. Lourderaj, U., Park, K., Hase, W. L. *Int. Rev. Phys. Chem.* **2008**, 27, 361–403.
6. Diels, O., Alder, K. *Justus Liebigs Annalen der Chemie.* **1928**, 460, 98–122.
7. Nicolaou, K. C., Snyder, S. A., Montagnon, T., Vassilikogiannakis, G. The Diels–Alder reaction in total synthesis. *Angew. Chem., Int. Ed.* **2002**, 41, 1668–1698.
8. Jeon, B.-s., Wang, S.-A., Ruszczycky, M. W., Liu, H.-w. *Chem. Rev.* 117, 5367–5388 (2017).
9. Oikawa, H., Tokiwano, T. *Nat. Prod. Rep.* **2004**, 21, 321–352.
10. Minami, A., Oikawa, H. *J. Antibiot.* **2016**, 69, 500–506.

11. Fage, C. D., Isiorho, E. A., Liu, Y. N., Wagner, D. T., Liu, H.-w., Keatinge-Clay, A. T. *Nat. Chem. Biol.* **2015**, 11, 256–258.
12. MacKerell Jr, A. D., Bashford, D., Bellott, M. L. D. R., Dunbrack Jr, R. L., Evanseck, J. D., Field, M. J., Fischer, S., Gao, J., Guo, H., Ha, S., Joseph-McCarthy, D. *J. Phys. Chem. B.* **1998**, 102, 3586–3616.
13. Karplus, M., McCammon, J. A. *Nat. Struct. Mol. Biol.* **2002**, 9, 646–652.
14. Lu, X., Fang, D., Ito, S., Okamoto, Y., Ovchinnikov, V., Cui, Q. *Mol. Simul.* **2016**, 42, 1056–1078.
15. Byrne, M. J., Lees, N. R., Han, L.-C., van der Kamp, M. W., Mulholland, A. J., Stach, J. E. M., Willis, C. L., Race, P. R. *J. Am. Chem. Soc.* **2016**, 138, 6095–6098.
16. Kneipp, K., Wang, Y., Kneipp, H., Perelman, L. T., Itzkan, I., Dasari, R. R., Feld, M. S. *Phys. Rev. Lett.* **1997**, 78, 1667–1670.
17. Lu, H. P., Xun, L., Xie, X. S. *Science* **1998**, 282, 1877–1882.
18. Ess, D. H., Wheeler, S. E., Iafe, R. G., Xu, L., Çelebi-Ölçüm, N., Houk, K. N. *Angew. Chem., Int. Ed.* **2008**, 47, 7592–7601.
19. Yang, Z., Yu, P., Houk, K. N. *J. Am. Chem. Soc.* **2016**, 138, 4237–4242.
20. Nieves-Quinones, Y., Singleton, D. A. *J. Am. Chem. Soc.* **2016**, 138, 15167–15176.
21. Yu, P., Chen, T. Q., Yang, Z., He, C. Q., Patel, A., Lam, Y.-h., Liu, C.-Y., Houk, K. N. *J. Am. Chem. Soc.* **2017**, 139, 8251–8258.
22. Hong, Y. J., Tantillo, D. J. *Nature Chem.* **2009**, 1, 384–389.
23. Hong, Y. J., Tantillo, D. J. *Nat. Chem.* **2014**, 6, 104–111.

24. Major, D. T., Weitman, M. *J. Am. Chem. Soc.* **2012**, 134, 19454–19462.
25. Warshel, A., Levitt, M. *J. Mol. Biol.* **1976**, 103, 227–249.
26. Yang, Z., Doubleday, C., Houk, K. N. *J. Chem. Theory Comput.* **2015**, 11, 5606–5612.
27. Medvedev, M. G., Zeifman, A. A., Novikov, F. N., Bushmarinov, I. S., Stroganov, O. V., Titov, I. Y., Chilov, G. G., Svitanko, I. V. *J. Am. Chem. Soc.* **2017**, 139, 3942–3945.
28. Noey, E. L., Tibrewal, N., Jiménez-Osés, G., Osuna, S., Park, J., Bond, C. M., Cascio, D., Liang, J., Zhang, X., Huisman, G. W., Tang, Y. *Proc. Natl. Acad. Sci.* 112, 7065–7072 (2015).
29. Lin, H., Truhlar, D. G. *Theor. Chem. Acc.* **2007**, 117, 185–199.
30. Masgrau, L., Truhlar, D. G. *Acc. Chem. Res.* **2015**, 48, 431–438.
31. Jeon, B.-s., Rusczycky, M. W., Russell, W. K., Lin, G.-M., Kim, N., Choi, S.-h., Wang, S.-A., Liu, Y.-n., Patrick, J., Russell, D. H., Liu, H.-w. *Proc. Natl. Acad. Sci.* **2017**, 114, 10408–10413.
32. Blake, J. F., Jorgensen, W. L. *J. Am. Chem. Soc.* **1991**, 113, 7430–7432.
33. Falzone, C. J., Wright, P. E., Benkovic, S. J. *Biochemistry* **1994**, 33, 439–442.
34. Agarwal, P.K., Billeter, S.R., Rajagopalan, P.R., Benkovic, S.J. and Hammes-Schiffer, S. *Proc. Natl. Acad. Sci.* **2002**, 99, 2794-2799.
35. Black, K., Liu, P.; Xu, L., Doubleday, C., Houk, K. N. *Proc. Natl. Acad. Sci. U. S. A.* **2012**, 109, 12860–12865.
36. Marenich, A. V., Cramer, C. J., Truhlar, D. G. *J. Phys. Chem. B.* **2009**, 113, 6378–6396.
37. Zhao, Y., Truhlar, D. G. *Theor. Chem. Acc.* **2008**, 120, 215–241.
38. Frisch, M. J., Trucks, G. W., Schlegel, H. B., Scuseria, G. E., Robb, M. A., Cheeseman, J. R., Scalmani, G., Barone, V., Mennucci, B., Petersson, G. A., Nakatsuji, H., Caricato, M.; Li, X.,

## CHAPTER 3.4

Hratchian, H. P., Izmaylov, A. F., Bloino, J., Zheng, G., Sonnenberg, J. L., Hada, M., Ehara, M., Toyota, K., Fukuda, R., Hasegawa, J., Ishida, M., Nakajima, T., Honda, Y., Kitao, O.; Nakai, H., Vreven, T., Montgomery Jr., J. A., Peralta, J. E., Ogliaro, F., Bearpark, M. J., Heyd, J., Brothers, E. N., Kudin, K. N., Staroverov, V. N., Kobayashi, R., Normand, J., Raghavachari, K., Rendell, A. P., Burant, J. C., Iyengar, S. S., Tomasi, J., Cossi, M., Rega, N., Millam, N. J., Klene, M., Knox, J. E., Cross, J. B., Bakken, V., Adamo, C., Jaramillo, J., Gomperts, R., Stratmann, R. E., Yazyev, O., Austin, A. J., Cammi, R., Pomelli, C., Ochterski, J. W., Martin, R. L., Morokuma, K., Zakrzewski, V. G., Voth, G. A., Salvador, P., Dannenberg, J. J., Dapprich, S., Daniels, A. D., Farkas, Ö., Foresman, J. B., Ortiz, J. V., Cioslowski, J., Fox, D. J. Gaussian 09, Gaussian, Inc.: Wallingford, CT, USA, **2009**.

39. Case, D. A., Babin, V., Berryman, J., Betz, R. M., Cai, Q., Cerutti, D.S., Cheatham Iii, T. E., Darden, T. A., Duke, R. E., Gohlke, H., Goetz, A. W. **2014**, Amber 14.

40. Truhlar, D. G., Gao, J., Alhambra, C., Garcia-Viloca, M., Corchado, J., Sánchez, M. L., Villa, J. *Acc. Chem. Res.* **2002**, 35, 341–349.

## Chapter 4. Summary

This thesis focuses on molecular reaction dynamics simulations of organic and enzymatic reactions. **Chapter 1** introduced the history of organic reaction dynamics, and reviewed the contribution of Houk group in this field. **Chapter 2** discusses the application of well-established gas-phase dynamics simulations to elucidate the time-resolved mechanism of organic reactions. In **chapter 2.1**, trajectory simulations were performed on dimethyldioxirane C-H oxidation reactions, which showed that polar acetone solvation favors diradical recombination, leading to the retention of stereospecificity. In **chapter 2.2**, the dynamic feature of concerted versus stepwise pathway of dehydro-Diels-Alder reaction were reported, which showed that concerted pathway involves a vibrational excitation, while stepwise pathway involves a rotational excitation. In **chapter 2.3**, we explored the dynamics of cyclopentadiene dimerization, the first reported ambimodal pericyclic reaction. Woodward and Katz proposed that the reaction involves a two-stage mechanism, with the TS leading to a Cope rearrangement TS, and then generating the dimerized product. Our simulations showed that two-stage pathway is involved in 17% of the reactive trajectories, which present a typical “dynamically stepwise” feature with time gap between formation of two bonds longer than 60 fs. In **chapter 2.4**, we collected 16 ambimodal reactions from previous work of Caramella, Singleton and Houk, and investigate how TS geometries influence the the product ratio from dynamics simulations. A linear correlation was found between TS bond lengths difference and the product ratio, serving as an empirical model

that would be used to diagnose new ambimodal reactions, and estimate product ratio without the expense of MD simulations.

**Chapter 3** involves the method development for reaction dynamics in solvent and in enzyme. In **chapter 3.1**, we proposed a solvent-perturbed transition state sampling (SPTSS) method, inspired by Truhlar's ensemble-average variational transition state theory. The method integrates the conformational sampling of solvent and quasi-classical sampling of reacting molecules. The method is applied to water-accelerated Diels-Alder reaction, cyclopentadiene + methylvinylketone, and show how water molecules dynamically form enhanced hydrogen bond to promote the reaction. This reaction was further explored in **chapter 3.2** by QM/QM'(PM3) method, which considers polarization effects on the bulk water. The results show that polarization does not significantly influence the dynamical behaviors of the reaction. In **chapter 3.3**, we applied SPTSS approach to study the chronology of CH-O and OH-O hydrogen bonding in the phosphoric acid-catalyzed allylboration reactions. The study reveals an intrinsic synergy of enhancement between the two H-bonds from reactant to transition state. The enhancement is diminished in toluene solvent. In **chapter 3.4**, we further developed the SPTSS method to allow the study of reaction dynamics, free energy, and kinetic isotope effect in enzyme. The new method is called environment perturbed transition state sampling (EPTSS). The method is used to study SpnF-catalyzed Diels-Alder reaction. We found that two TS conformers are involved in the reaction, with Diels-Alder TS favored in water and ambimodal TS favored in the gas phase and in enzyme. Trajectory simulations show that ambimodal TS leads to the formation of [4+2]

and [6+4] adduct with a ratio of 11:1 in the enzyme, and 1.1:1 in the gas phase, indicative of enzymatic control of product ratio in femtosecond time scale.

In a summary, this thesis demonstrates important dynamic features of organic reactions that remain largely unexplored in the circle. More importantly, my work established a methodology for studying time-resolved mechanism of chemical reaction in solvent and in enzyme, which would unravel deeper insight into chemical and biological processes, and has the potential of facilitating new design of enzymes and catalysts.

## REFERENCE

## REFERENCE

1. Dynamics of Chemical Reactions: Atomistic Visualization of Organic Reactions and Homage to Van't Hoff. **Yang, Z.**; Houk, K. N. (Submitted to *Chemistry, A European Journal* as an homage to Van't Hoff.)
2. Molecular Dynamics of Dimethyldioxirane C-H Oxidation. **Yang, Z.**; Yu, P.; Houk, K. N. *Journal of the American Chemical Society*, **2016**, *138*, 4237-4242.
3. Distortion-Controlled Reactivity and Molecular Dynamics of Dehydro-Diels–Alder Reactions. Yu, P.\*; **Yang, Z.\***; Liang, Y.; Hong, X.; Li, Y.; Houk, K. N. *Journal of the American Chemical Society*, **2016**, *138*, 8247-8252. (\* co-first author)
4. Molecular Dynamics of the Two-Stage Mechanism of Cyclopentadiene Dimerization: Concerted or Stepwise? **Yang, Z.**; Zou, L.; Liu, F.; Yu, Y.; Dong, X.; Houk, K. N. (Submitted to *Chemical Physics* in honor of Raphael Levine for his 80<sup>th</sup> birthday)
5. Prediction of Product Ratio for Ambimodal Pericyclic Reactions. **Yang, Z.**; Dong, X.; Yu, P.; Yu, Y.; Li, Y.; Houk, K. N. (In preparation)
6. QM/MM Protocol for Direct Molecular Dynamics of Chemical Reactions in Solution: the Water-Accelerated Diels–Alder Reaction. **Yang, Z.**; Doubleday, C.; Houk, K. N. *Journal of Chemical Theory and Computation*, **2015**, *11*, 5606-5612.
7. QM/QM' Direct Molecular Dynamics of Water-Accelerated Diels-Alder Reaction. Liu, F\*.; **Yang, Z.\***; Mei, Y.; Houk, K.N. *Journal of Physical Chemistry B*, **2016**, *120*, 6250-6254. (\* co-first author)



## REFERENCE

8. Chronology of CH $\cdots$ O Hydrogen Bonding from Molecular Dynamics Studies of the Phosphoric Acid-Catalyzed Allylboration of Benzaldehyde. Grayson, M. N.; **Yang, Z.\***; Houk, K. N. *Journal of the American Chemical Society*, **2017**, *139*, 7717-7720 (\* co-first author)
9. Enzymatic Control of Reaction Dynamics. **Yang, Z.**; Yang, S.; Yu, P.; Li, Y.; Park, J.; Patel, A.; Doubleday, C.; Houk, K. N. (Submitted to *Proceedings of the National Academy of Sciences*)
10. Bimodal Evans-Polanyi Relationships in Dioxirane Oxidations of sp<sup>3</sup> CH: Non-perfect Synchronization in Generation of Delocalized Radical Intermediates. Liu, F.; **Yang, Z.**; Yu, Y.; Mei, Y.; Houk, K. N. *Journal of the American Chemical Society*, **2017**, *139*, 16650-16656
11. Prediction and Understanding of Intrinsic Selectivities in Hydrogen Abstraction by a Model for the Fe(IV)oxo-porphyrin unit of Cytochrome P450s. Comparing to Hydroxyl Radical. Yu, Y.; **Yang, Z.\***; Liu, F.; Houk, K. N. (\* co-first author) (In preparation)
12. Mechanism of Enzyme PyrI4-catalyzed Diels-Alder Reaction. Li, W.\*; Yang, S.\*; **Yang, Z.\***; Yu, P.; Houk, K. N. (\* co-first author) (In preparation)
13. Origins of Regioselectivity in the Fischer Indole Synthesis of a Selective Androgen Receptor Modulator. Noey, E. L.; **Yang, Z.**; Li, Y.; Yu, H.; Richey, R. N.; Merritt, J. M.; Kjell, D. P.; Houk, K. N. *Journal of Organic Chemistry*, **2017**, *82*, 5904-5909.
14. Dynamically Concerted and Stepwise Trajectories of the Cope Rearrangement of 1,5-Hexadiene. Mackey, J. L.; **Yang, Z.**; Houk, K. N. *Chemical Physics Letters*, **2017**, *683*, 253-257.
15. Dynamically Complex Enzyme-catalyzed [6+4] and [4+2] Cycloadditions in the Biosynthesis of Spinosyn A. Patel, A.; Chen, Z.; **Yang, Z.**; Gutiérrez, O.; Liu, H. -w.; Houk, K.

## REFERENCE

- N.; Singleton, D. A. *Journal of the American Chemical Society*, **2016**, *138*, 3631-3634.
16. Mechanisms and Origins of Periselectivity of the Ambimodal [6+ 4] Cycloadditions of Tropone to Dimethylfulvene. Yu, P.; Chen, T. Q.; **Yang, Z.**; He, C. Q.; Patel, A.; Lam, Y. H.; Liu, C. Y.; Houk, K. N. *Journal of the American Chemical Society*, **2017**, *139*, 8251-8258
17. Mechanism and Dynamics of Intramolecular C–H Insertion Reactions of 1-Aza-2-azoniaallene Salts. Hong, X.; Bercovici, D. A.; **Yang, Z.**; Al-Bataineh, N.; Srinivasan, R.; Dhakal, R. C.; Houk, K. N.; Brewer, M. *Journal of the American Chemical Society*, **2015**, *137*, 9100-9107.
18. SAM-Dependent Enzyme-Catalysed Pericyclic Reactions in Natural Product Biosynthesis Ohashi, M.; Liu, F.; Hai, Y.; Chen, M.; Tang, M. C.; **Yang, Z.**; Sato, M.; Watanabe, K.; Houk, K. N. and Tang, Y. *Nature*, **2017**, *549*, 502-506.
19. Direct Single-Molecule Dynamic Detection of Chemical Reactions Guan, J.; Jia, C.; Li, Y.; Liu, Z.; Wang, J.; **Yang, Z.**; Gu, C.; Su, D.; Houk, K. N.; Zhang, D.; Guo, X. (*Science Advance*, in revision)
20. Bridged [2.2.1] Bicyclic Phosphine Oxide Facilitates Catalytic Staudinger Reduction and  $\gamma$ -Umpolung Addition–Wittig Olefination Zhang, K.; Cai, L.; **Yang, Z.**; Houk, K.; Kwon, O. (Submitted to *Chemical Science*)
21. Effect of Trehalose Polymer Regioisomers on Protein Stabilization. Messina, M. S.; Ko, J. H.; **Yang, Z.**; Strouse, M. J.; Houk, K. N.; Maynard, H. D. *Polymer Chemistry*, **2017**, *8*, 4781-4788.
22. Photocycloaddition Through Visible Light-Induced Energy Transfer. Zhao, J.; Brosmer, J. L.; Tang, Q.; **Yang, Z.**; Houk, K. N.; Diaconescu, P. L.; Kwon, O. *Journal of the American*

## REFERENCE

*Chemical Society*, **2017**, *139*, 9807-9810

23. What a Difference Dibenzannulation Makes: Direct Dynamics of Chlorocarbene Additions to Cyclooctyne and Dibenzocyclooctyne. **Yang, Z.**; Urquilla, A.; Saperstein, Y.; Houk, K. N.; Merrer, D. C. (In preparation)